

**SIMULATION STUDY OF THE EFFECT OF WELL SPACING, EFFECT OF
PERMEABILITY ANISOTROPY, AND EFFECT OF PALMER AND
MANSOORI MODEL ON COALBED METHANE PRODUCTION**

A Thesis

by

ISMAIL ZULKARNAIN

Submitted to the Office of Graduate Studies of
Texas A&M University
in partial fulfillment of the requirements for the degree of

MASTER OF SCIENCE

December 2005

Major Subject: Petroleum Engineering

**SIMULATION STUDY OF THE EFFECT OF WELL SPACING, EFFECT OF
PERMEABILITY ANISOTROPY, AND EFFECT OF PALMER AND
MANSOORI MODEL ON COALBED METHANE PRODUCTION**

A Thesis

by

ISMAIL ZULKARNAIN

Submitted to the Office of Graduate Studies of
Texas A&M University
in partial fulfillment of the requirements for the degree of

MASTER OF SCIENCE

Approved by:

Chair of Committee,	Robert A. Wattenbarger
Committee Members,	James B. Maggard
	Michael S. Pilant
Head of Department,	Stephen A. Holditch

December 2005

Major Subject: Petroleum Engineering

ABSTRACT

Simulation Study of the Effect of Well Spacing, Effect of Permeability Anisotropy, and Effect of Palmer and Mansoori Model on Coalbed Methane Production. (December 2005)

Ismail Zulkarnain, B.S., Institut Teknologi Bandung, West Java-Indonesia

Chair of Advisory Committee: Dr. Robert A. Wattenbarger

Interference for adjacent wells may be beneficial to Coalbed-Methane production. The effect is the acceleration of de-watering which should lead to earlier and higher gas rate peaks. It is inherent that permeability anisotropy exists in the coalbed methane formation. It means that the placement of wells (wells configuration) has an effect on the development of coalbed methane field.

The effect of Palmer-Mansoori Theory is increasing effective permeability at lower pressures due to matrix shrinkage during desorption. This effect should increase the gas recovery of coalbed methane production. Palmer and Mansoori model should be considered and included to coalbed methane reservoir simulation.

These effects and phenomena can be modeled with the CMG simulator. A systematic sensitivity study of various reservoir and operating parameters will result in generalized guidelines for operating these reservoirs more effectively.

DEDICATION

This work is dedicated to:

To my parents for their unlimited love and for all they have done for me;

To all my brothers and sisters for their encourageness and support;

And to my beloved fiancée Olivia Hidayat and her family.

ACKNOWLEDGEMENTS

I wish to express my sincere appreciation to the following members of my graduate advisory committee for their contributions toward the success of this thesis.

Special thanks to the chairman of my graduate advisory committee, Dr. Robert A. Wattenbarger, for his patience, guidance, courage, and fatherly support in helping me bring this research to completion.

Thanks to Dr. J Bryan Maggard and Dr. Michel S. Pilant, for serving as members of my advisory committee.

Thank you to the faculty and staff of the Harold Vance Department of Petroleum Engineering–Texas A&M University, for providing the facility and accommodations, as well as support resources for this work.

Finally, I wish to thank the committee of the Overseas Scholarship Program for Graduate Studies Pertamina-PSCs (Production Sharing Contractors) Educational Consortium and Chevron Texaco Indonesia for their financial support.

TABLE OF CONTENTS

	Page
ABSTRACT.....	iii
DEDICATION.....	iv
ACKNOWLEDGEMENTS.....	v
TABLE OF CONTENTS.....	vi
LIST OF FIGURES	ix
LIST OF TABLES	xiv
 CHAPTER	
I INTRODUCTION.....	1
1.1 Coalbed Methane Reservoir.....	1
1.2 Well Spacing Effects on Coalbed Methane Production.....	3
1.3 Permeability Anisotropy	4
1.4 Cleats Compression and Matrix Shrinkage Effect (Palmer and Mansoori Theory).....	4
1.5 Objectives	5
1.6 Organization of Thesis.....	6
II LITERATURE REVIEW	7
2.1 Introduction.....	7
2.2 Well Spacing Effect (Interference Effect)	7
2.3 Permeability Anisotropy	9
2.4 Cleats Compression and Matrix Shrinkage Effect (Palmer and Mansoori Theory).....	9
III RESERVOIR ENGINEERING AND MODELING OF COALBED METHANE RESERVOIR	11
3.1 Introduction.....	11
3.2 Reservoir Engineering of Coalbed Methane.....	11
3.2.1 Coalbed Methane Reservoir.....	11
3.2.2 Coal Porosity.....	13
3.2.3 Gas Storage Properties.....	14
3.2.4 Adsorption Isotherm	15
3.2.5 Methane Flow Properties of Coal	18
3.2.5.1 Gas Diffusion of Coalbed Methane Reservoir.....	18
3.2.5.2 Gas Flow of Coalbed Methane Reservoir.....	19

CHAPTER	Page
3.2.6 Permeability	19
3.2.7 Saturation	19
3.2.8 Effects of Cleat Compression and Matrix Shrinkage on Coalbed Methane Reservoir.....	20
3.2.8.1 Cleats Compression	20
3.2.8.2 Matrix Shrinkage	21
3.3 Reservoir Modeling of Coalbed Methane Reservoir	24
IV THEORY AND BACKGROUND OF SIMULATION STUDY	27
4.1 Well Spacing Effects (Interference Effects)	27
4.2 Effects of Permeability Anisotropy	30
4.3 Transformation of Anisotropic Reservoirs into Equivalent Isotropic Reservoirs	31
4.4 Effects of Cleat Compression and Matrix Shrinkage	35
V SIMULATION STUDY	37
5.1 Introduction.....	37
5.2 Reservoir Model and Simulation Data.....	37
5.2.1 Base Case Reservoir Model	37
5.2.2 Reservoir Data	38
5.3 Effects of Well Spacing	39
5.4 Permeability Anisotropy	40
5.4.1. Permeability Anisotropy on 20 Acre Spacing	40
5.4.2 Permeability Anisotropy on 5 Acre Spacing	42
5.5 Transformation of an Anisotropic System to an Isotropic System.....	44
5.5.1 Permeability Anisotropy 10:1	44
5.5.2 Permeability Anisotropy 100:1	47
5.6 Cleat Compression and Matrix Shrinkage Simulation Procedure	49
VI DISCUSSIONS	51
6.1 Introduction.....	51
6.2 Discussions	51
6.2.1 Well Spacing Effects (Interference Effects)	51
6.2.2 Transformation of Anisotropic Reservoirs into Equivalent Isotropic Reservoirs	59
6.2.3 Effects of Permeability Anisotropy on Coalbed Methane Reservoirs	61
6.2.4 Effect of Cleats Compression and Matrix Shrinkage (Permeability Changes) on Coalbed Methane Production.....	67
6.2.4.1 Young's Modulus.....	68
6.2.4.2 Poisson's Ratio.....	70

CHAPTER	Page
6.2.4.3 Strain Maximum	72
6.2.5 Formation Compressibility	73
VII CONCLUSIONS AND RECOMMENDATIONS.....	74
7.1 Conclusions.....	74
7.2 Recommendations.....	74
NOMENCLATURE	75
REFERENCES.....	77
APPENDIX A DESCRIPTION OF CMG SIMULATOR	80
APPENDIX B CMG BASE CASE DATA FILE.....	85
APPENDIX C MODULI DEFINITIONS	92
APPENDIX D INPUT DATA FOR CLEATS COMPRESSION AND MATRIX SHRINKAGE MODEL (PALMER AND MANSOORI THEORY).....	94
APPENDIX E SIMULATION RESULTS	99
VITA.....	120

LIST OF FIGURES

FIGURE	Page
1.1 Typical production performance of coal bed methane reservoir.....	2
1.2 Typical production performance of conventional gas reservoir.....	3
3.1 Schematic of coal-seam cleat system.....	12
3.2 Schematic of methane flow dynamics in coal-seam.....	13
3.3 Illustration of the large internal surface area possessed by coal particles....	14
3.4 Description of Langmuir volume (V_L) on a typical Langmuir adsorption-desorption isotherm curve.....	16
3.5 Description of Langmuir pressure (p_L) on a typical Langmuir adsorption-desorption isotherm curve.....	17
3.6 Effect of Langmuir pressure (p_L) on Langmuir isotherm curve.....	17
3.7 Schematic of cleats compression phenomenon.....	21
3.8 Schematic of matrix shrinkage phenomenon.....	22
3.9 Effect of matrix shrinkage on permeability (Palmer and Mansoori Model)..	24
3.10 Idealization coal seam model from an actual model to an idealized model (dual porosity modeling).....	25
4.1 Comparison for gas rates of reservoir with one-well system and reservoir with two-wells system for conventional gas reservoir.....	27
4.2 Comparison for water rates of reservoir with one-well system and reservoir with two-wells system for conventional gas reservoir.....	28
4.3 Pressure drawdown profile of a single well system.....	29
4.4 Pressure drawdown profile of a multi wells system.....	29
4.5 Schematic of diffusion of gas into the fracture (cleats) system.....	31
4.6 Transformation of an anisotropic square reservoir system into an equivalent isotropic rectangular reservoir system.....	34
4.7 Example of application of Palmer and Mansoori Theory on coalbed methane reservoir.....	35
5.1 21*21*1 grid model. The reservoir dimension is 1866.76 ft x 1866.76 ft x 30 ft.....	37

FIGURE	Page
5.2 Scenario A for study of well placement effect on coalbed methane with permeability anisotropic for wells with 20 acre drainage area.....	41
5.3 Scenario B for study of well placement effect on coalbed methane with permeability anisotropic for wells with 20 acre drainage area	41
5.4 Scenario C for study of well placement effect on coalbed methane with permeability anisotropic for wells with 20 acre drainage area	42
5.5 Scenario A for study of well placement effect on coalbed methane with permeability anisotropic for wells with 5 acre drainage area.....	43
5.6 Scenario B for study of well placement effect on coalbed methane with permeability anisotropic for wells with 5 acre drainage area	43
5.7 Scenario C for study of well placement effect on coalbed methane with permeability anisotropic for wells with 5 acre drainage area	44
5.8 Reservoir system with anisotropic 10:1 for transformation from anisotropic reservoir system to isotropic reservoir system	45
5.9 Isotropic reservoir system of transformation from anisotropic reservoir system to isotropic reservoir system for permeability anisotropy 10:1.....	46
5.10 Reservoir system with anisotropic 100:1 for transformation from anisotropic reservoir system to isotropic reservoir system.....	48
5.11 Isotropic reservoir system of transformation from anisotropic reservoir system to isotropic reservoir system for permeability anisotropy 100:1.....	49
6.1 Effect of well spacing (interference effect) on gas production rate, conventional gas reservoir.....	51
6.2 Effect of well spacing (interference effect) on water production rate, conventional gas reservoir.....	52
6.3 Comparison of gas rates for an 80 acre well and an 40 acre well in an isotropic reservoir (Base Case).....	53
6.4 Comparison of water rates for an 80 acre well and an 40 acre well in an isotropic reservoir (Base Case).....	54

FIGURE	Page
6.5 Comparison of total gas rates for various well spacings in an 80 acre reservoir.....	55
6.6 Comparison of total water rates for various well spacings in an 80 acre reservoir.....	56
6.7 Comparison of recovery factor of gas production for various well spacings in an 80 acre reservoir.....	57
6.8 Comparison of recovery factor of water production for various well spacings in an 80 acre reservoir.....	58
6.9 Gas rates for transformation of square-anisotropic 80 acre reservoir to rectangular-isotropic 80 acre reservoir	60
6.10 Cumulative gas production rates for transformation of square-anisotropic 80 acre reservoir to rectangular-isotropic 80 acre reservoir.....	61
6.11 Comparison of gas rates for three types of well configurations.....	62
6.12 Comparison of recovery factor of gas production for three types of well configurations.....	63
6.13 Schematic of reservoir model for transformation of square-anisotropic 80 acre reservoir to rectangular-isotropic 80 acre reservoir.....	64
6.14 Comparison of water rates for three types of well configurations.....	65
6.15 Comparison of recovery factor of water production for three types of well configurations.....	66
6.16 Simulation results show that gas production rate increases with increasing magnitude in the Young's Modulus.....	69
6.17 Simulation results show that cumulative gas production increases with increasing magnitude in the Young's Modulus.....	70
6.18 Simulation results show that gas production rate increases with decreasing magnitude in the Poisson's ratio.....	71
6.19 Simulation results show that cumulative gas production increases with decreasing magnitude in the Poisson's ratio.....	71

FIGURE	Page
6.20 Simulation results show that gas rate increases with increasing magnitude in the strain maximum (strain at infinite pressure).....	72
6.21 Simulation results show that cumulative gas production increases with increasing magnitude in the maximum strain (strain at infinite pressure)....	73
B.1 21*21 simulation model grid model.....	85
C.1 Schematic of axial modulus.....	92
C.2 Schematic of Poisson's ratio.....	93
D.1 For cases with Palmer and Mansoori model, changes in fracture compressibility result in no changes in gas production rate.....	96
D.2 For cases with Palmer and Mansoori model, changes in matrix compressibility result in no changes in gas production rate.....	96
D.3 For cases without Palmer and Mansoori model, changes in fracture compressibility result in no changes in gas production rate.....	97
D.4 For cases without Palmer and Mansoori model, changes in matrix compressibility result in no changes in gas production rate.....	98
E.1 Comparison of total gas rates for various well spacings in an 80 acre reservoir.....	99
E.2 Comparison of total water rates for various well spacings in an 80 acre reservoir.....	100
E.3 Comparison of cumulative gas production for various well spacings in an 80 acre reservoir.....	101
E.4 Comparison of cumulative water production for various well spacings in an 80 acre reservoir.....	102
E.5 Comparison of recovery factor of gas production for various well spacings in an 80 acre reservoir.....	103
E.6 Comparison of recovery factor of water production for various well spacings in an 80 acre reservoir.....	104
E.7 Comparison of gas rates for three types of well configurations for wells with 20 acre drainage area.....	106

FIGURE	Page
E.8 Comparison of water rates for three types of well configurations for wells with 20 acre drainage area.....	107
E.9 Comparison of recovery factor of gas production for three types of well configurations for wells with 20 acre drainage area	108
E.10 Comparison of recovery factor of water production for three types of well configurations for wells with 20 acre drainage area	109
E.11 Comparison of gas rates for three types of well configurations for wells with 5 acre drainage area	111
E.12 Comparison of water rates for three types of well configurations for wells with 5 acre drainage area	112
E.13 Comparison of recovery factor of gas production for three types of well configurations for wells with 5 acre drainage area	113
E.14 Comparison of recovery factor of water production for three types of well configurations for wells with 5 acre drainage area	114
E.15 Gas rates for transformation of square-anisotropic 80 acre reservoir to rectangular-isotropic 80 acre reservoir with permeability anisotropic 1:0.1.....	116
E.16 Cumulative gas production rates for transformation of square-anisotropic 80 acre reservoir to rectangular-isotropic 80 acre reservoir with permeability anisotropic 1:0.1	117
E.17 Gas rates for transformation of square-anisotropic 80 acre reservoir to rectangular-isotropic 80 acre reservoir with permeability anisotropic 1:0.01.....	118
E.18 Cumulative gas production rates for transformation of square-anisotropic 80 acre reservoir to rectangular-isotropic 80 acre reservoir with permeability anisotropic 1:0.01.....	119

LIST OF TABLES

TABLE	Page
3.1 Input Data for Matrix Shrinkage Effect Calculation.....	23
4.1 Data for an Anisotropic Reservoir System.....	32
4.2 Equivalent Isotropic Reservoir System for Reservoir System in Table 4.1...	34
5.1 Base Case Reservoir Data.....	38
5.2 Anisotropic Reservoir System ($k_x : k_y = 1 : 0.1$).....	45
5.3 Isotropic Reservoir System ($k_x : k_y = 1 : 0.1$).....	46
5.4 Anisotropic Reservoir System ($k_x : k_y = 1 : 0.01$).....	47
5.5 Isotropic Reservoir System ($k_x : k_y = 1 : 0.01$).....	48
6.1 Comparison of Results for Various Well Spacings for 80 Acre Reservoir System.....	59
6.2 Comparison Results for Three Types of Well Configurations.....	66
E.1 Comparison of Results for Various Well Spacings.....	105
E.2 Comparison Results for Various Well Configurations - 20 Acre Spacing ...	110
E.3 Comparison Results for Various Well Configurations - 5 Acre Spacing.....	115

CHAPTER I

INTRODUCTION

1.1 Coalbed Methane Reservoir

Coal bed methane is considered unconventional reservoirs in that methane gas is stored in micropores and bedding planes, as well as free gas within natural fractures or cleats¹. This Reservoir acts both as the source rock and storage reservoir for methane gas. Coal bed methane is peculiar in that methane is predominantly stored in a molecular adsorbed phase within micropores of the coal. High-cost natural gas produced from deep (greater than 15,000 feet) low permeability sands may also be termed unconventional, as may gas produced from geopressured (initial reservoir pressure exceeding 0.465 *psi/vertical foot of depth*) brines (greater than 10,000 *ppm* total dissolved solids). In comparison, conventional gas reservoirs contain gas molecules within interstitial pore-spaces, for example between sand grains in a sandstone reservoir, and in fractures. Gas trapped in a conventional reservoir generally is considered to have migrated from its place of genesis to a different geologic zone or horizon into the reservoir rock.

The ability of the coal bed methane reservoir to store methane is dependant upon numerous factors: reservoir pressure, composition and rank of the coal, micropores structure and its surface properties, the molecular properties of the adsorbed gas constituents, and reservoir temperature².

Coal beds are an attractive prospect for development because of their ability to retain a higher amount of gas at shallow depths in comparison to conventional reservoirs at comparable depths and reservoir pressures. It has been estimated that during the formation of 1 *ton* of coal, gas is produced up to 46 *Mscf*³. Darton⁴ found that most mature coal contains between 20-100 *Mscf* of methane per *ton*.

This thesis follows the style of *Society of Petroleum Engineers Journal*.

Since methane gas is stored (adsorbed) on micropores of the coal, and storage is a function of pressure (the higher the pressure the greater the storage potential), production of gas is dependent upon reduction of pressure within the coal beds. Methane can be produced from the coal beds by reducing overall reservoir pressure or by reducing the partial pressure of the methane alone, while sustaining reservoir pressure. Pressure reduction frees the methane molecules from the coal and allows gas migration. A reduction of reservoir pressure is most often accomplished through formation water removal.

Water and gas separators used for conventional gas production were modified to accommodate copious amounts of produced water and associated coal fines. The produced water is often fresher (lower dissolved solids) than is characteristic of the relatively small amounts of produced water derived from conventional gas reservoirs. With hydrostatic pressure reduction at depth, methane gas is desorbed from the coal and is free to migrate through permeable strata, cleats and fractures to an area of lower pressure, ideally into the well bores that created the pressure reduction. In near-surface coal outcrops, hydrostatic pressure reduction may allow locally desorbed gas to migrate entrained with groundwater or rise vertically through porous soils to the surface.

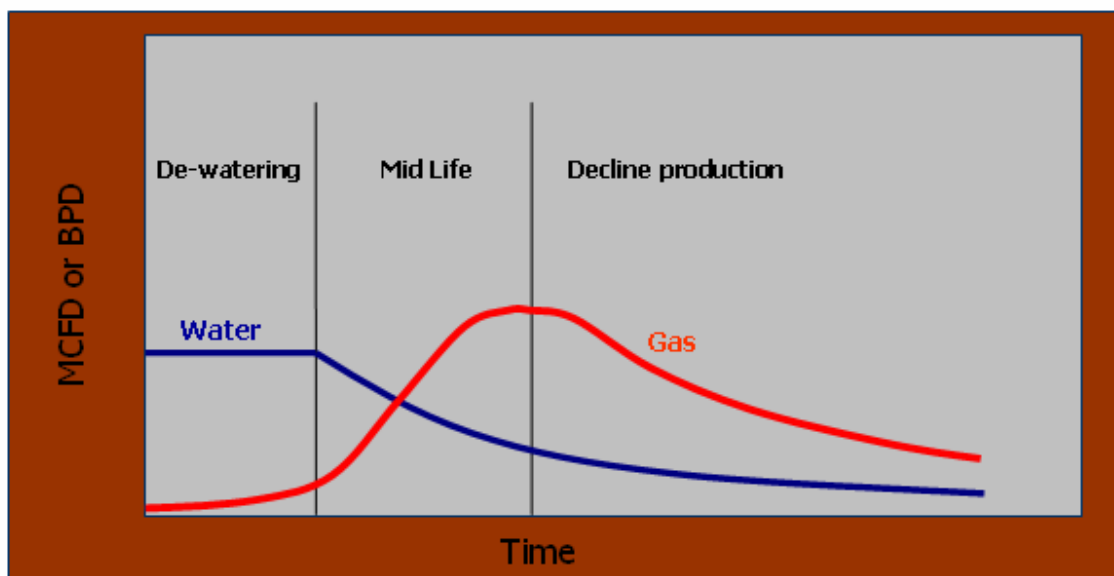


Fig. 1.1–Typical production performance of coal bed methane reservoir. First stage of production life is the dewatering stage, the second stage (mid-life) is the increasing of gas production rate (negative decline), and the third stage is the decline of gas production rate until the abandonment of production.

As coal bed water is withdrawn and formation pressure declines, the volume of gas produced tends to build from a low initial rate to a maximum rate several years after the onset of production (**Fig. 1.1**). The progressively increased gas production rate to a maximum flow years later is in direct contrast with conventional pressure-depletion reservoirs from which gas production rates tend to be greatest at the onset, then steadily decline over the life of the well (**Fig. 1.2**). While a reduction in reservoir pressure frees the methane from the coal, greatly reduced pressure may deprive the fluids of the energy needed to migrate efficiently to the well bore and enable desorption of increasing proportions of carbon dioxide. It is estimated that less than 50 percent of the coal bed methane in place can be economically recovered by reservoir pressure depletion strategy².

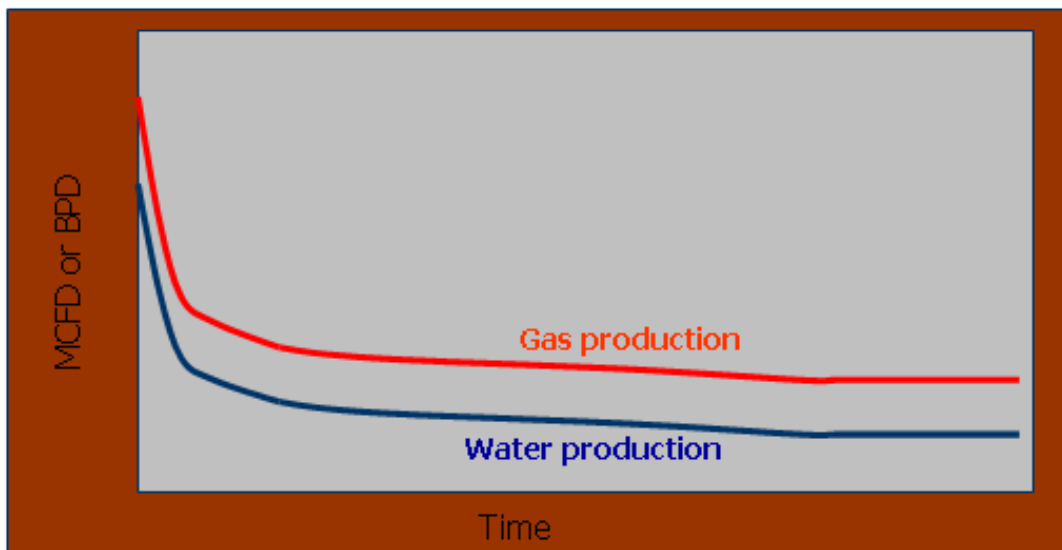


Fig. 1.2–Typical production performance of conventional gas reservoir. Gas rate and water rate decline directly as well as the production begins.

1.2 Well Spacing Effects on Coalbed Methane Production

The interference between wells has a beneficial effect on coal bed methane reservoir, unlike conventional gas reservoirs. It has been proved that the closer well spacing we drill, the faster dewatering process we have. The dewatering process results in pressure depletion. As the pressure depleted, gas will be released from the coal matrix into the coal fracture (cleats). With closer well spacing, we produce more gas rapidly. It is

primarily different from conventional gas reservoirs, where wells are drilled at larger spacing in order to minimize the effect of interference.

In coal bed methane reservoir, gas production rate peaks higher at earlier time as the well spacing decreases. The impact on the ultimate gas recovery will depend on specific reservoir conditions as early time increases in production may or may not be offset by earlier production decline in later life of the wells.

1.3 Permeability Anisotropy

Coal bed methane reservoir is considered as naturally fractured reservoir. Coal beds are characterized as a dual porosity reservoir, fractures (cleats) and matrix. The fractures (cleats) system is consisted of two major fractures system, the face cleat and butt cleat. The face cleat is long and continuous fractures throughout the coal seams and butt cleat is a short and discontinuous fractures perpendicular to the face cleat. The butt cleat is discontinuous because it is usually intersected by the face cleat. The face cleat has a larger contact area with the matrix compare to the butt cleat, therefore it is capable to drain larger area of coal seams and assumed as the maximum permeability direction. In some cases, this assumption may not be applicable (e.g. Bowen basin, Australia)⁵.

Coal matrix acts as the storage of gas but has very little permeability. As the pressure decreases, gas is desorbed from the surface of coal and diffuses into the fractures system. Once in the cleat system, gas will flow through the fractures into the wellbore. The fractures contribute to the formation permeability. The existence of face cleat and butt cleat develop permeability anisotropy. This permeability anisotropy tends to create a preferential flow.

In facts, the permeability has impacts on the coal bed methane production. One of the well known impacts is the drainage pattern shape.

1.4 Cleats Compression and Matrix Shrinkage Effect (Palmer and Mansoori Theory)

In the naturally fracture formation such as coal bed methane reservoir, the permeability is critically sensitive to changes in effective stress (pore pressure). During the drawdown,

the desorption of methane from the coal matrix leads to matrix shrinkage. This matrix shrinkage has an impact to the formation permeability⁶.

The following phenomena have been explained by Palmer and Mansoori⁷ that:

1. During drawdown of a reservoir by primary production, effective stress increases and permeability decreases due to cleat compression.
2. However, in coal beds, drawdown leads to desorption of methane, and this is accompanied by matrix shrinkage which opens the cleats and leads to permeability increase.

This theory, in facts, has impacts on coal bed methane production. Because the matrix shrinkage phenomenon tends to develop permeability rebound at lower pressure. It might also have implications for enhanced coal bed methane recovery such as CO₂ injection.

1.5 Objectives

A systematic sensitivity study of various reservoir and operating parameters will result in generalized guidelines for operating coal bed methane reservoirs more effectively. Interference for adjacent wells may be beneficial to coal bed methane production. One effect is the acceleration of de-watering which should lead to earlier gas rate peaks. The existence of permeability anisotropy also has impacts on coal bed methane production. The other effect is the Palmer-Mansoori theory of increasing effective permeability at lower pressures due to matrix shrinkage during desorption.

The main goal of this research is to develop guidelines for coal bed methane production operation based on various reservoir and operating parameters. This research is emphasized on study of the following parameters:

1. The effect of interference between wells on coal bed methane production. It also has implication on the well spacing effects.
2. The effect of permeability anisotropy on coal bed methane production. This parameter is also related to the placement of the well (well configuration).
3. The impacts of Palmer and Mansoori theory on coal bed methane production.

1.6 Organization of Thesis

The outline and organization of this thesis are as follows:

We begin this thesis with the introduction, Chapter I. It presents about the coal bed methane reservoirs, problems description, objectives, and organization of thesis.

Chapter II presents a comprehensive literature review related with the technology of coal bed methane, as well as modeling and simulation developed and presented by various authors.

Chapter III, presents the theories and fundamentals of coal bed methane reservoir engineering, coalbed methane modeling, and coalbed methane simulation.

Chapter IV, presents the theory and background of simulation study

Chapter V, presents simulation study to investigate the well spacing effects (well interference effects), permeability anisotropy, and matrix shrinkage effects.

Chapter VI, discusses several aspects and results from this research.

Chapter VII, presents summary, conclusions, and some recommendation for future work.

Finally, we present the nomenclature, reference, and some appendixes developed in this research.

CHAPTER II

LITERATURE REVIEW

2.1 Introduction

This chapter presents the review of technical literature on several topics related to the operational parameters of coalbed methane production. The review will be categorized into three major topics: effects of interference, permeability anisotropy, and matrix shrinkage effect (Palmer and Mansoori Theory).

The first section reviews the effects of interference between wells on coalbed methane production. We focus on the difference between the interference effects on conventional gas reservoir and coalbed methane reservoir. The second section reviews the effect of permeability anisotropy. The third section reviews the development of matrix shrinkage effect (Palmer and Mansoori theory).

The goal in this literature review is to investigate what are the effects of the wells interference, effects of the permeability anisotropy, and effects of the Palmer and Mansoori theory on coalbed methane production. With doing literature review, we also know what have been done by researchers and we can apply and do similar thing in this research.

2.2 Well Spacing Effect (Interference Effect)

Methane is stored in the matrix system as an adsorbed gas. We need to lower the pressure to let methane desorbed from the surface of coal. Lowering the pressure needs to remove the water from the cleat system (dewatering). Therefore, it has strong implication on well interference. Interference between wells in conventional gas reservoir has been known with negative interference effects. Several authors and researchers have been investigated the effects of well interference on coalbed methane reservoir.

Remner *et. al.*⁸ conducted a parametric study to investigate the impacts of interference effects on gas and water production in multiple well system. They found that the pressure drawdown caused by the interference between wells enhanced the desorption of methane to the cleat system, therefore creates a beneficial impacts on gas production

unlike the gas conventional gas reservoir. However, the water rate has the same performance with conventional interference effect.

Wicks *et. al.*⁹ also studied the effect of well spacing for coalbed methane in the Warrior basin. They reported that closer well spacing would increase methane recovery. Drilling in a 160 acres with 8 wells produced almost 85 percent of gas in place while Drilling only one well only produced 25 percent of gas in place. However, the consideration of optimum well spacing must be made based on economic decision.

Young *et. al.*¹⁰ conducted the simulation study of the beneficial effects of well interference in coalbed methane production using the data from the basal Fruitland coals in the Northern San Juan Basin. They proved that the well interference has a beneficial effect in coalbed methane production. They also did the simulation study to investigate the effect of well spacing and fracture length in coalbed methane production using the data from Fruitland coalbed methane reservoir. He concluded that there is an optimum well spacing to produce the coalbed methane from one field. And the optimum well spacing is due to the variability in reservoir properties of Fruitland coalbed reservoir in the San Juan Basin. They also stated that unlike the conventional gas wells, well interference effects are potentially useful in exploiting coalbed methane resources.

Young *et. al.*¹¹ also investigated the effect of well spacing and well interference for Fruitland coalbed methane reservoir, San Juan basin. They also indicated the beneficial effect of well interference. This phenomenon is totally different from conventional gas reservoir, where wells are drilled at large spacing to minimize the interference effects. They found that closer well spacing resulted in higher peak gas rate occurring earlier in production life. However, this higher and earlier gas rate caused a more rapid production decline.

Chaianansutcharit *et. al.*¹² investigated the effects of well interference on coalbed methane performance. They conducted simulation study to study the effects. They proved that well interference has positive impacts on coalbed methane reservoir. Well interference could increase methane recovery. They stated that the well interference would accelerate the gas production in term that 2 wells system would reach total recovery earlier than one well system.

2.3 Permeability Anisotropy

Permeability anisotropy in porous media has been investigated by many authors and researchers. The presence of parallel natural fracturing is one of the major important reasons of permeability anisotropy. In coalbed methane reservoir, the presence of face cleat and butt cleat creates permeability anisotropy.

Several studies have been reported that the drainage pattern shape should be designed according to the permeability anisotropy. It has been showed that the permeability anisotropy has a major impact to the drainage pattern. Wicks *et. al.*⁹ reported that the rectangular drainage pattern is better than square pattern on coalbed methane production. Rectangular pattern has a better methane recovery compare to the square pattern. The rectangular pattern can improve gas recovery about 15 percent.

Bumb and Mckee¹³ indicated improvement in water production when well pattern was planned according to permeability anisotropy.

Sung and Ertekin¹⁴, in their simulation study, proposed that if more vertical wells drilled in the direction of face cleats, methane would be transmitted to the wells more effectively.

Young *et. al.*¹⁰ conducted simulation study for Cedar Hill Field, Northern San Juan Basin. They stated that the degree of permeability anisotropy should be considered in the development of a coalbed methane reservoir due to the impact on field drainage. The consideration should be made particularly with regard to well placement.

Chaianansutcharit *et. al.*¹² analyzed the impacts of permeability anisotropy on coalbed methane performance. They identified the “dual peak” gas rate behavior. They analyzed that the dual peak is caused by the different timing of boundary effects. They also confirmed that rectangular drainage shape should planned for coalbed methane field development.

2.4 Cleats Compression and Matrix Shrinkage Effect (Palmer and Mansoori

Theory)

Gray¹⁵ reported that coal has been shown to shrink during the desorption of methane and expand during the readsorption.

Harpalani *et. al.*⁶ conducted an experimental study to investigate the effect of desorption of methane on the formation permeability. They indicated that the desorption of gas causes the coal to shrink. The shrinkage of coal matrix is turned out to cause the formation permeability to increase significantly, particularly when the pressure decreases below the desorption pressure. The increasing permeability resulted in higher amount of gas production.

In 1990, Sawyer *et. al.*¹⁶ developed a coal matrix shrinkage and permeability model. This model was developed for COMET simulator and known as ARI model. The ARI model uses gas concentration as an important parameter to calculate the changes of permeability according to matrix shrinkage.

Palmer and Mansoori⁷, in 1996, published a new model to calculate the permeability changes according to the stress effects and matrix shrinkage. They proposed a new equation for calculating pore volume compressibility and permeability in coals as a function of effective stress and matrix shrinkage. This equation described the changes of permeability as reservoir pressure decreases during drawdown and showed a permeability rebound at lower pressure.

CHAPTER III

RESERVOIR ENGINEERING AND MODELING OF COALBED METHANE RESERVOIR

3.1 Introduction

World demand on fossil energy, especially oil and gas, continuously increase. The ability of conventional oil to supply energy does no longer meet the demand. Therefore, the unconventional reservoir appears as an important player to supply the energy. Unconventional natural gas can be defined as gas produced from resources other than those historically exploited by the oil and gas industry¹⁷. Unconventional gas resources include tight gas formation, gas shales, coal bed methane, and geopressured aquifers¹⁸.

Coal bed methane as the unconventional reservoir plays an important role on recently energy supply. Effective Development of coal bed methane reservoir needs a better understanding of coal bed methane reservoir. In order to deeply understand the behavior and performance of coal bed methane reservoir, the knowledge of coalbed methane reservoir engineering is the key points. Reservoir engineering of coalbed methane includes the phenomena and physical parameters of coal bed methane. This Chapter presents the fundamentals of coal bed methane reservoir and reservoir modeling of coal bed methane reservoir.

3.2 Reservoir Engineering of Coalbed Methane

3.2.1 Coalbed Methane Reservoir

Reservoir characteristic of coalbed methane is quite complicated. Coalbeds are naturally fractured and low pressure systems with gas adsorbed into the coal matrix. Coalbeds are characterized as a dual porosity reservoir, fractures (cleats) and matrix. The fractures (cleats) system is consisted of two major fractures system, the face cleat and butt cleat. The face cleat is long and continuous fractures throughout the coal seams and butt cleat is a short and discontinuous fractures perpendicular to the face cleat. The butt cleat is discontinuous because it is usually intersected by the face cleat. The matrix system is the part of the formation that exists between the fractures system. The face cleat has larger contact area with the matrix compare to the butt cleats, therefore it is capable to drain

larger area of coal seams. The face cleats provide the main pathways for gas to flow into the wellbore (see **Fig. 3.1**).

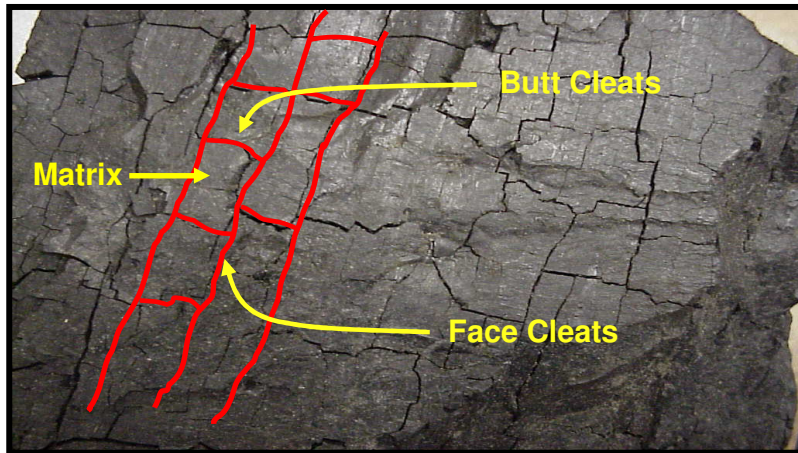


Fig. 3.1–Schematic of coal-seam cleat system. The red lines show the face cleats and butt cleat on a piece of coal. Face cleats are long and continuous while butt cleats are short and discontinuous (intersected by face cleats).

At the original conditions of reservoir, most of gas is stored in the matrix with a very little gas in the fractures, negligible. Fractures system is saturated with water. Gas is stored in the matrix in adsorption condition rather than stored as a free gas like in the conventional gas reservoirs. The majority of gas is adsorbed on the internal surface of the micropores of coal matrix.

Primary production of coalbed methane occurs by initially de-watering the naturally fractured system and hence reducing the pressure in the fracture system. The reduced pressure causes the desorption of gas from the surface of coal matrix and release of gas to the fractures. Gas diffuses from the surface of coal matrix towards the fracture system. Once in the fractures, gas flows throughout the fractures into the wellbore. The degasification of coalbed methane is consisted of three major processes:

1. Desorption process, the release of gas from the internal surface of micropores of the coal matrix.
2. Diffusion process, the desorbed gas flows throughout the coal matrix into the fractures system.
3. Gas flows throughout the fractures (cleats) into the wellbore.

See Fig. 3.2 for details.

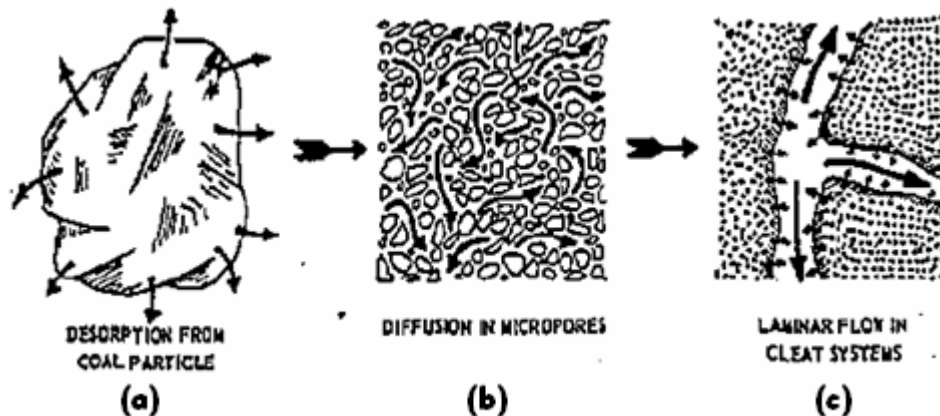


Fig. 3.2–Schematic of methane flow dynamics in coal-seam (After Remner *et.al*⁸). (a) Desorption process, the release of gas from the internal surface of micropores of the coal matrix. (b) Diffusion process, the desorbed gas flows throughout the coal matrix into the fractures system. (c) Gas flows throughout the fractures (cleats) into the wellbore.

3.2.2 Coal Porosity

Coal is both the source rock and reservoir rock for a coalbed methane well. Methane is stored in the same place where it is formed. As with conventional reservoirs, some barrier must be in place to prevent the gas from migrating out of the reservoir rock. Coal is solid substance separated by fractures or cleats. Like conventional reservoirs, some gas is stored in the space between the solid particles. However, the interstitial pore space represents a small portion of the overall available storage space within coal. Most of the gas is stored within the microscopic structure of the coal itself. The microscopic structure of coal creates a complex, intricate maze, providing a tremendous amount of surface area upon which the methane can attach.

Coal bed methane comprises three majors porosity:

1. Fractures, the face cleats and the butt cleats. It provides the path flow of gas from the coal matrix to the wellbore. At original reservoir condition, Fracture is almost a hundred percent saturated with water.
2. Macropores, interstitial pore spaces within the coal matrix that store the methane gas in the coalbed methane reservoir as a free gas. It is assumed as the porosity of the coal matrix.
3. Micropores, pore spaces within the coal matrix with very small size in diameter. Micropores store the methane gas in the coal bed methane reservoir as an

adsorbed gas. These micropores are not considered as the porosity because of its very small size, but assumed as the internal surface area of coal matrix.

3.2.3 Gas Storage Properties

Coal is considered as a porous medium (reservoir rocks) because of its ability to store and flow the methane. However it has a remarkable difference from other conventional reservoirs in that the volume of gas, which it can store, is high beyond its pore volume capacity. In fact, the methane stored in coal reservoir is mainly adsorbed onto the internal micropores surface. Due to the very small size of an individual micropores, typically $5 \times 10^{-10} - 10 \times 10^{-10} \text{ m}$ in diameter, the internal micropores surface in coal can be very large¹⁹. For some coals, the internal micropores surface area may reach several hundreds m^2 per gram of solid, thus making available large amount of surface adsorbing gas. Some authors concluded that the surface area of coals is mostly in the range of 2150 – 3150 ft^2/g . This also means that if 18 gram of coal is crushed its surface area can be as large as a 360 ft X 160 ft football field. This is illustrated in **Fig. 3.3**.

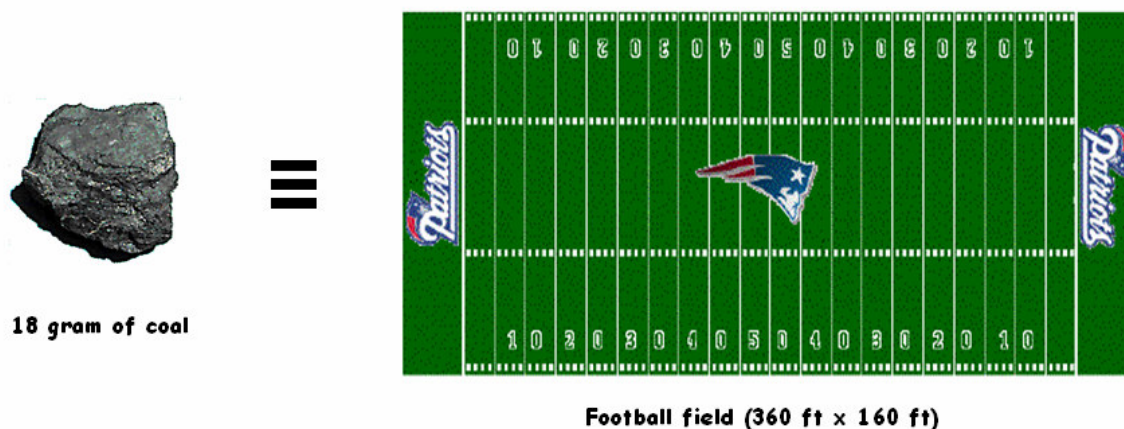


Fig. 3.3—Illustration of the large internal surface area possessed by coal particles. 18 gram of coal has internal surface are equals to a football field.

For a given coal, the amount of gas adsorbed in the surface of coal matrix is a function of the pressure within the pore volume only. The amount of adsorbed gas is limited by the available free pore surface. The relationship of the amount (concentration)

of adsorbed gas and pressure at a given temperature is well known as the Langmuir adsorption isotherm curve and is fundamental reservoir property of coal seam.

If we lower the coal seam pressure, gas will be released from the coal matrix until a new equilibrium condition between the new pressure and adsorbed gas is reached. The time required for the coal to reach a new equilibrium condition depends on the diffusion properties of coal. Reducing the pressure until zero absolute (0 *psia*) will cause the coal releasing all of the adsorbed gas.

For reservoir modeling purposes, the total amount of gas stored in the coal bed methane reservoir comprises the following category.

1. Free gas, stored in the pore spaces follows normal gas law. The amount of this free gas can be calculated if the porosity and pressure are known. Free gas is very small compared to the adsorbed gas.
2. Adsorbed gas, stored in the internal surface area of micropores by surface attraction forces. The relationship of the amount (concentration) of adsorbed gas and pressure at a given temperature is described by Langmuir Isotherm Curve. Adsorbed gas contributes most of the gas in the coal bed methane reservoir.

3.2.4 Adsorption Isotherm

Coal has the ability to store a large amount of gas. Methane (gas) is adsorbed in the coal bed methane under the adsorption mechanism. Adsorption can be described by imagining dust attached to a surface of solid, sand attached to surface of solid. This is different from absorption where one substance becomes trapped inside another, such as a sponge soaking up water. However, Adsorption is a reversible process because that involves weak attraction forces.

Methane is adsorbed in the internal surface of coal matrix. The adsorbed methane on the internal surface of coal matrix is modeled using the Langmuir adsorption isotherm. The Langmuir adsorption isotherm assumes that the gas attaches to the surface of the coal and covers the surface as a single layer of gas (monolayer). Nearly all of the gas stored by adsorption coal exists in a condensed, near liquid state¹⁹. The following equation is the Langmuir equation that describes the amount of gas stored on the surface of coal matrix as a function of pressure:

$$C(p) = V_L \frac{p}{p + p_L} \dots\dots\dots 3.1$$

Langmuir isotherm equation assumes that the concentration of methane adsorbed on the surface of coal matrix is a function of pressure only.

In the **Eqn. 3.1**, $C(p)$ is the amount of adsorbed gas in scf/ft^3 , V_L is the Langmuir volume constant in scf/ft^3 , p_L is Langmuir pressure in $psia$, and p is instantaneous pressure in $psia$.

The Langmuir isotherm equation has 2 parameters:

1. Langmuir volume (V_L): is the maximum amount of methane adsorbed on the surface of the coal matrix when the pressure, p , reaches infinity. This value is asymptotically approached by the isotherm as the pressure increases. The following figure (**Fig. 3.4**) is of a typical isotherm and shows its relationship with V_L .

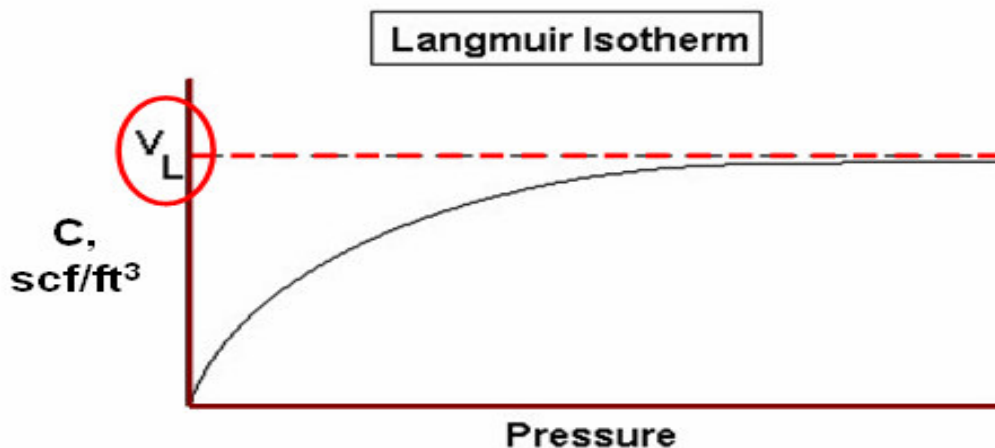


Fig. 3.4—Description of Langmuir volume (V_L) on a typical Langmuir adsorption-desorption isotherm curve. The figure shows that V_L is the maximum volume of adsorbed gas (methane).

2. Langmuir pressure (P_L): is the pressure where the amount of adsorbed methane is one half of its maximum amount, V_L , i.e. when $p = p_L$, $C = 0.5 V_L$. This is illustrated in **Fig. 3.5**.

Fig. 3.6 shows how Langmuir pressure, p_L , affects the shape of Langmuir isotherm curve. The higher the p_L is the lower the curve is. However, eventually all of the curves will coincide at the same V_L .

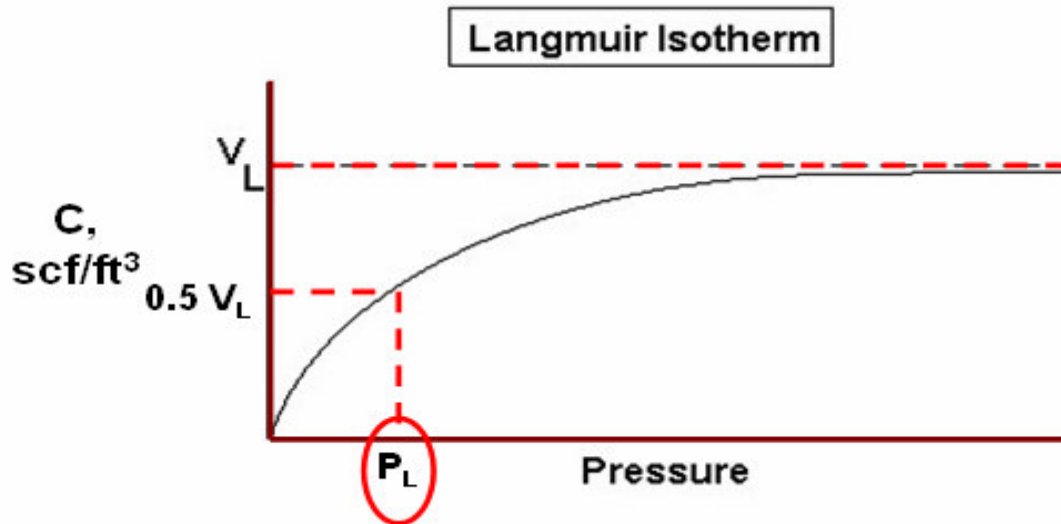


Fig. 3.5–Description of Langmuir pressure (p_L) on a typical Langmuir adsorption-desorption isotherm curve. The figure shows that p_L is the pressure where the volume of the adsorbed gas is one half V_L .

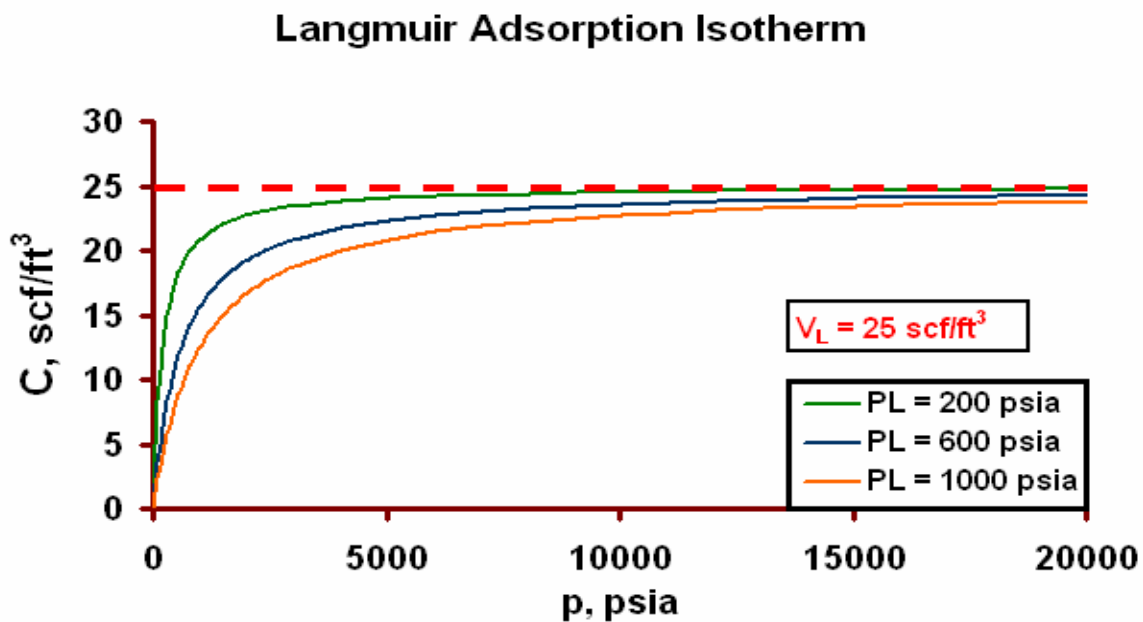


Fig. 3.6–Effect of Langmuir pressure (p_L) on Langmuir isotherm curve. The higher the p_L is the lower the curve is. However, eventually all of the curves will coincide at the same V_L .

The amount of adsorbed gas, ($C(p)$) mentioned in **Eqn. 3.1**, also can be stated in *scf/ton*. **Eqn. 3.2** determines the amount of adsorbed gas in *scf/ton*.

$$V = V_m \frac{bp}{1+bp} \dots\dots\dots 3.2$$

and

$$b = \frac{1}{p_L} \dots\dots\dots 3.3$$

Where V_m is the Langmuir isotherm constant in *scf/ton*, b is the Langmuir pressure constant constant in *psia⁻¹*, and p is instantaneous pressure in *psia*. V_L is related to the V_m with the following equation (Seidle and Arri²⁰):

$$V_L = 0.031214V_M \rho_B \dots\dots\dots 3.4$$

Where ρ_B is bulk density of coal deposit in *gram/cm³*.

3.2.5 Methane Flow Properties of Coal

The ability of coalbed methane reservoir to transport the methane is measured by flow properties such as diffusivity and permeability. In the very small pores, such as micropores, gas is released from the internal micropores surface (desorption). The released gas is transported very slowly through the coal matrix into the fractures (cleats) with gradient of concentration as the driving force. In the fractures (cleats), gas released from the coal matrix flows throughout the fractures system into the wellbore with gradient of pressure as the driving force.

3.2.5.1 Gas Diffusion of Coalbed Methane Reservoir

Throughout the very small micropores in the coal matrix, the desorbed gas will flow in the diffusion state rather than flowing following Darcy's Law. The desorbed gas could not flow freely following Darcy's Law due to the very high drag force in the pathways of size micropores. This diffusion process is described using the Fick's Law¹⁸:

$$Q_{gas} = -DA \frac{dC}{dL} \dots\dots\dots 3.5$$

where D is the diffusion constant in ft^2/day and A is the surface area of matrix element, ft^2 . We can see that the driving force for the diffusion process is the gradient of concentration rather than gradient of pressure in Darcy's Law. However, the concentration of gas is a function of pressure as described by *Langmuir Isotherm Theory*.

3.2.5.2 Gas Flow of Coalbed Methane Reservoir

The desorbed gas from the coal matrix system, gas flows throughout the fractures into the wellbore. The flow of gas throughout the fractures system is governed by Darcy's Law¹⁸. The following equation describes the Darcy's Law¹⁸:

$$q = -\frac{kA}{\mu} \frac{dp}{dL} \dots\dots\dots 3.6$$

We can see clearly that the driving force for the flow of gas throughout the fractures system is the pressure gradient.

3.2.6 Permeability

Coal is a naturally fractured formation. It consists of fractures (face cleats and butt cleats) and the matrix. Most of the gas is stored inside the matrix system (on the surface of micropores). Gas is desorbed from the surface of matrix and flows throughout the matrix into the fractures by diffusion.

Fractures, initially, is saturated with water. Producing gas from coal bed methane reservoir is associated with dewatering the fractures. Dewatering the fractures decreases the reservoir pressure, therefore initiates gas to desorb from the surface of micropores. Gas diffuses throughout the coal matrix in to the fracture.

Fractures provide the pathway for water and gas to flow into the wellbore. Flow of fluids (water and gas) in the fractures follows the Darcy's Law. For CBM reservoir, permeability refers to the permeability of fractures system, not the permeability of the matrix system.

3.2.7 Saturation

Coal is a naturally fractured formation. It consists of fractures (face cleats and butt cleats) and the matrix. Fractures are almost a hundred percent saturated with water. The matrix

consists of macropores and micropores. Macropores stores the gas as free gas, whereas micropores stores the gas by adsorption.

For CBM production, saturation (S_w or S_g) refers to the saturation of the cleats and macropores, not the micropores in the matrix.

3.2.8 Effects of Cleat Compression and Matrix Shrinkage on Coalbed Methane

Reservoir

Several authors have been reported from the laboratory experiments and field data that coal matrix shrinkage and the resulting change in cleat (fracture) system porosity can have a profound effect on the formation permeability and thus on production performance.

In the naturally fracture formation such as coal bed methane reservoir, the permeability is critically sensitive to changes in effective stress (pore pressure). During the drawdown, the desorption of methane from the coal matrix leads to matrix shrinkage. This matrix shrinkage has an impact to the formation permeability⁶.

The following phenomena have been explained by Palmer and Mansoori⁷ that:

1. During drawdown of a reservoir by primary production, effective stress increases and permeability decreases due to cleats compression.
2. However, in coalbeds, drawdown leads to desorption of methane, and this is accompanied by matrix shrinkage which opens the cleats and leads to permeability increase.

3.2.8.1 Cleats Compression

As the reservoir pressure decreases, the overburden compresses the cleats thereby reducing the permeability. A schematic of this phenomenon is shown in the following figure (**Fig. 3.7**).

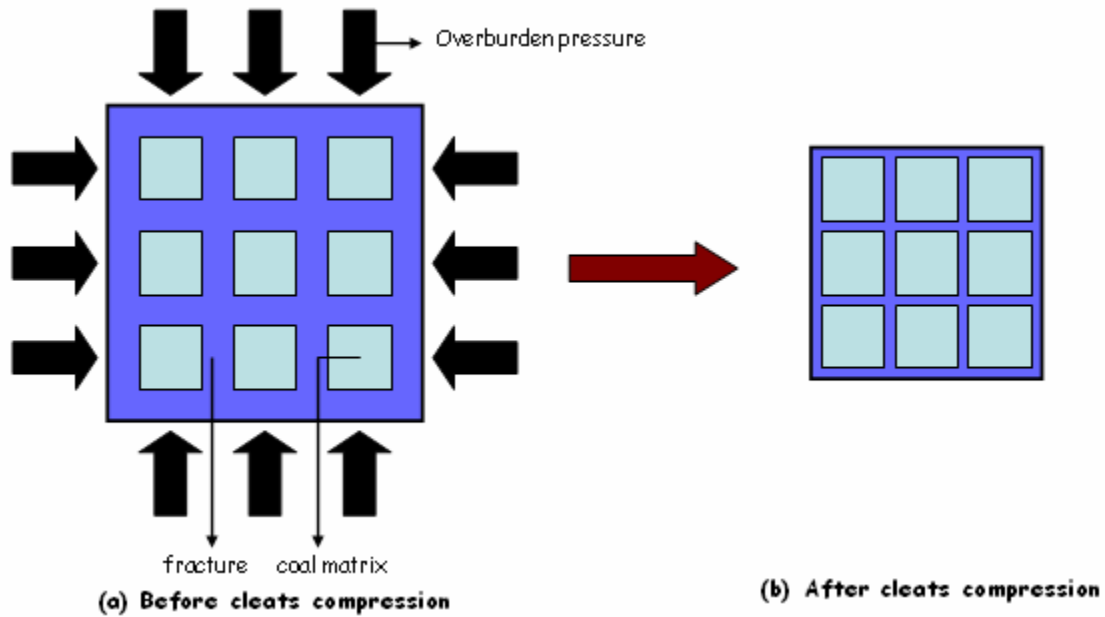


Fig. 3.7—Schematic of cleats compression phenomenon. (a) schematic of coal seam before cleats compression and (b) schematic of coal seam after cleats compression.

3.2.8.2 Matrix Shrinkage

Coal matrix adsorbs gas on the surface of micropores. The desorption of gas from the coal matrix leads to decrease the pressure exerted by the gas in these pores. This causes the volume of the coal matrix to reduce in size. A reduction in the matrix size simultaneously acts to widen the cleats thereby increasing permeability. This is illustrated in **Fig. 3.8**.

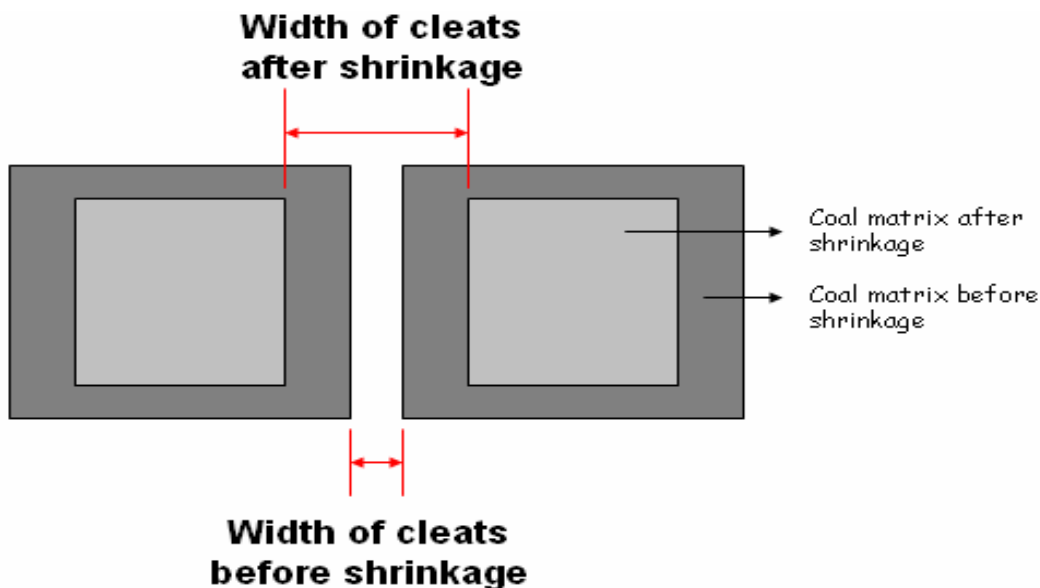


Fig.3.8–Schematic of matrix shrinkage phenomenon. The increasing of width of cleats is caused by the matrix shrinkage.

Palmer and Mansoori⁷, in 1996, published a new model to calculate the permeability changes according to the stress effects and matrix shrinkage. They proposed a new equation for calculating pore volume compressibility and permeability in coals as a function of effective stress and matrix shrinkage. This equation described the changes of permeability as reservoir pressure decreases during drawdown and showed a permeability rebound at lower pressure.

The Palmer and Mansoori model is presented as:

$$\frac{\phi}{\phi_o} = 1 + \frac{c_m}{\phi_o} (p - p_o) + \frac{c_o}{\phi_o} \left(\frac{K}{M} - 1 \right) \left(\frac{bp}{1+bp} - \frac{bp_o}{1+bp_o} \right) \dots\dots\dots 3.7$$

And the permeability is calculated using the following equation

$$\frac{k}{k_o} = \left(\frac{\phi}{\phi_o} \right)^3 \dots\dots\dots 3.8$$

Using **Eqn. 3.7** and **Eqn. 3.8**, therefore we can calculate the changes in permeability as functions of elastic moduli (Young's modulus, bulk modulus, constrained axial modulus, and Poisson ratio). Those equations are for one gas component only. They also assumed that the shape of the volumetric strain is similar to a Langmuir isotherm curve²².

Palmer and Mansoori⁷ Stated that

$$c_m = \frac{1}{M} - \left(\frac{K}{M} + f - 1 \right) \beta \dots\dots\dots 3.9$$

$$\frac{M}{E} = \frac{1 - \nu}{(1 + \nu)(1 - 2\nu)} \dots\dots\dots 3.10$$

$$\frac{K}{M} = \frac{1}{3} \left(\frac{1 + \nu}{1 - \nu} \right) \dots\dots\dots 3.11$$

If sufficient matrix shrinkage exists, there will be permeability rebound at lower pressure drawdown.

An example of application of the model has been presented by Palmer and Mansoori. The application of the model applies for data from San Juan basin. The following shows the changes of permeability as the function of cleats compression and matrix shrinkage effects.

The input parameter used in the calculation shown in the table below, **Table 3.1**:

TABLE 3.1-INPUT DATA FOR MATRIX SHRINKAGE EFFECT CALCULATION	
Parameter	Large Scale San Juan Basin Reservoir
ϕ_o (%)	0.1 – 0.5
ν	0.39
E (psi)	1.24E+05 – 4.45E+05
K/M	0.76
M/E	2.0
F	0.5
β (psi ⁻¹)	0
B (psi ⁻¹)	0.0016
c_o/b (psi)	8
P_i	1100
V_L	500
c_p	$\frac{1}{2}E\phi$

Fig. 3.9 shows the results from the model. As we can see from the figure, there is a permeability rebound if the matrix shrinkage is strong enough. This phenomenon has been explained by Palmer and Mansoori⁷ that:

1. During drawdown of a reservoir by primary production, effective stress increases and permeability decreases due to cleat compression.
2. However, in coalbeds, drawdown leads to desorption of methane, and this is accompanied by matrix shrinkage which opens the cleats and leads to permeability increase.

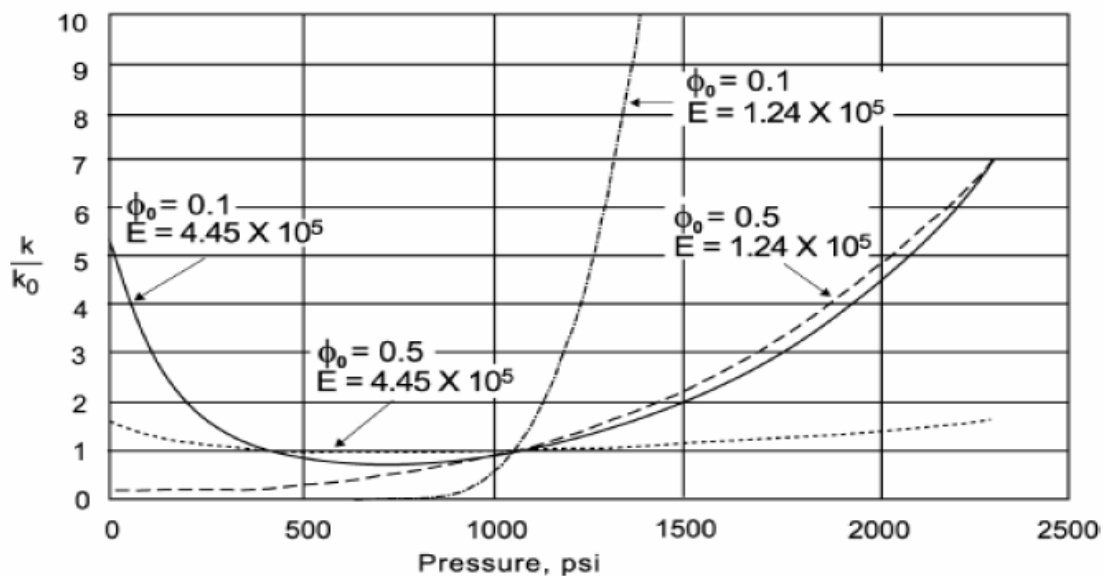


Fig. 3.9–Effect of matrix shrinkage on permeability (Palmer and Mansoori Model). Reproduced from SPE paper 36737⁷. Two competing effects, cleats compression and matrix shrinkage, result in the permeability rebound on the lower pressure.

3.3 Reservoir Modeling of Coalbed Methane Reservoir

The easiest way to describe a coal bed methane reservoir is to think of a conventional reservoir in a dual-porosity mode. Usually a conventional dual-porosity simulator is used to model a system such as a fractured carbonate reservoir where there is a low-permeability matrix coupled to a high-permeability fracture network. Each system has its own unique permeability and porosity, and a matrix/fracture transfer term governs the fluid flow from the matrix into the fractures.

In a CBM model, the fracture network represents the coal cleats. However, the matrix portion of the system has no effective permeability and porosity and is used only as a gas source with gas release controlled by a gas concentration vs. pressure relationship supplied as input data. While it is common to refer to CBM models as dual-porosity models, they are really only single-porosity models with a pressure-dependent source term coupled to the reservoir.

If the system modeled is entirely coal, the simulation approach is straightforward. Coal properties must be supplied as input data as well as system permeability, porosity, initial pressure, and initial fluid saturations. As water is removed from the cleat system, the reservoir pressure declines, gas is desorbed from the coal into the cleats, and gas production begins. This approach has been used successfully over the years in models representing simple single-well systems as well as larger, more-complex models containing thousands of producing CBM wells.

For mathematical purposes, the coal-seam is modeled by a dual porosity model. The well known dual porosity model was proposed by Warren and Root²¹ and Kazemi²³ to simulate naturally fractured reservoirs. **Fig. 3.10** shows idealization coal seam model from an actual model to an idealized model. In the idealized model, a systematic array of matrix is surrounded by fractures. The matrix has a very low permeability but very high storage of gas, fractures has very high permeability but low storage of gas.

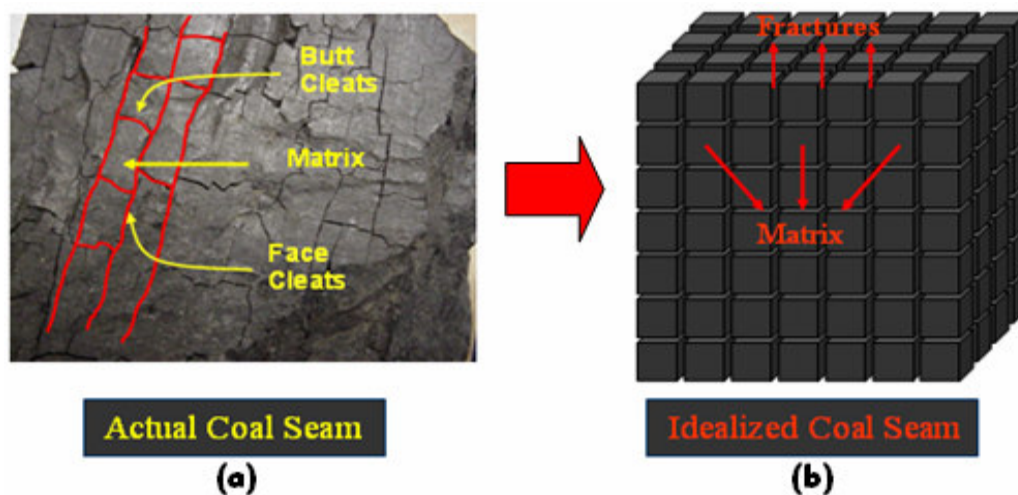


Fig. 3.10–Idealization coal seam model from an actual model to an idealized model (dual porosity modeling). (a) actual coal seam model and (b) idealized coal seam model similar with Warren and Root model²¹.

Matrix system has very high storage ability compare to fractures system. Matrix system of coal seam has very large surface area. Darton⁴ found that most mature coal contains between 20 and 100 *scf* {0,566 and 2.832 *std. m*³) of methane per ton. Gas is stored in the matrix as an adsorbed gas. The amount of gas stored in matrix is dependent to the reservoir pressure. The amount of gas (concentration of gas) as the function of pressure is described by Langmuir isotherm equation as follows²²:

$$C(p) = V_L \frac{P}{p + p_L} \dots\dots\dots 3.12$$

As mentioned earlier, the coal matrix has very low permeability but it has very large surface area. Because coal matrix has very-very low permeability, mass transport through the matrix system is in diffusion state. Gas diffuses throughout the matrix rather than flows. The diffusion of gas through the matrix is described using the following equations²²:

$$Q_{gas}(P) = Coef(\bar{C} - C(p)) \dots\dots\dots 3.13$$

Where

$$Coef = D(aA)N_e \dots\dots\dots 3.14$$

And *a* is *D* is the diffusion constant in *ft*²/*day*, *a* shape factor in *ft*⁻¹, *A* is the surface area of a matrix *ft*², and *N_e* is the number of matrix elements within a grid block. As we can see from the **Eqn. 3.13** above, the diffusion of gas through the matrix system is proportional to the difference of the average gas concentration in the coal matrix, \bar{C} and the gas at matrix-fracture (cleat) interface, *C(p)*.

\bar{C} is calculated using the basic material balance. *C(p)* is calculated from the Langmuir adsorption isotherm equation.

Once gas arrives in the fractures (cleats), the mass transport of gas is described using the Darcy's Law²². The following equation describes Darcy's Law mathematically:

$$q = -\frac{kA}{\mu} \frac{dP}{dL} \dots\dots\dots 3.15$$

CHAPTER IV

THEORY AND BACKGROUND OF SIMULATION STUDY

4.1 Well Spacing Effects (Interference Effects)

We have known that well interference has a negative effect on gas production for conventional gas reservoir. Usually, wells are drilled at sufficient spacing to minimize the effect of well interference. The typical gas production rate and water production rate for conventional gas reservoir are shown in the **Fig. 4.1** and **Fig. 4.2**. The figures show the negative effect of well interference on conventional gas reservoir.

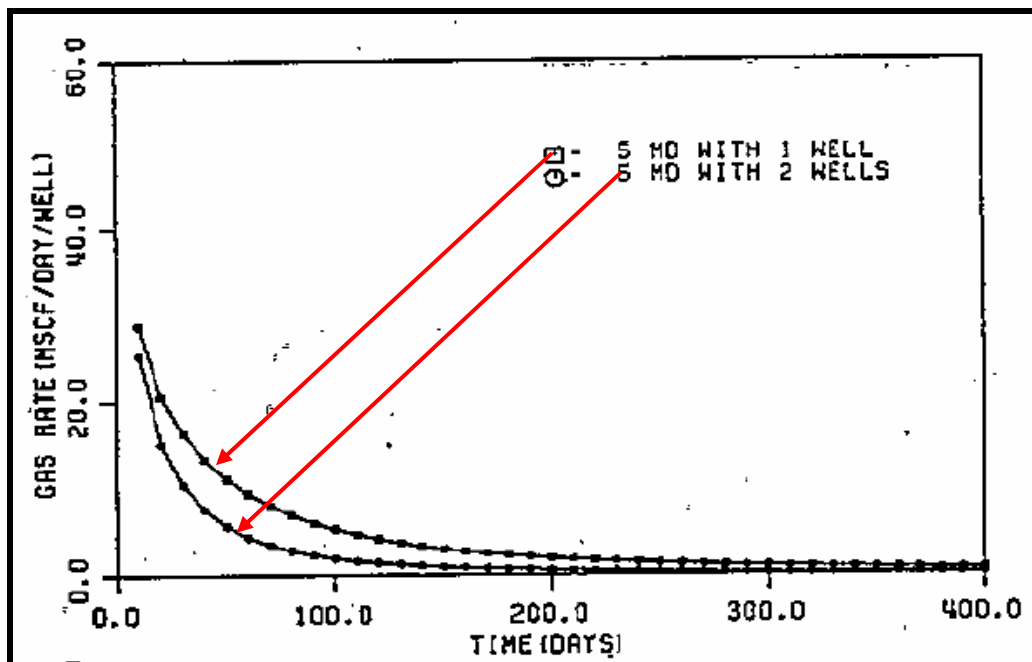


Fig. 4.1—Comparison for gas rates of reservoir with one-well system and reservoir with two-wells system for conventional gas reservoir (after Remner *et. al*⁸). The reservoir has exactly similar dimensions and properties. Additional well decreases the gas production rates for the whole production life.

It can be seen clearly from **Fig. 4.1** that gas production rate from an individual well in one well system is higher than in two wells system. Additional well tends to decrease the gas production rates for the whole production life. Also, we can see the same profile for water production rate (**Fig. 4.2**).

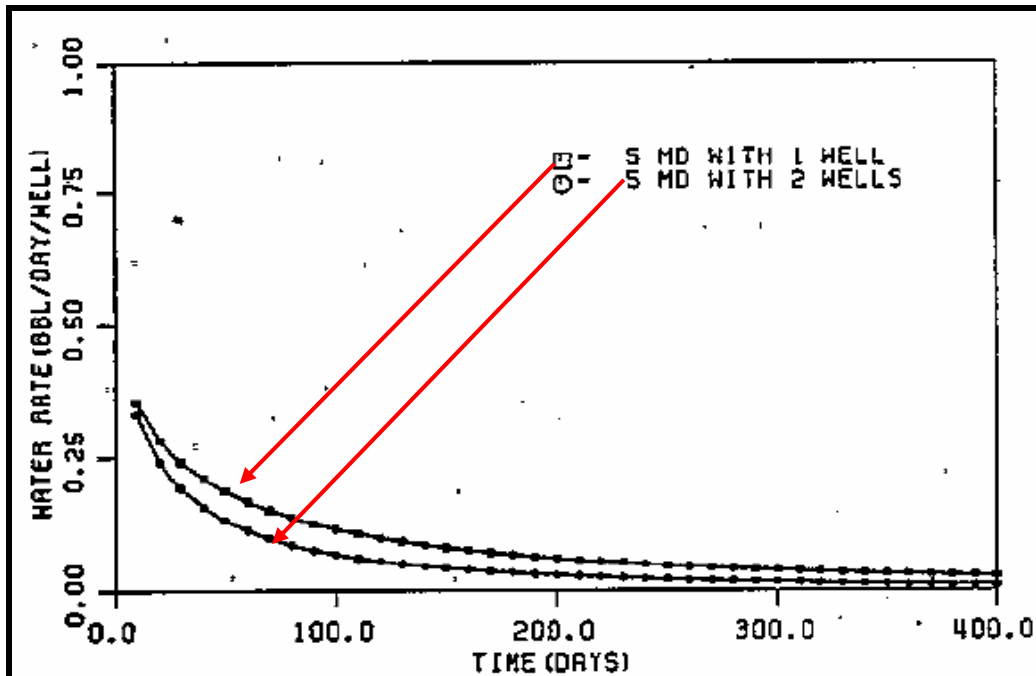


Fig. 4.2—Comparison for water rates of reservoir with one-well system and reservoir with two-wells system for conventional gas reservoir (after Remner *et. al*⁸). The reservoir has exactly similar dimensions and properties. Additional well decreases the water production rates for the whole production life.

However, it has different effect on coal bed methane production. Based on the theory, the effect of interference for adjacent wells is acceleration of de-watering which should lead to earlier and higher gas rate peaks. Water is one of the primary concerns. If we don't drill enough wells, we may not be able to dewater the reservoir sufficiently to get economic gas rates, or it may take very long time to recover the gas.

According to the Langmuir isotherm theory, the gas desorbs from coal surface if reservoir pressure reaches the desorption pressure. We need to lower the pressure in order to let the methane desorb from the coal surface. It has an implication to the well interference to lower the pressure immediately. The more wells deplete the reservoir the faster reservoir pressure reaches the desorption pressure. **Fig. 4.3** and **Fig. 4.4** show us the comparison between pressure profile of one well system and multi well system.

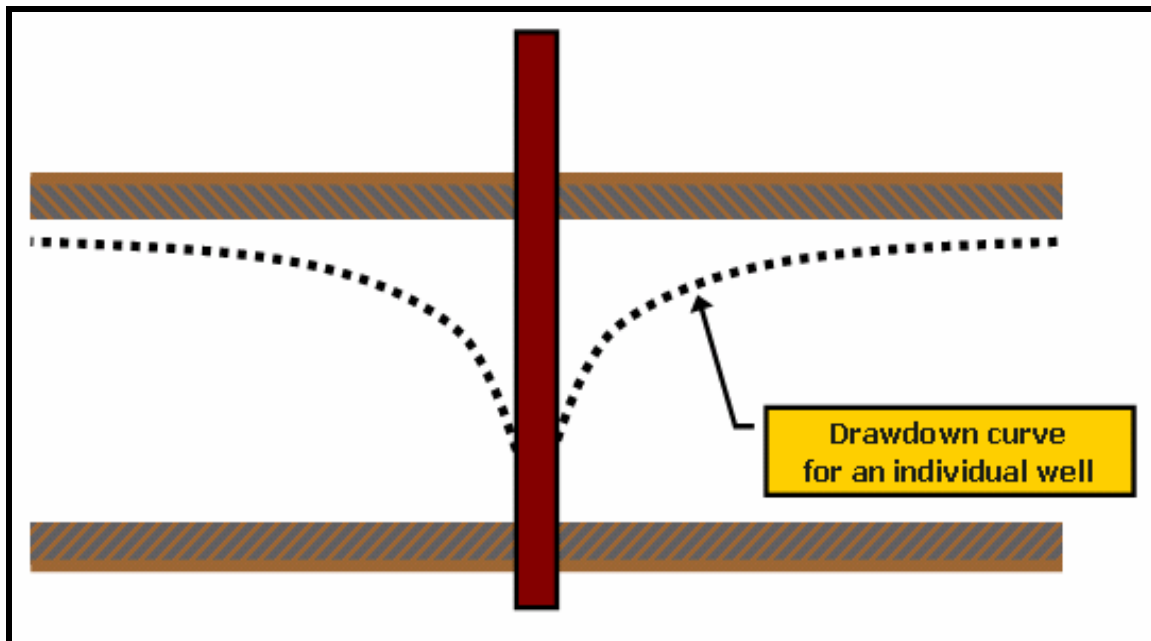


Fig. 4.3–Pressure drawdown profile of a single well system.

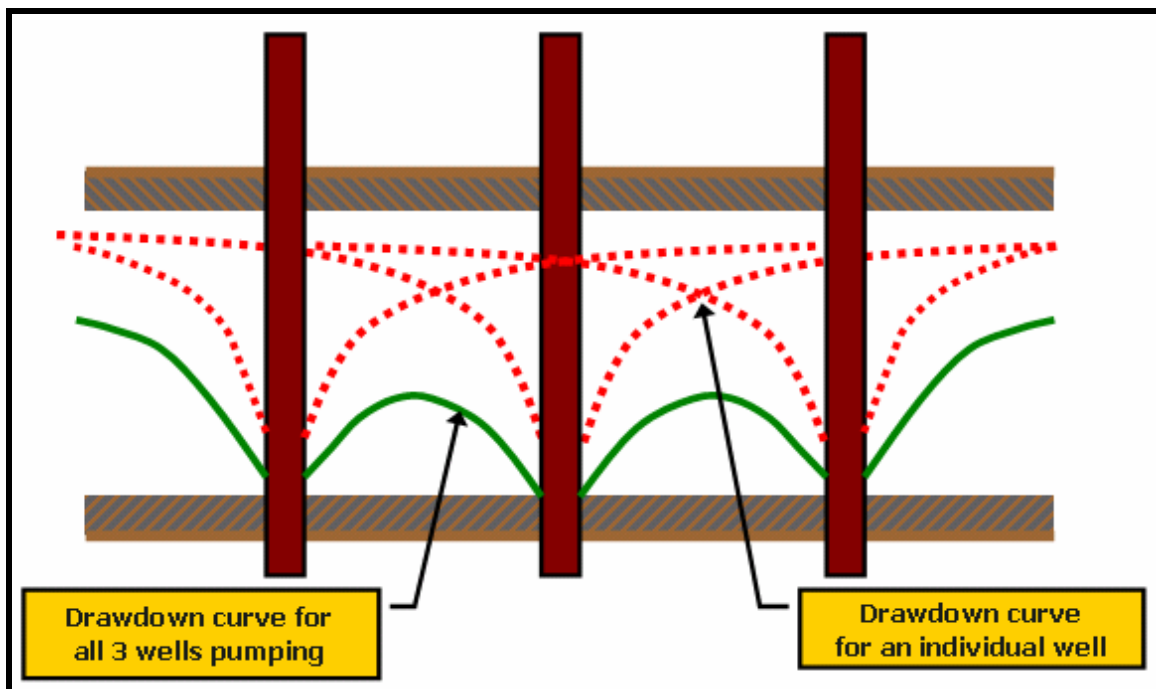


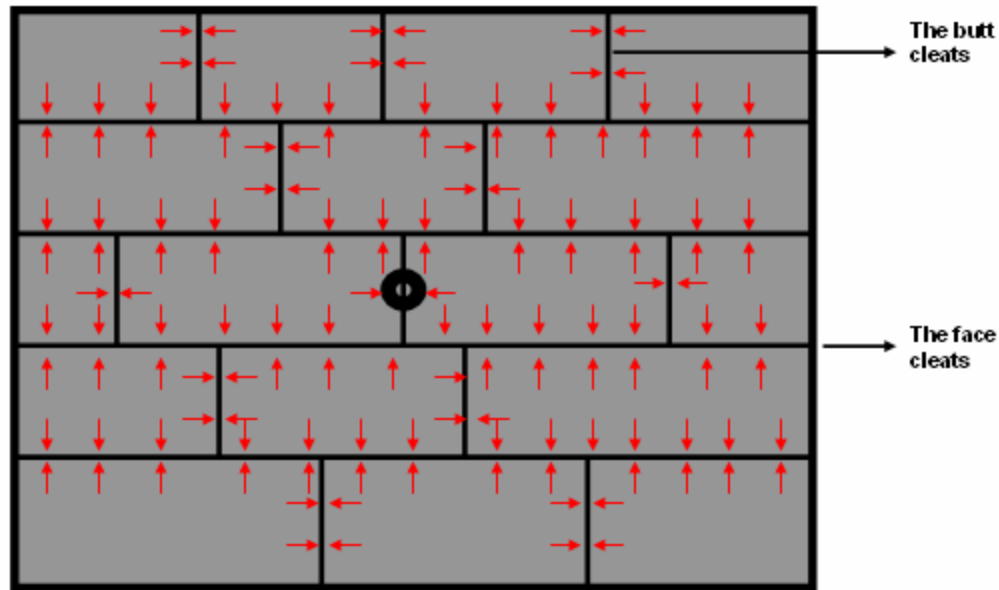
Fig. 4.4–Pressure drawdown profile of a multi wells system. With additional wells, the pressure drawdown for each well will be much lower and it tends to accelerate the dewatering stage.

Fig. 4.3 and **Fig. 4.4** above show that multi-well system may deplete the coalbed methane reservoir effectively. Multi-well system accelerates the dewatering stage, therefore accelerates recovery of the gas. Using the simulator, we can evaluate and investigate the impacts of this theory on coal bed methane production.

Also, during the dewatering phase, the relative permeability to gas increases as water is being produced from the reservoir. Therefore gas rates increase during initial stage of production. This may result in a negative decline effect in the gas production rate. The closer the spacing is, the sooner we can dewater the coalbed methane reservoir.

4.2 Effects of Permeability Anisotropy

Coal bed methane reservoir is considered as naturally fractured reservoir. Coal beds are characterized as a dual porosity reservoir, fractures (cleats) and matrix. The fractures (cleats) system is consisted of two major fractures system, the face cleats and butt cleats. The face cleats are long and continuous fractures throughout the coal seams and butt cleats are short and discontinuous fractures perpendicular to the face cleat. The butt cleats are discontinuous because they are usually intersected by the face cleats. The face cleats has larger contact area with the matrix compare to the butt cleats, therefore it is capable to drain larger area of coal seams and assumed as the maximum permeability direction. In some cases, this assumption may not be applicable (e.g. Bowen basin, Australia)⁵.



Flow in Anisotropic-Square Reservoir System

Fig. 4.5–Schematic of diffusion of gas into the fracture (cleats) system. Most of gas will diffuse into the face cleats, since the face cleats has larger contact area with the matrix compare to the butt cleat.

The existence of face cleats and butt cleats creates permeability anisotropy in coalbed methane reservoir. This permeability anisotropy tends to force most of the gas to diffuse into the face cleats, since the face cleats has larger contact area with the coal matrix compare to the butt cleats. Therefore, most of desorbed gas diffuses from the coal matrix into the face cleats. **Fig. 4.5** shows the schematic of diffusion of gas into the fractures in the permeability anisotropic reservoir.

In facts, the permeability anisotropy has impacts on the coal bed methane production. One of the well known impacts is well pattern. To optimally produce the gas from coalbed methane reservoir, we have to investigate the effect of well pattern on coalbed methane production.

4.3 Transformation of Anisotropic Reservoirs into Equivalent Isotropic Reservoirs

An anisotropic square system can be transform into an equivalent isotropic rectangle system. This equivalent isotropic rectangle system can be calculated using a mathematical transformation. Villagran²⁴ developed a method for the transformation of anisotropic reservoir into isotropic reservoir. They primarily developed this method to investigate the effect of permeability anisotropy on tight gas wells. However, this time

we will use this transformation to determine an equivalent isotropic reservoir dimensions for a given anisotropic reservoir. The following equations are used to calculate the transformation of an anisotropic square system to an equivalent isotropic rectangular system. Absolute permeability is calculated as follows:

$$\bar{k} = \sqrt{k_x k_y} \dots\dots\dots 4.1$$

The dimensions in the x and y directions could be transformed to x-new and y-new dimensions using Equation 4.2 and Equation 4.3:

$$X_{new} = x_e \sqrt{\frac{\bar{k}}{k_x}} = x_e \left(\frac{k_y}{k_x} \right)^{\frac{1}{4}} \dots\dots\dots 4.2$$

$$Y_{new} = y_e \sqrt{\frac{\bar{k}}{k_y}} = y_e \left(\frac{k_x}{k_y} \right)^{\frac{1}{4}} \dots\dots\dots 4.3$$

Now, we are going to show the transformation of anisotropic system to the isotropic system. In this calculation, we use the hypothetical data tabulated in the **Table 4.1**.

TABLE 4.1–DATA FOR AN ANISOTROPIC RESERVOIR SYSTEM		
Drainage Area, A	80	<i>acre</i>
x-dimension, x_e	1866.76	<i>ft</i>
y-dimension, y_e	1866.76	<i>ft</i>
Permeability x-direction, k_x	1.00	<i>md</i>
Permeability y-direction, k_y	0.01	<i>md</i>

For coal bed methane reservoir, permeability is associated to the permeability in the fractures system not the permeability in the matrix system. Therefore in this calculation we concern about the permeability in the fracture system. In the **Table 4.1** the calculation only included the permeability in the fractures system.

The area of the square reservoir is evaluated as follows:

$$A = x_e * y_e = 80acres \dots\dots\dots 4.4$$

where x_e and y_e dimensions are calculated from the above relationship as follows:

$$x_e = y_e = (80 \times 43,560)^{0.5} = 1866.76 \text{ ft} \dots\dots\dots 4.5$$

And the effective permeability for this case is calculated as (this permeability is used as the new permeability for isotropic reservoir system):

$$\bar{k} = [(1md)(0.01md)]^{0.5} = 0.1md \dots\dots\dots 4.6$$

Now, we will evaluate the transformation from anisotropy system to isotropy system. x_{new} is evaluated as follows.

$$\left(\frac{k_y}{k_x}\right)^{\frac{1}{4}} = \left(\frac{0.01md}{1md}\right)^{\frac{1}{4}} = 0.316228 \dots\dots\dots 4.7$$

and

$$x_{new} = x_e \left(\frac{k_y}{k_x}\right)^{\frac{1}{4}} = (1866.76)(0.316228) = 590.322 \text{ ft} \dots\dots\dots 4.8$$

y_{new} dimension is evaluated as follows.

$$\left(\frac{k_x}{k_y}\right)^{\frac{1}{4}} = \left(\frac{1md}{0.01md}\right)^{\frac{1}{4}} = 3.16228 \dots\dots\dots 4.9$$

and

$$y_{new} = y_e \left(\frac{k_x}{k_y}\right)^{\frac{1}{4}} = (1866.76)(3.16228) = 5903.22 \text{ ft} \dots\dots\dots 4.10$$

From the calculations above, we show that a square reservoir with dimensions of 1866.76 ft in the x and y-directions and permeability anisotropy, k_x of 1 md and k_y of 0.01 md, has an equivalent rectangle reservoir of 590.322 ft in x-direction and 5903.22 ft in y-direction with the isotropic effective permeability (\bar{k}) of 0.1 md. **Table 4.2** shows the equivalent isotropic reservoir for the reservoir system mentioned in the **Table 4.1**.

TABLE 4.2–EQUIVALENT ISOTROPIC RESERVOIR SYSTEM FOR RESERVOIR SYSTEM IN TABLE 4.1		
Drainage Area, A	80	<i>Acre</i>
x-dimension, x_e	590.322	<i>ft</i>
y-dimension, y_e	5903.22	<i>ft</i>
Permeability x-direction, k_x	0.1	<i>md</i>
Permeability y-direction, k_y	0.1	<i>md</i>

As conclusions, we show that the presence of permeability anisotropy is caused by the presence the face cleats and butt cleats. This permeability anisotropy restricts the flow of gas along the direction that parallel to the direction of butt cleats. The permeability anisotropy tends to transform an anisotropic square reservoir into a long and skinny equivalent isotropic reservoir. **Fig. 4.6** shows that the equivalent isotropic reservoir is longer in the direction parallel to the lower permeability direction (k_y) and narrower in the direction parallel to the higher permeability direction (k_x). This conclusion explains that the permeability anisotropy has an effect on the placement of wells (well pattern) on coal bed methane reservoir production. An optimal placement of well accelerates and increases recovery, otherwise decelerates and decreases recovery.

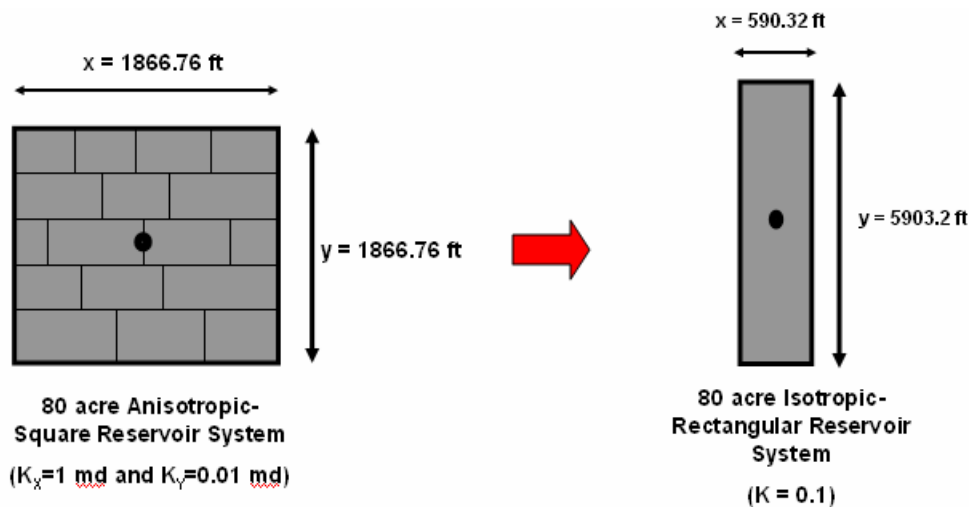


Fig. 4.6–Transformation of an anisotropic square reservoir system into an equivalent isotropic rectangular reservoir system. Equivalent isotropic reservoir is longer to the direction parallel to the lower permeability direction and narrower in the direction parallel to the higher permeability direction.

4.4 Effects of Cleat Compression and Matrix Shrinkage

In the naturally fracture formation such as coalbed methane reservoir, the permeability is critically sensitive to changes in effective stress (pore pressure). During the drawdown, there are two major phenomena related to permeability changes in the reservoir rock:

1. During drawdown of a reservoir by primary production, effective stress increases and permeability decreases due to cleats compression.
2. Drawdown also leads to desorption of methane, and this is accompanied by matrix shrinkage which opens the cleats and leads to permeability increase.

This two phenomena change the permeability into opposite direction, and the competition of this effect will direct permeability into a certain direction. However, at low pressure the competition of matrix shrinkage and cleats compression will increase the absolute permeability of reservoir rock. The following figure (**Fig. 4.7**) shows a typical permeability change as a function of pressure due to matrix shrinkage and cleats compression process.

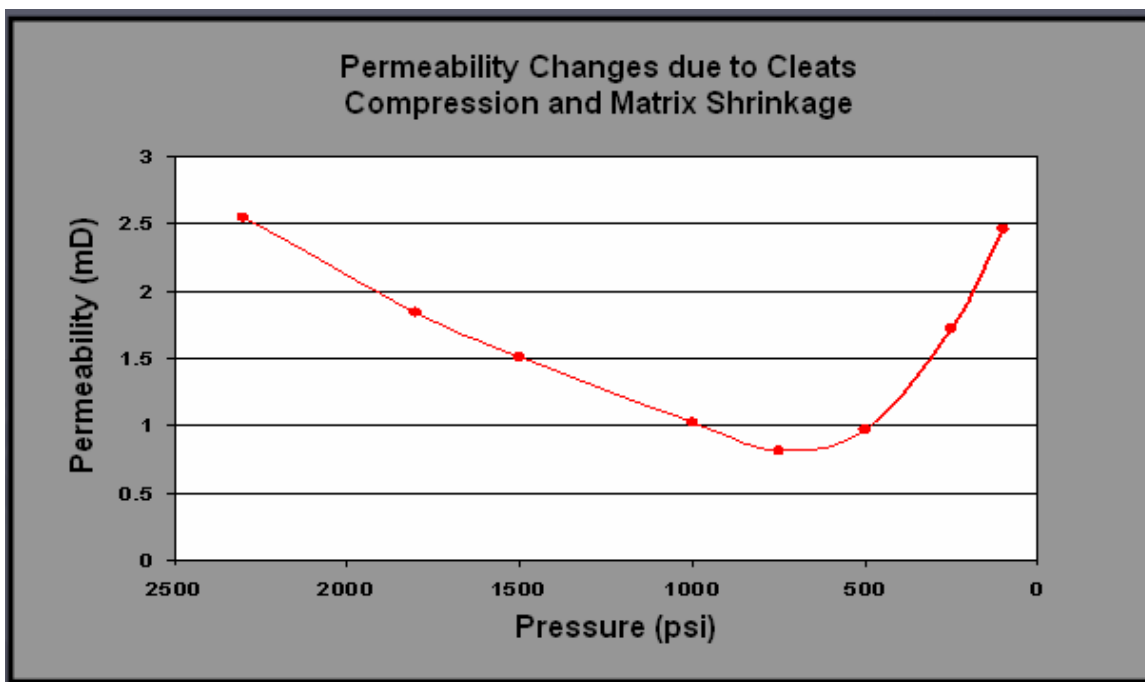


Fig. 4.7—Example of application of Palmer and Mansoori Theory on coalbed methane reservoir. The permeability decreases as the pressure decreases but in a certain pressure (around 600 psi) the permeability increases because of matrix shrinkage effect (Palmer and Mansoori Theory).

Based on Palmer and Mansoori theory, the changes of permeability is caused by the following parameters:

- Poisson's ratio
- Young's modulus, and
- Infinite strain of reservoir rock

As mentioned in **CHAPTER III** the changes on the above parameter, affect the absolute permeability of the reservoir rock. Therefore, the changes on the above parameters will affect the flow performance of gas production and water production that governed by the Darcy's Law.

The following equation describes the Darcy's Law¹⁸:

$$q = -\frac{kA}{\mu} \frac{dP}{dL}$$

The simulation study conducted in this research is intended to study the effects of those parameters on coal bed methane production, how the changes of the Poisson's ratio, Young's modulus, and infinite strain of reservoir rock affect the gas recovery.

CHAPTER V SIMULATION STUDY

5.1 Introduction

Simulation study to investigate the well interference effects, permeability anisotropy, and matrix shrinkage effects has been made. This chapter is emphasized to discuss about the simulation study. This chapter includes the discussion about the reservoir model and simulation data, wells interference simulation procedure, permeability anisotropy simulation procedure, and matrix shrinkage simulation procedure. The simulation studies are conducted using *CMG-GEM 2004.10*.

5.2 Reservoir Model and Simulation Data

5.2.1 Base Case Reservoir Model

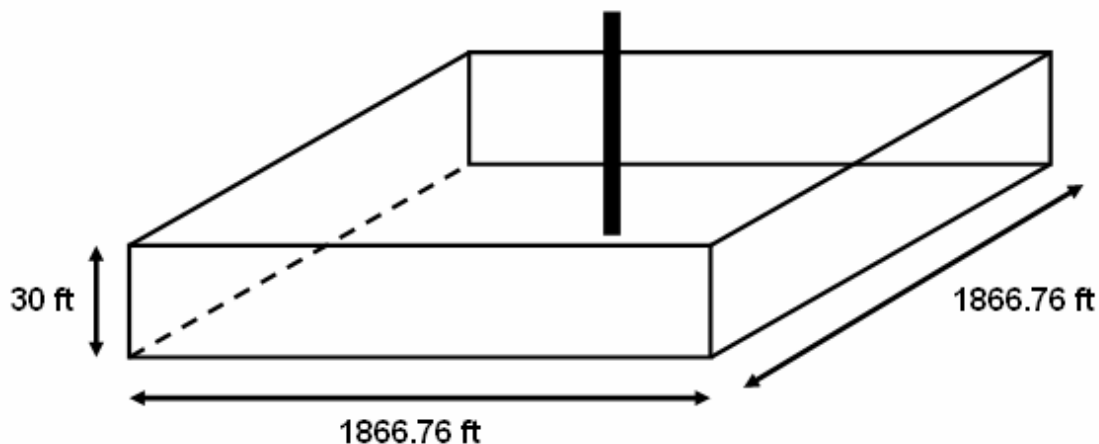


Fig. 5.1–21*21*1 grid model. The reservoir dimension is 1866.76 ft x 1866.76 ft x 30 ft. The reservoir is square isotropic reservoir.

The base case reservoir model used in this simulation study is described by the **Fig. 5.1** above. The reservoir area is 80 acres with 30 ft of thickness. The reservoir contains both fractures system and matrix system (dual porosity system). The fractures system represents the face cleats and butt cleats.

CMG simulator uses Warren and Root model to model the dual porosity reservoir. In this simulation, coal matrix acts the source of gas and fractures acts as the media for gas to flow into the well bore.

5.2.2 Reservoir Data

The following **Table 5.1** is the tabulated input data for simulation study.

TABLE 5.1–BASE CASE RESERVOIR DATA	
Variable	Numerical Value
Well radius, ft	0.1197
Length, ft (x-direction)	1866.76
Length, ft (y-direction)	1866.76
Seam thickness, ft	30
Initial pressure, psi	725.18
Reservoir temperature, F	113
<u>Fracture</u>	
Porosity, %	0.001
Permeability, md	1
Fracture spacing, ft	0.0042
<u>Matrix</u>	
Porosity, %	0.005
Permeability, md	0.00001
Langmuir pressure, psia	725.18
Langmuir volume, gmol/lb of rock	32.3
Difussion time (σ), day	100

As we can see from the **Table 5.1** above, the initial reservoir pressure is same as the Langmuir pressure. It means that the reservoir is a saturated reservoir.

The simulator disables all matrix-to-fracture Darcy flow when coalbed option is activated, since the assumption is that the flow is a diffusive process. This inherently makes the matrix permeability redundant, a small positive value is needed to indicate a

pathway for diffusion to occur between matrix (coal) and fracture (cleat)²². Therefore, In **Table 5.1** we input the permeability of the matrix with very small value.

5.3 Effects of Well Spacing

In this simulation study, we intend to investigate the effect of well spacing on coalbed methane production. As we already knew, interference between wells has negative effects on conventional gas reservoir. However, several authors have been conducted study to investigate those effects on coalbed methane production. They found that interference between wells has beneficial effects on coalbed methane reservoir, unlike conventional gas reservoir.

In this simulation study, we want to investigate what really the beneficial effects of wells interference (well spacing). Does it improve the recovery or only accelerate the gas production? However, acceleration of gas production is a beneficial effect in terms present worth of revenue and cutting down the operating cost. We use CMG (Computer Modeling Group)-GEM 2004.10 to study the interference effects. This study is conducted using the following procedure:

Suppose that we found a new coalbed methane reservoir. The reservoir is big reservoir. We want to develop this new field. We will develop the reservoir using the following scenarios:

- 80 acre spacing, the reservoir model and reservoir data is exactly same as the base case reservoir. Therefore, I called it the base case reservoir.
- 40 acre spacing, the reservoir is square and the well is located exactly in the center of the reservoir. The input data is exactly same as the base case reservoir.
- 20 acre spacing, the reservoir is square and the well is located exactly in the center of the reservoir. The input data is exactly same as the base case reservoir.
- 5 acre spacing, the reservoir is square and the well is located exactly in the center of the reservoir. The input data is exactly same as the base case reservoir.

5.4 Permeability Anisotropy

Coal bed methane reservoir is inherently a naturally fractured reservoir. It is caused by the presence of the face cleats and butt cleats. The presence of face cleats and butt cleats creates permeability anisotropy on coalbed methane reservoir.

Permeability anisotropy, reported by several authors, causes a strong impact on well pattern. It also causes a linear flow in the reservoir. Therefore, this simulation study is intended to investigate the effects of permeability anisotropy on coal bed methane production. We are conducting the simulation studies to investigate the effect of well pattern on coalbed methane production because of the existence of permeability anisotropy.

The simulation study is conducted on an 80 acres reservoir with 30 feet of thickness. The base case reservoir is changed into anisotropic reservoir system. The following explanation will describe in detail the reservoir model used in the simulation studies.

5.4.1. Permeability Anisotropy on 20 Acre Spacing

The reservoir model is exactly same as base case reservoir unless the fracture permeability. The fracture permeability in this simulation is set to be anisotropic. The fracture permeability for x-direction is set to be 1 *md* and the fracture permeability for y-direction is set to be 0.01 *md*. The matrix permeability is set to be as same as the base case reservoir data. Okeke²⁵ investigated that the changes of matrix permeability has no effects on coalbed methane production performance.

In this simulation, we want to investigate what is the effect of well placement in an anisotropic coalbed methane reservoir. Therefore, we set the reservoir as we mentioned above and the following scenarios are simulated using CMG-GEM 2004.10:

- Scenario A

Fig. 5.2 illustrates the schematic of this reservoir model. The reservoir is 80 *acre* area. The reservoir has 4 wells. Each of the well has the same drainage area, 20 *acre*. Each of the well is located in the center of square reservoir area.

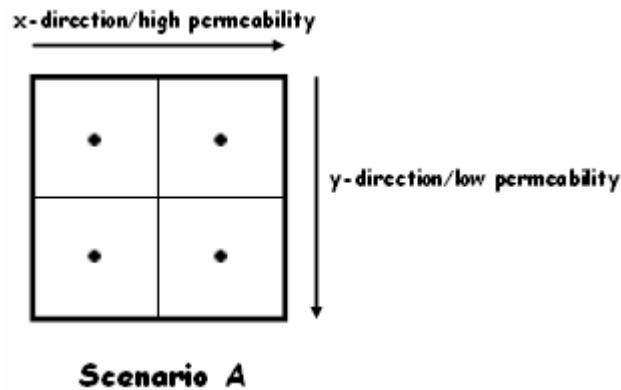


Fig. 5.2–Scenario A for study of well placement effect on coalbed methane with permeability anisotropic for wells with 20 acre drainage area. The reservoir is 80 acre area. The reservoir has four wells. Each of the well is located in the center of square area, 20 acre.

- Scenario B

Fig. 5.3 illustrates the schematic of this reservoir model. The reservoir is 80 *acre* area. The reservoir has 4 wells. Each of the well has the same drainage area, 20 *acre*. Each of the well is located in the center of rectangular reservoir area. Placement of wells is aligned to the direction of lower permeability direction.

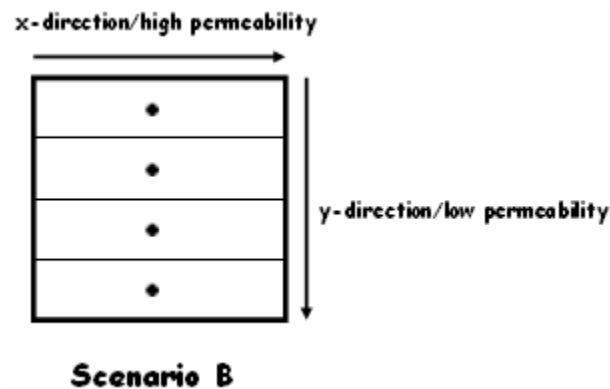


Fig. 5.3–Scenario B for study of well placement effect on coalbed methane with permeability anisotropic for wells with 20 acre drainage area. The reservoir is 80 acre area. The reservoir has four wells. Each of the well is located in the center of rectangular area, 20 acre. Placement of wells is aligned to the direction of lower permeability direction.

- Scenario C

Fig. 5.4 illustrates the schematic of this reservoir model. The reservoir is 80 *acre* area. The reservoir has 4 wells. Each of the well has the same drainage area, 20

acre. Each of the well is located in the center of rectangular reservoir area. Placement of wells is aligned to the direction of higher permeability direction.

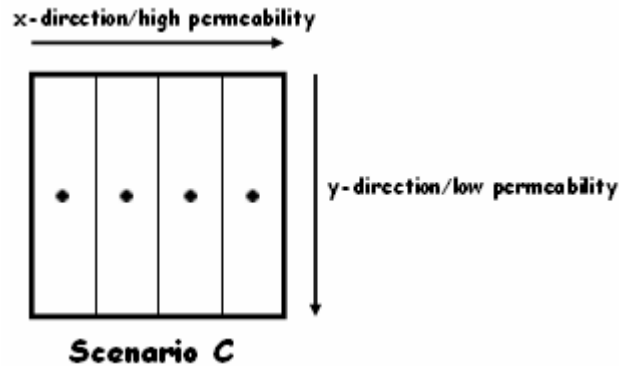


Fig. 5.4–Scenario C for study of well placement effect on coalbed methane with permeability anisotropic for wells with 20 acre drainage area. The reservoir is 80 acre area. The reservoir has four wells. Each of the well is located in the center of rectangular area, 20 acre. Placement of wells is aligned to the direction of higher permeability direction.

5.4.2 Permeability Anisotropy on 5 Acre Spacing

The reservoir model is exactly same as base case reservoir unless the fracture permeability. The fracture permeability in this simulation is set to be anisotropic. The fracture permeability for x-direction is set to be 1 *md* and the fracture permeability for y-direction is set to be 0.01 *md*. The matrix permeability is set to be as same as the base case reservoir data.

In the simulation, we want to investigate what is the effect of well placement in an anisotropic coalbed methane reservoir. Therefore, we set the reservoir as we mentioned above and the following scenarios are simulated using CMG-GEM 2004.10:

- Scenario A

Fig. 5.5 illustrates the schematic of this reservoir model. The reservoir is 80 *acre* area. The reservoir has 16 wells. Each of the well has the same drainage area, 5 *acre* spacing. Each of the well is located in the center of square reservoir area.

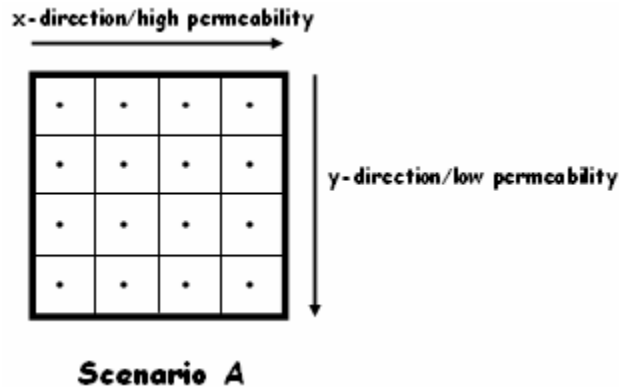


Fig. 5.5–Scenario A for study of well placement effect on coalbed methane with permeability anisotropic for wells with 5 acre drainage area. The reservoir is 80 acre area. The reservoir has sixteen wells. Each of the well is located in the center of square area, 5 acre.

- Scenario B

Fig. 5.6 illustrates the schematic of this reservoir model. The reservoir is 80 acre area. The reservoir has 16 wells. Each of the well has the same drainage area, 5 acre. Each of the well is located in the center of rectangular reservoir area. Placement of wells is aligned to the direction of lower permeability direction.

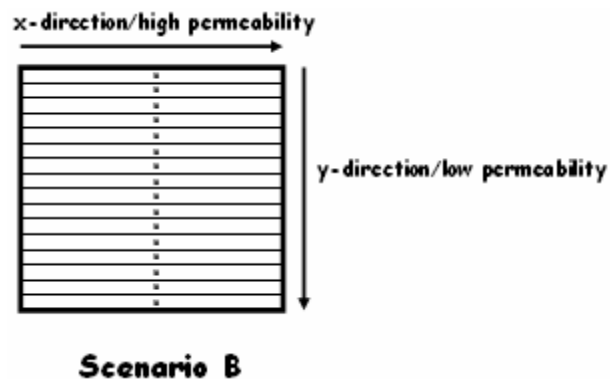


Fig. 5.6–Scenario B for study of well placement effect on coalbed methane with permeability anisotropic for wells with 5 acre drainage area. The reservoir is 80 acre area. The reservoir has sixteen wells. Each of the well is located in the center of rectangular area, 5 acre. Placement of wells is aligned to the direction of lower permeability direction.

- Scenario C

Fig. 5.7 illustrates the schematic of this reservoir model. The reservoir is 80 acre area. The reservoir has sixteen wells. Each of the well has the same drainage area, 5 acre. Each of the well is located in the center of rectangular reservoir area. Placement of wells is aligned to the direction of higher permeability direction.

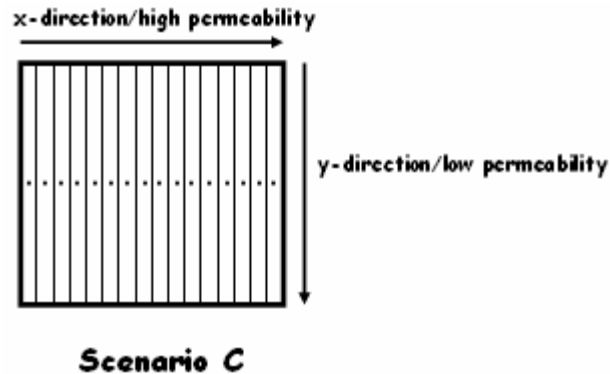


Fig. 5.7–Scenario C for study of well placement effect on coalbed methane with permeability anisotropic for wells with 5 acre drainage area. The reservoir is 80 acre area. The reservoir has sixteen wells. Each of the well is located in the center of rectangular area, 5 acre. Placement of wells is aligned to the direction of higher permeability direction.

5.5 Transformation of an Anisotropic System to an Isotropic System

These simulations are conducted to apply and study the transformation of an anisotropic system into an isotropic system. The reservoir system is an 80 acres area with 30 feet of thickness. The reservoir is depleted by only one well. All the reservoir properties data used in the following simulations are the same data used in the previous simulations. All the transformation that we did in the following simulations is the same transformation like we discuss previously in Chapter IV. The simulations are divided into the following category.

5.5.1 Permeability Anisotropy 10:1

In this time we want to compare the production performance between the following simulation scenarios. Both of the following scenarios are determined from the Transformation method that mentioned in Chapter IV. The simulations are based on the permeability anisotropy 10:1, permeability in x-direction is 1 *md* and permeability in y-direction is 0.1 *md*.

Anisotropic square system

The reservoir model and reservoir data is as same as base case reservoir unless the properties shown in the following **Table 5.2**:

TABLE 5.2–ANISOTROPIC RESERVOIR SYSTEM ($k_x : k_y = 1 : 0.1$)	
Variable	Numerical Value
Number of wells	1
Length, ft (x-direction)	1866.76
Length, ft (y-direction)	1866.76
Area, (acres)	80
<u>Fracture Permeability</u>	
x-direction	1
y-direction	0.1
<u>Matrix Permeability</u>	
x-direction	0.0001
y-direction	0.0001

The following figure, **Fig. 5.8**, shows the schematic anisotropic reservoir grid system for permeability 10:1.

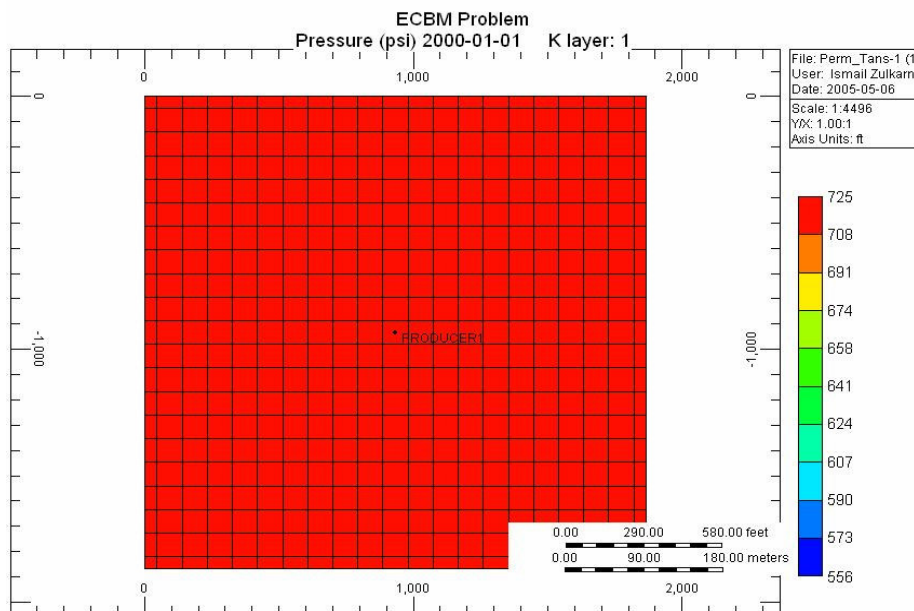


Fig. 5.8–Reservoir system with anisotropic 10:1 for transformation from anisotropic reservoir system to isotropic reservoir system. Reservoir is square 80 acre and anisotropic. Fracture Permeability for x-direction is 1 md and fracture permeability for y-direction is 0.1 md. Well is located in the center of reservoir.

Isotropic rectangular system

The reservoir has the same input data as base case reservoir unless the properties shown in the following **Table 5.3**:

TABLE 5.3–ISOTROPIC RESERVOIR SYSTEM ($k_x : k_y = 1 : 0.1$)	
Variable	Numerical Value
Number of wells	1
Length, ft (x-direction)	1049.757362
Length, ft (y-direction)	3319.624254
Area, (acres)	80
<u>Fracture Permeability</u>	
x-direction	0.316227766
y-direction	0.316227766
<u>Matrix Permeability</u>	
x-direction	0.0001
y-direction	0.0001

And the following figure, **Fig. 5.9**, shows the schematic reservoir grid system.

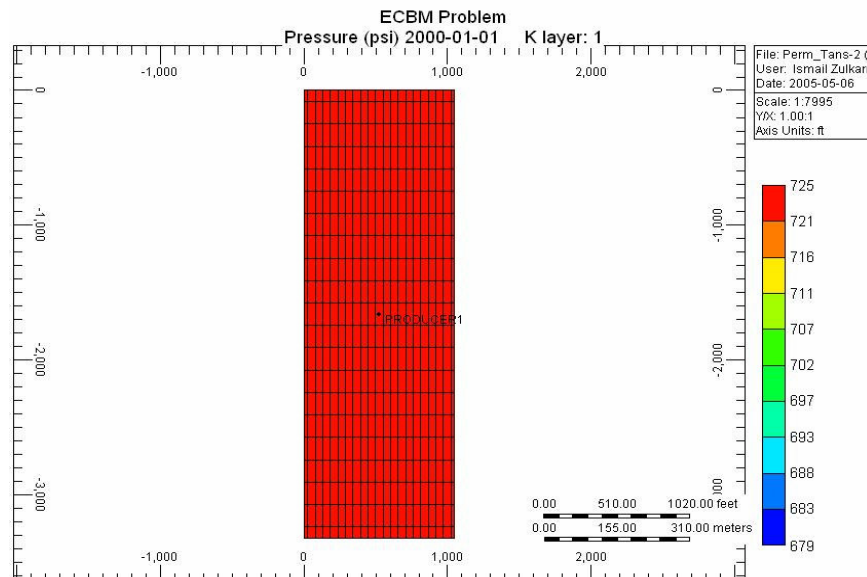


Fig. 5.9–Isotropic reservoir system of transformation from anisotropic reservoir system to isotropic reservoir system for permeability anisotropy 10:1. Reservoir is rectangular 80 acre and isotropic. Fracture Permeability for x-direction and y-direction is same, 0.31623 md. Well is located in the center of rectangular reservoir.

5.5.2 Permeability Anisotropy 100:1

In this time we want to compare the production performance between the following simulation scenarios. Both of the following scenarios are determined from the Transformation method that mentioned in Chapter IV. The simulations are based on the permeability anisotropy 100:1, permeability in x-direction is 1 *md* and permeability in y-direction is 0.01 *md*.

Anisotropic square system

The reservoir model and reservoir data is as same as base case reservoir unless the properties shown in the following **Table 5.4**:

TABLE 5.4–ANISOTROPIC RESERVOIR SYSTEM ($k_x : k_y = 1 : 0.01$)	
Variable	Numerical Value
Number of wells	1
Length, ft (x-direction)	1866.76
Length, ft (y-direction)	1866.76
Area, (acres)	80
<u>Fracture Permeability</u>	
x-direction	1
y-direction	0.01
<u>Matrix Permeability</u>	
x-direction	0.0001
y-direction	0.0001

Fig. 5.10 shows the schematic anisotropic reservoir grid system for permeability 100:1.

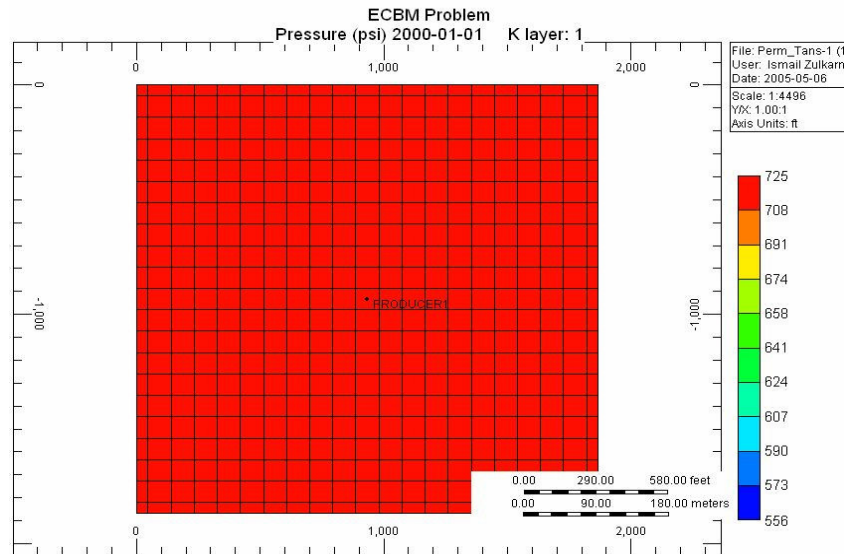


Fig. 5.10– Reservoir system with anisotropic 100:1 for transformation from anisotropic reservoir system to isotropic reservoir system. Reservoir is square 80 acre and anisotropic. Fracture Permeability for x-direction is 1 *md* and fracture permeability for y-direction is 0.01 *md*. Well is located in the center of reservoir.

Isotropic rectangular system

The reservoir has the same input data as base case reservoir unless the properties shown in the following **Table 5.5**:

TABLE 5.5–ISOTROPIC RESERVOIR SYSTEM ($k_x : k_y = 1 : 0.01$)	
Variable	Numerical Value
Number of wells	1
Length, ft (x-direction)	590.3219461
Length, ft (y-direction)	5903.219461
Area, (acres)	80
<u>Fracture Permeability</u>	
x-direction	0.1
y-direction	0.1
<u>Matrix Permeability</u>	
x-direction	0.0001
y-direction	0.0001

And the following figure (**Fig. 5.11**) shows the schematic reservoir grid system.

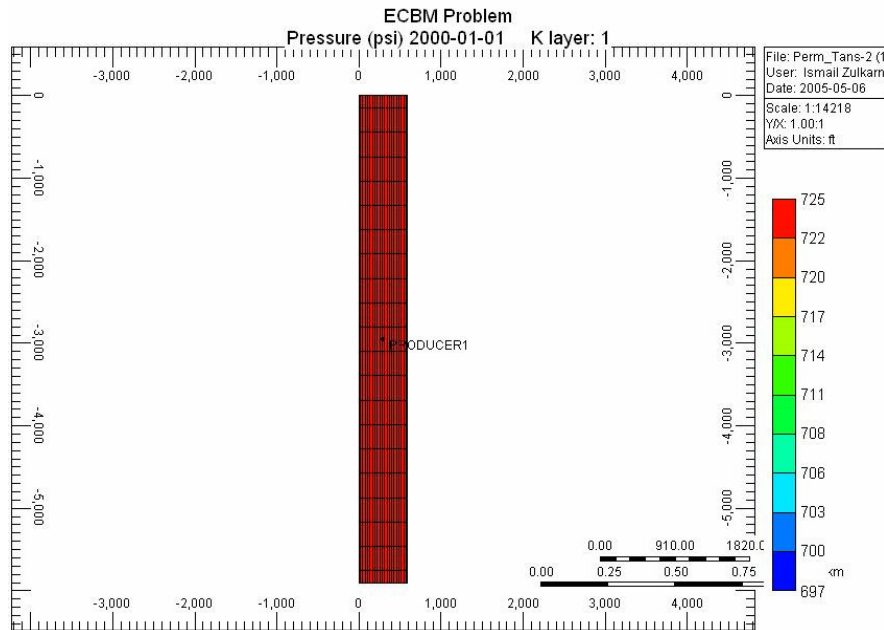


Fig. 5.11–Isotropic reservoir system of transformation from anisotropic reservoir system to isotropic reservoir system for permeability anisotropy 100:1. Reservoir is rectangular 80 acre and isotropic. Fracture Permeability for x-direction and y-direction is same, 0.131623 md. Well is located in the center of rectangular reservoir.

5.6 Cleat Compression and Matrix Shrinkage Simulation Procedure

This part of research is intended to investigate the effects of matrix shrinkage and cleats compression on coal bed methane production. We all knew that Palmer and Mansoori^{7,26} developed a model to calculate the permeability changes as a function of pressure. In this theory, it is shown that there is a permeability rebound at lower pressure. It has an implication that this phenomenon could increase methane production at lower pressure.

To investigate the effect of matrix shrinkage and cleats compression on gas recovery, we conduct the sensitivity analysis of the following parameters.

A. Effects of Young's Modulus

To investigate the effects of Young's modulus on the production performance of coal bed methane we conduct sensitivity analysis. We are varying the Young's modulus: 500,000 *psia*, 750,000 *psia*, 1,000,000 *psia*, 1,500,000 *psia*, 2,000,000 *psia*, 3,000,000 *psia*, 4,000,000 *psia*, and 5,000,000 *psia*.

B. Effects of Poisson's ratio

To investigate the effects of Poisson's ratio on the production performance of coal bed methane we conduct sensitivity analysis. We are varying the Poisson's ratio: 0.1, 0.2, 0.3, 0.4, and 0.5.

C. Effects of Infinite Strain

To investigate the effects of infinite strain on the production performance of coal bed methane we conduct sensitivity analysis. We are varying the infinite strain: 0.0025, 0.0050, 0.0075, 0.01, 0.0125, 0.0150, 0.0175, and 0.02.

We expect that the sensitivity analysis may help us to understand how the matrix shrinkage and cleats compression affect the performance of gas production rate, water production rate, and the total recovery of coal bed methane reservoir.

Appendix C. explains how to set up the input data for Palmer and Mansoori model.

CHAPTER VI DISCUSSIONS

6.1 Introduction

This chapter discusses several aspects and results from this research. Only the remarkable results will be presented here, the complete simulation results are included in the Appendix D. Discussions of well-spacing effects (interference effects), permeability anisotropy effects, transformation of anisotropic system to isotropic system, and cleats compression and matrix shrinkage effects are presented in this chapter.

6.2 Discussions

6.2.1 Well Spacing Effects (Interference Effects)

We have been used CMG-GEM simulator to investigate the effect of wells interference. This simulator was employed to predict the gas production rate, water production rate and pressure performance during 10 years production. The simulation study at first was conducted for single well system and 2 wells system in as discussed earlier in Chapter IV.

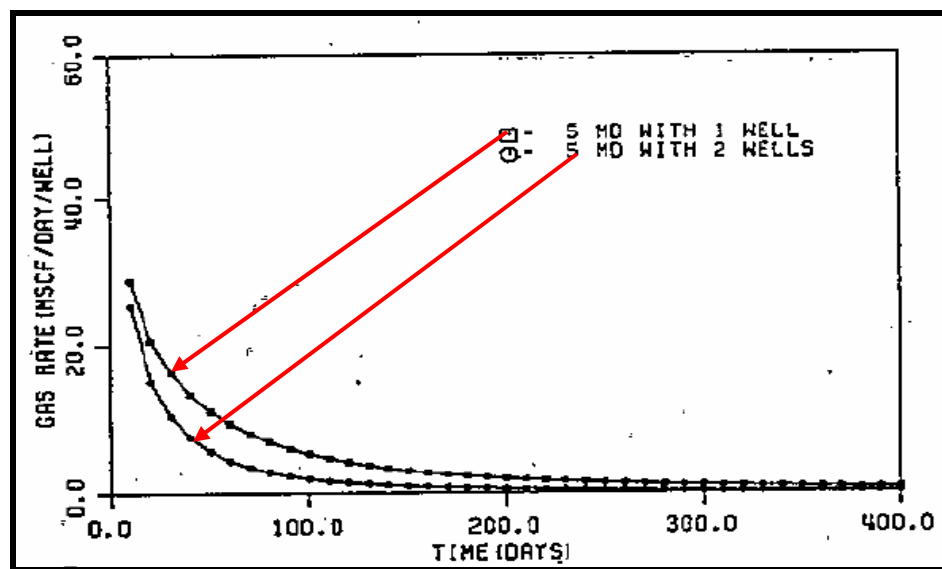


Fig. 6.1—Effect of well spacing (interference effect) on gas production rate, conventional gas reservoir (After Remner⁸).

The effects of well interference on conventional gas reservoir are presented in **Fig. 6.1** and **Fig. 6.2**. **Fig. 6.1** presents the gas production rate for reservoir with single well system and reservoir with 2-wells system. Both of reservoirs have the same drainage area. As we can see from the **Fig. 6.1**, gas production rate from an individual well in 2-well system is less than that of single well system. It has been known as negative interference effects on conventional gas reservoir. However, the total gas production rate from 2-well system is greater than that of single well system. **Fig. 6.2** shows the water production rate for conventional gas reservoir. As we can see from **Fig. 6.2**, it shows a similar performance with gas rate.

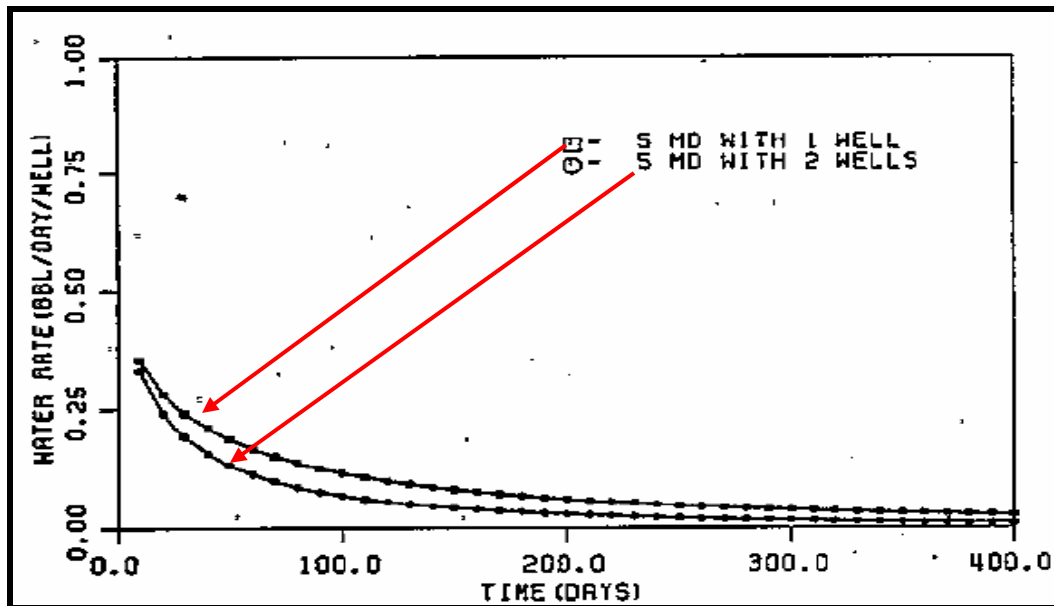


Fig. 6.2—Effect of well spacing (interference effect) on water production rate, conventional gas reservoir (After Remner⁸).

The effect of well interference on coal bed methane reservoir is somewhat different from that of conventional gas reservoir. As we can see from the simulation results (**Fig. 6.3**), the effect of additional well creates a positive effect on gas production rate. Gas production rate for an individual well from 40 *acre* spacing system is higher than that of 80 *acre* system in the early stage of production. Decreasing well spacing (interference effect) tends to accelerate the production of gas from the reservoir. Closer spacing (interference effect) accelerates the depressuring of the reservoir. It can be explained in such a way that the additional pressure reduction caused by the second well

increases the desorption rate, thus providing the system with more gas. In other words, the contacts between pressure transient between wells in a drainage system will accelerate the pressure drawdown and consequently will increase the desorption of gas. **Fig. 6.3** clearly shows us the reversal effects of interference on coal bed methane.

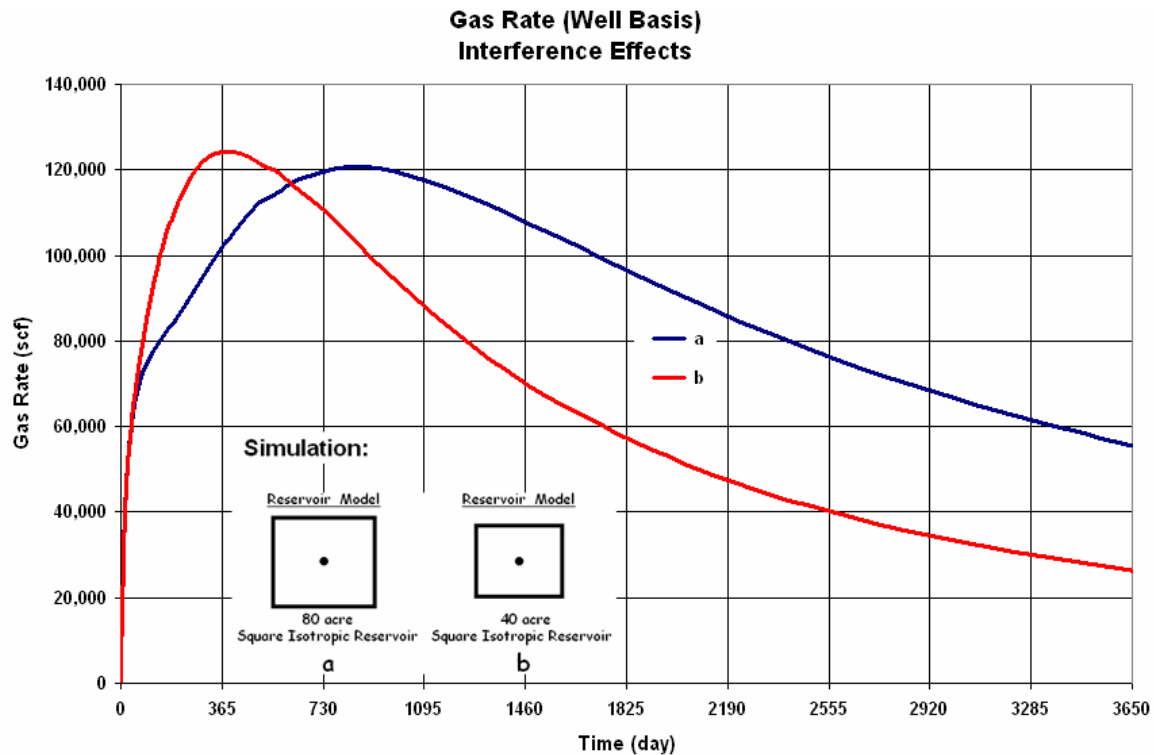


Fig. 6.3—Comparison of gas rates for an 80 acre well and an 40 acre well in an isotropic reservoir (Base Case). Each well is centered in a square drainage area. The improved early gas rate for the 40 acres well is caused by dewatering effects.

During the early stage of production, the relative permeability to gas increases as water is being produced from the reservoir. Therefore, gas rate increase during the initial stage of production. Instead of continuously increase, gas production at a certain time starts to decline. At this point of time, gas production rate will behave similarly with conventional negative interference. Gas production start to declines when the rate of desorption in the matrix system is less than the production rate in the fracture to the wellbore. The rate of desorption starts to decline at a certain time because the supply of gas from the matrix system already declined.

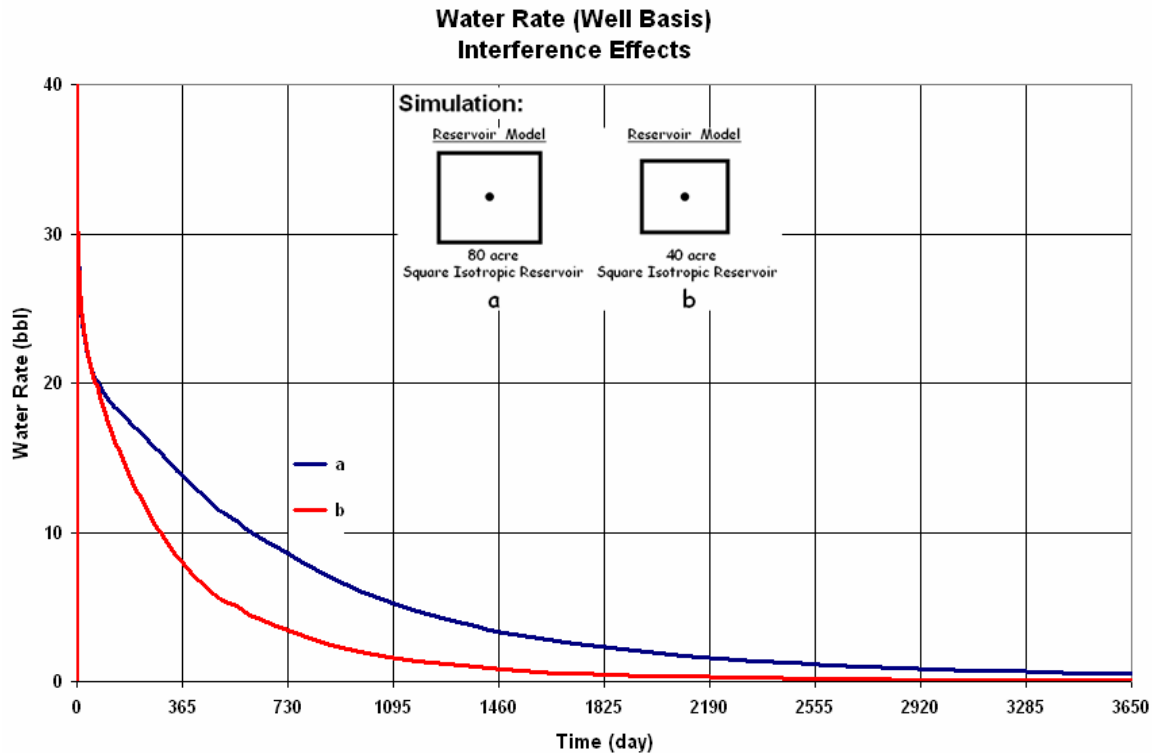


Fig. 6.4—Comparison of water rates for an 80 acre well and an 40 acre well in an isotropic reservoir (Base Case). Each well is centered in a square drainage area. The early water rate for the 40 acres well tends to be greater than half the 80 acres well, causing earlier dewatering and higher gas rates.

Although interference creates a beneficial effect to gas production rate, water rate behaves somewhat similar with conventional interference (see **Fig. 6.4**). Closer well spacing tends to accelerate the water production. As we can see from **Fig. 6.4**, the early water production rate for 40 *acre* spacing tends to be greater than half the 80 *acre* spacing. It is believed that the desorbing gas associated with the coal seam acts as a shield, thus diminishing the interference effect caused by the additional well.

As discussed above, the interference occurs when the pressure transients of different wells meet. It means that well spacing is a critical parameter in the methane drainage process. The more interference is created between wells, the sooner the dewatering and the higher the gas rate.

The investigation of interference effect is extended to 80 *acre* spacing, 40 *acre* spacing, 20 *acre* spacing, and 5 *acre* spacing. We conducted and compared the simulations for 80 *acre* spacing, 40 *acre* spacing, 20 *acre* spacing, and 5 *acre* spacing.

The following figure shows the simulation results.

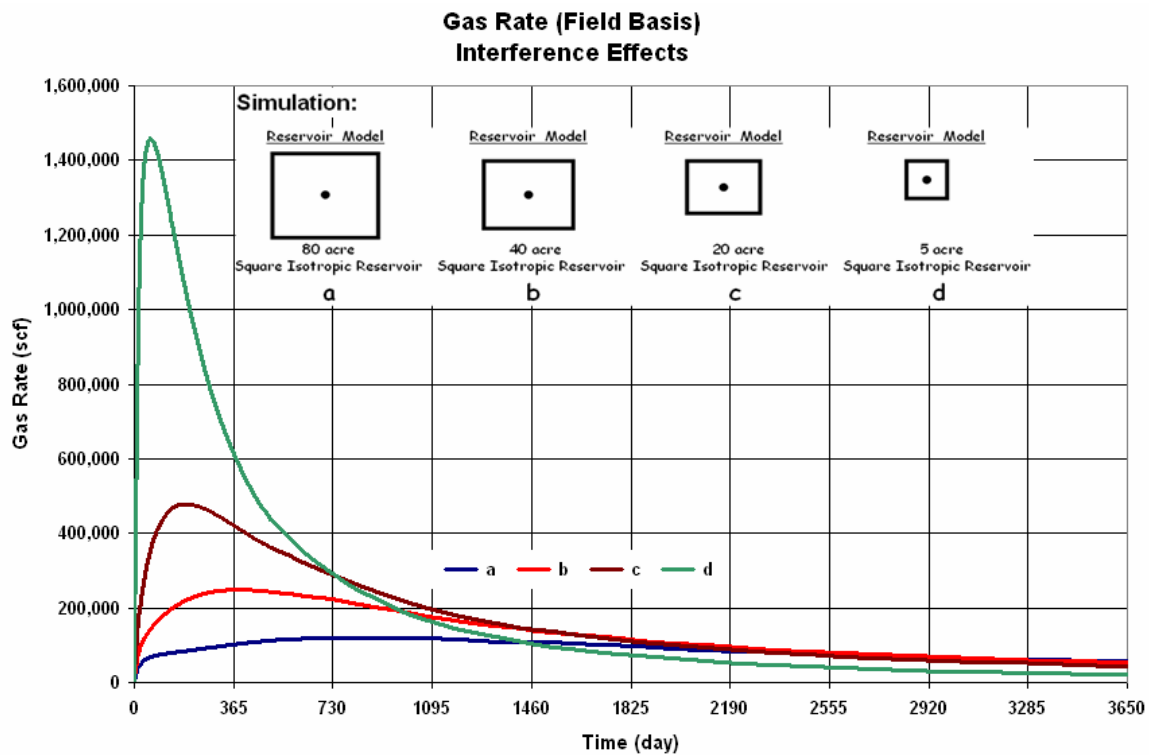


Fig. 6.5—Comparison of total gas rates for various well spacings in an 80 acre reservoir. Each well is centered in its square drainage area. More wells (closer spacing) give higher early rates but then their rates become lower after a 2 to 4 years.

The results presented here are the total production rate for a reservoir system. In the **Fig. 6.5** above, we see that the 5 acre spacing system peaks the highest and the earliest and the 80 acre spacing peaks the lowest and the latest. Also, we present the results for water rate (**Fig. 6.6**), recovery of gas (**Fig. 6.7**), and recovery of water (**Fig. 6.8**).

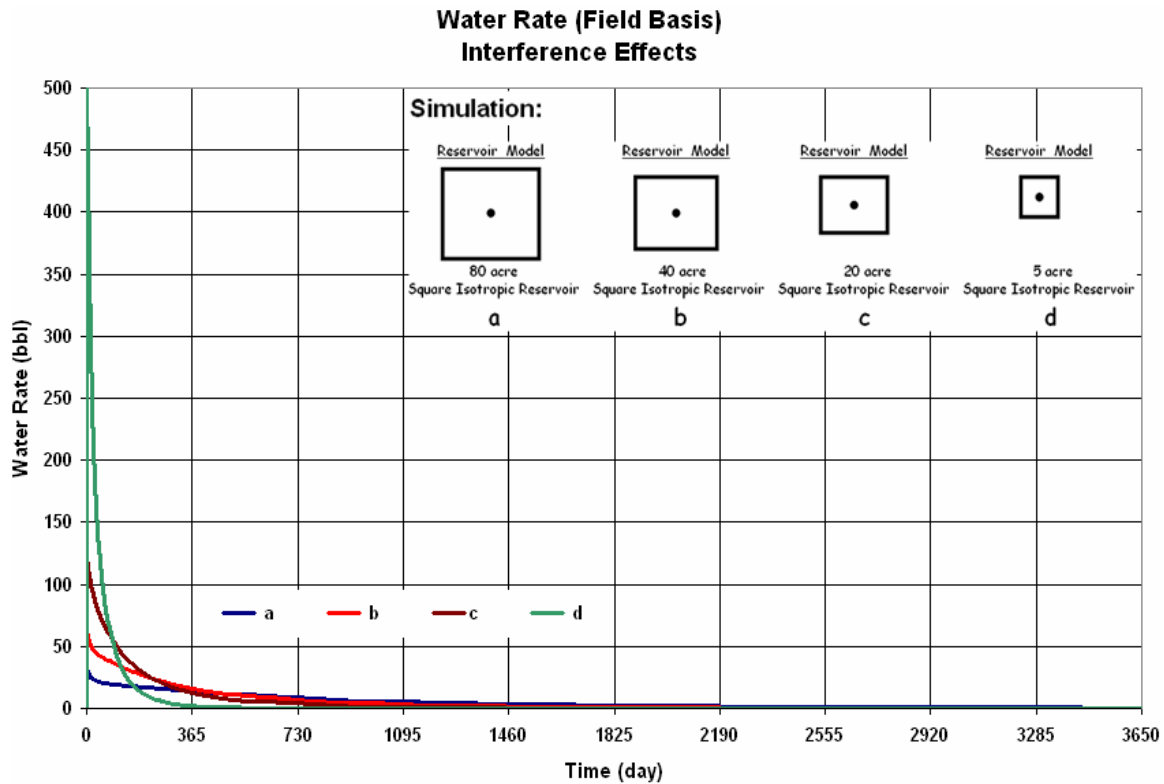


Fig. 6.6—Comparison of total water rates for various well spacings in an 80 acre reservoir. Each well is centered in its square drainage area. More wells (closer spacing) give higher early rates but then their rates become lower after a half to 2 years.

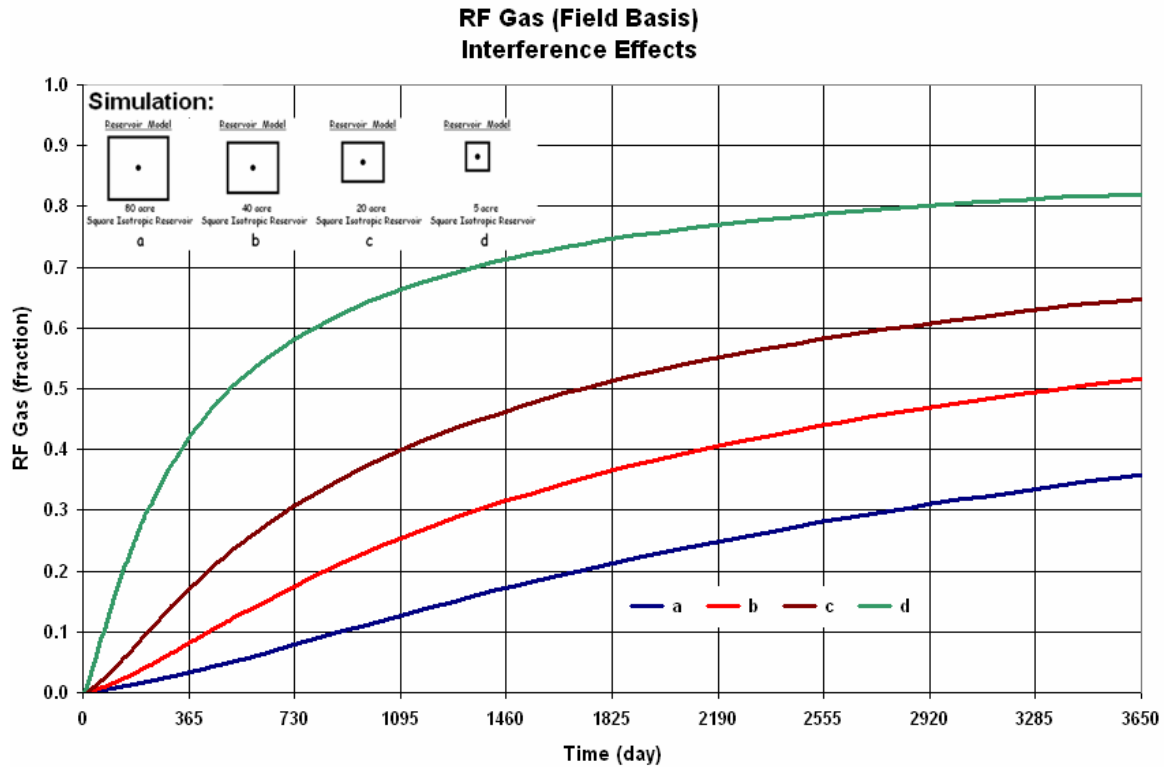


Fig. 6.7—Comparison of recovery factor of gas production for various well spacings in an 80 acre reservoir. Each well is centered in its square drainage area. More wells (closer spacing) accelerates gas production. Closer spacing also produces higher cumulative recovery factor in the ten years simulation.

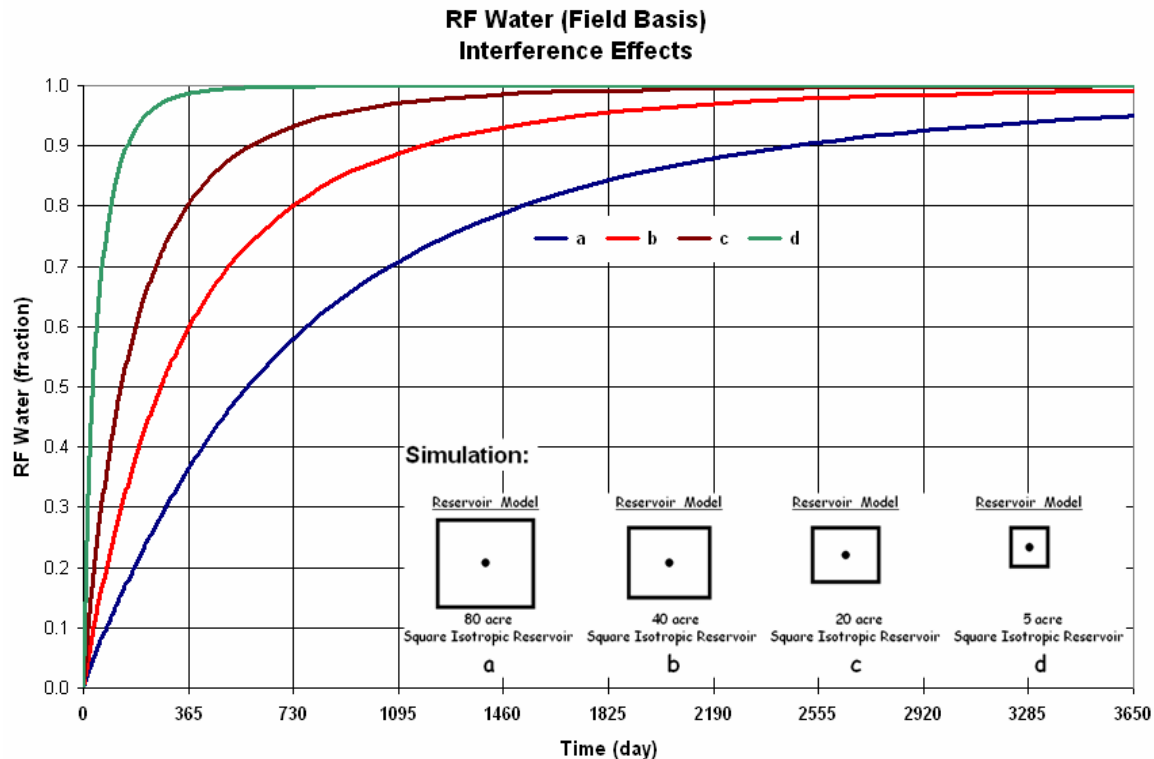


Fig. 6.8—Comparison of recovery factor of water production for various well spacings in an 80 acre reservoir. Each well is centered in its square drainage area. More wells (closer spacing) accelerates water production but eventually three of various well-spacings produce the same recovery factor in the tenth years simulation.

We can say that the highest and the earliest peak resulted from 5 acre spacing system is caused by the highest number of interference between wells. The more wells, the more interference is created. We can see from **Fig. 6.8** that, 5 acre spacing system produces most of water in early year of production. It produces more than 95 percent of water in only one year.

Also from **Fig. 6.8**, it shows that 5 acre spacing system produces the highest cumulative production during 10 years simulation followed by 20 acre spacing system, 40 acre spacing system, and 80 acre spacing system respectively.

Table 6.1 shows the tabulated results for ten years simulation of interference effect investigation.

TABLE 6.1—COMPARISON OF RESULTS FOR VARIOUS WELL SPACINGS FOR 80 ACRE RESERVOIR SYSTEM					
<i>OGIP</i> =		9.04E+08	<i>scf</i>		
<i>OWIP</i> =		1.79E+04	<i>stb</i>		
No.	Type of simulation	Cum. Gas Production (<i>scf</i>)	Cum. Water Production (<i>stb</i>)	RF Gas	RF Water
1	80 acre	3.28E+08	17077.5	36.27%	95.24%
2	40 acre	4.71E+08	17783.3	52.09%	99.17%
3	20 acre	5.89E+08	17914.2	65.15%	99.90%
4	5 acre	7.43E+08	17931.7	82.23%	100.00%

However, economical analysis should be considered to determine the optimal well spacing. The drilling cost, well completion costs, development costs have to be considered to determine what the optimal well spacing is for a specific coal bed methane reservoir development.

6.2.2 Transformation of Anisotropic Reservoirs into Equivalent Isotropic Reservoirs

We discussed how to transform an anisotropic reservoir system to an isotropic reservoir system in Chapter IV. In this chapter we are discussing simulation results for the transformation method. We will discuss only the transformation for permeability anisotropy 100:1. The complete results for the simulations of this transformation are presented in Appendix D.

The following **Fig. 6.9** is the simulation results for permeability anisotropy 100:1. We can see from the figure that both of the reservoir system, the anisotropic system and the isotropic system, show a similar performance. Both of the gas production performance falls on the same curve. Simulation from CMG verifies the method discussed in Chapter IV is applicable for coal bed methane reservoir.

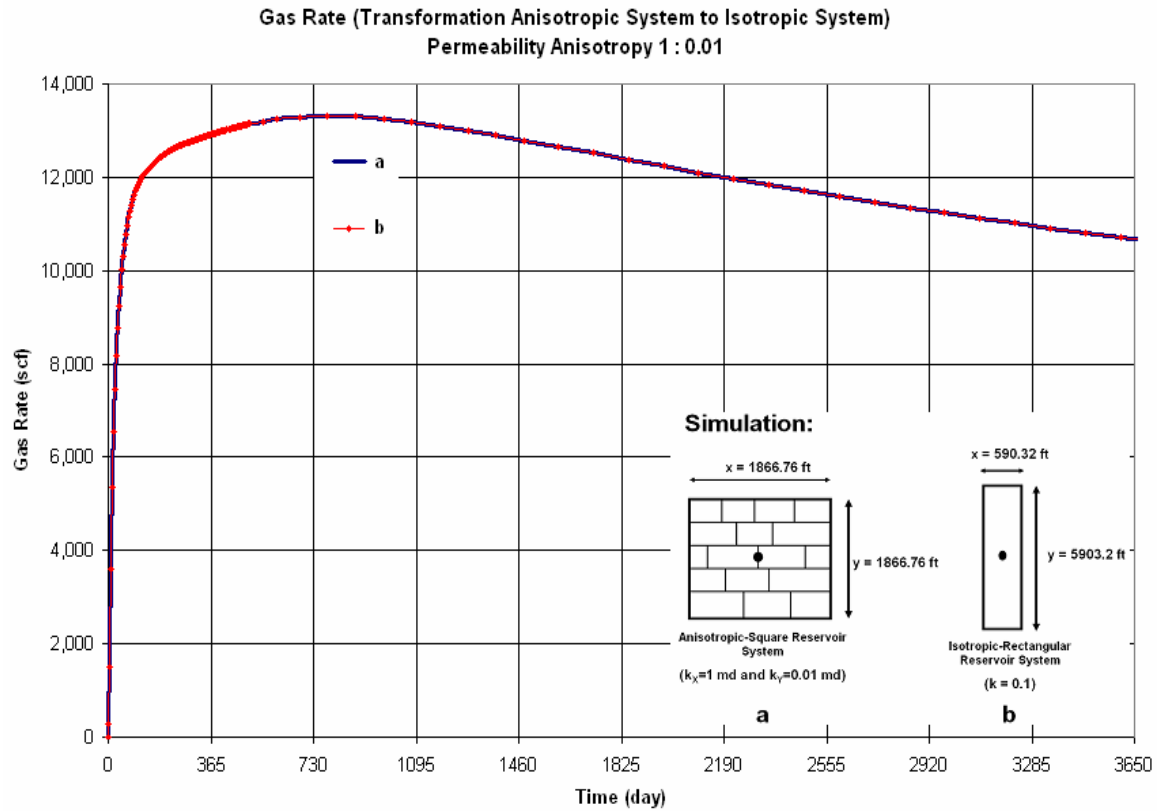


Fig. 6.9—Gas rates for transformation of square-anisotropic 80 acre reservoir to rectangular-isotropic 80 acre reservoir. Both of reservoir system show similar performance for gas production rate.

Also we present the simulation result for cumulative gas rate from both reservoir systems, **Fig. 6.10**.

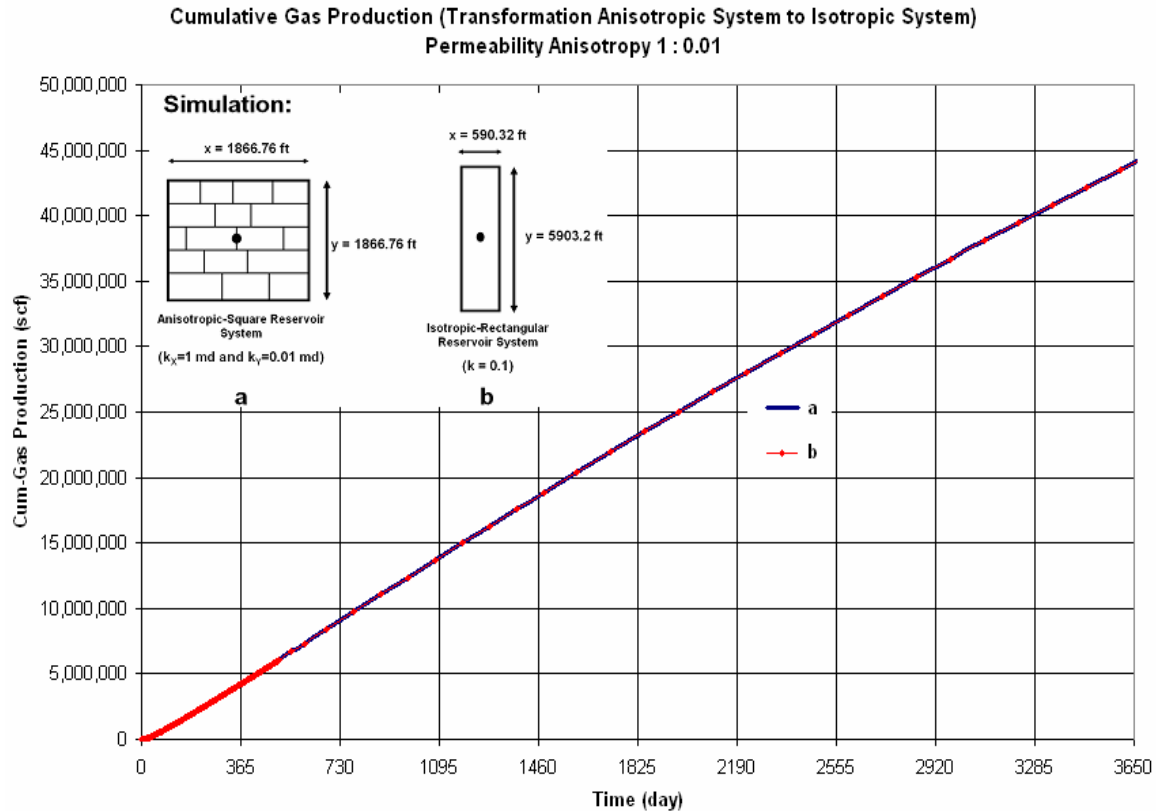


Fig. 6.10–Cumulative gas production rates for transformation of square-anisotropic 80 acre reservoir to rectangular-isotropic 80 acre reservoir. Both of reservoir system show similar performance for cumulative gas production.

The transformation helps us to understand the effect of permeability anisotropy to the performance of coal bed methane reservoir. Permeability anisotropy changes a square anisotropic reservoir system into a rectangular isotropic reservoir system. The more permeability anisotropy is, the more skinny the rectangular reservoir is.

This transformation also helps us to investigate the effect of well placement caused by the permeability anisotropy of the coal bed methane reservoir.

6.2.3 Effects of Permeability Anisotropy on Coalbed Methane Reservoirs

Permeability anisotropy is an inherent property of coal bed methane. The simulations are conducted to investigate the effect of well placement on coal bed methane production. The reservoir model used in these simulations is already discussed in Chapter V. The reservoir is an anisotropic reservoir.

The results presented here are only the simulation results for Subchapter 5.4.1 (Permeability anisotropy on 20 acre spacing). The complete simulation results are presented in Appendix D.

For permeability anisotropy modeling, permeability along x-axis is set as 1 md and permeability along y-axis is set as 0.01 md. In this case, the reservoir provides more flow-path for the fluid to flow along the x-axis. The rate of depletion along the x-axis is higher than the rate of depletion along the y-axis. **Fig. 6.11** shows the results for gas rates for permeability anisotropy on 20 acre spacing, Subchapter 5.4.1.

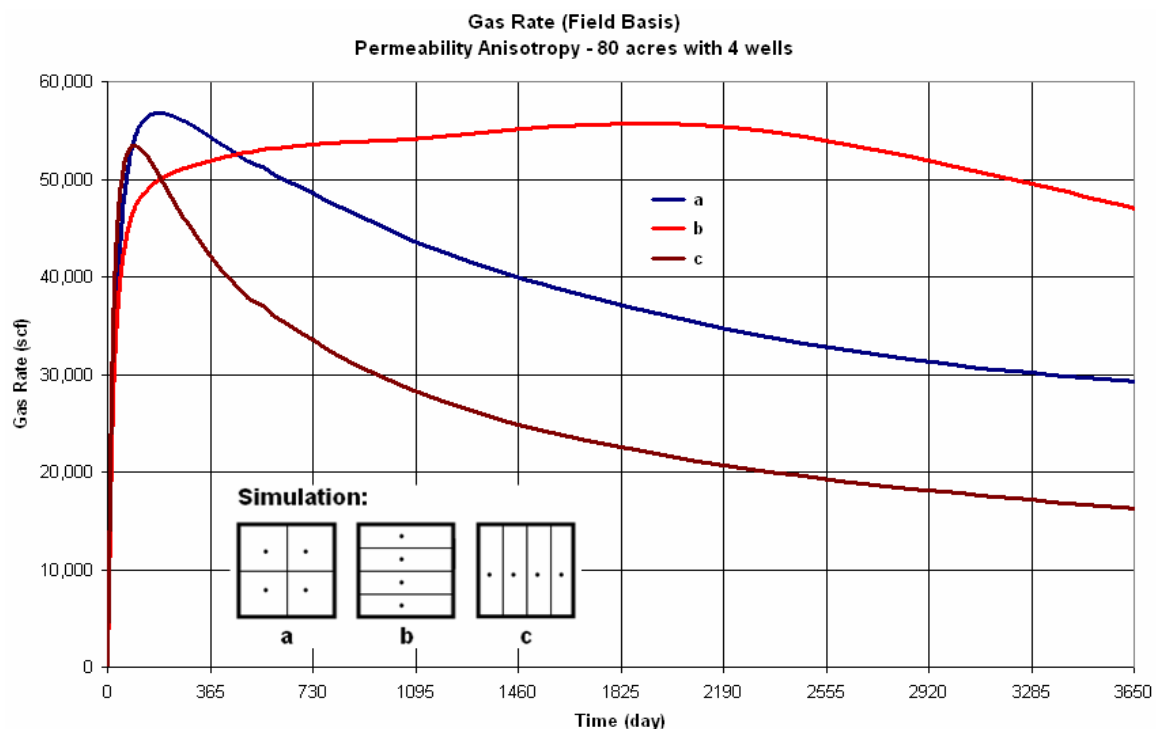


Fig. 6.11—Comparison of gas rates for three types of well configurations. Reservoir is anisotropic, $k_x = 1$ md and $k_y = 0.01$ md. Configuration type b gives the highest gas rate for most of ten years simulation and type c gives the lowest.

Fig. 6.11 shows that scenario A has the highest gas rate in the first year of production. Scenario B peaks the latest but it has the highest gas rate compare to others for almost the late 9 years. It indicates that scenario B is the best well placement method regarding to the permeability anisotropy. It also will be more useful if we also see the cumulative gas production for these simulations.

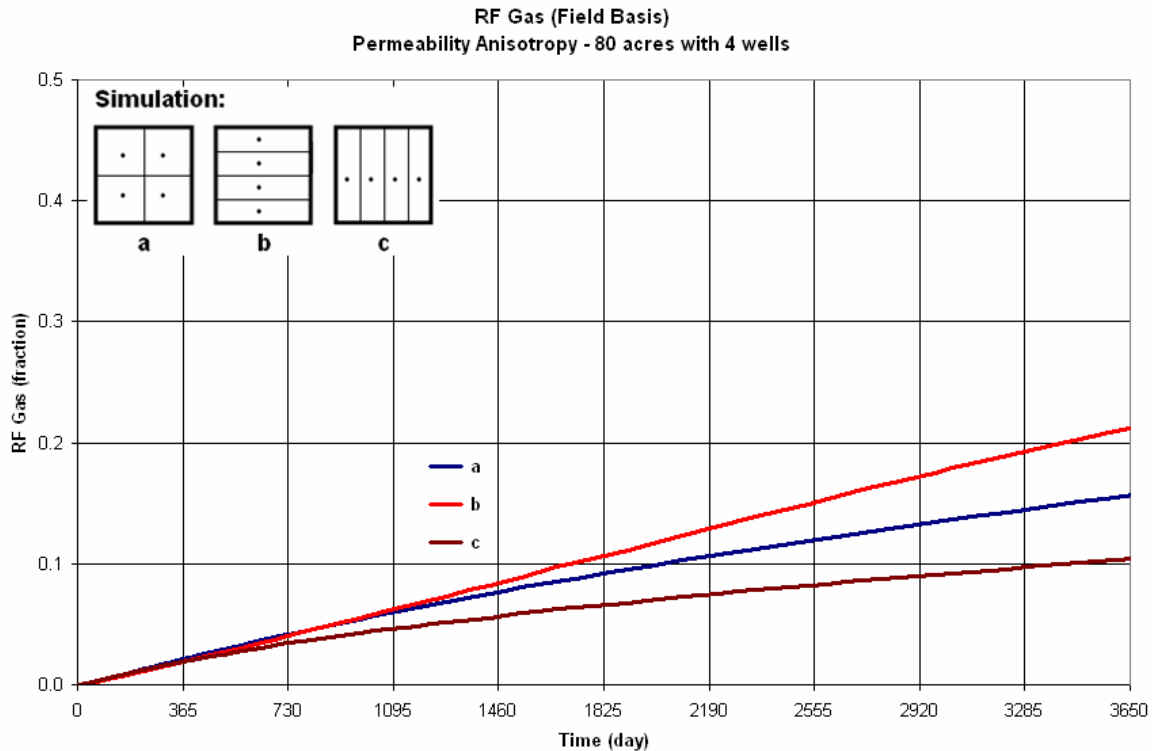


Fig. 6.12–Comparison of recovery factor of gas production for three types of well configurations. Configuration type b gives the highest cumulative production for ten years simulation and type c gives the lowest.

From the **Fig. 6.12** above, we see that for 10 years simulation scenario B produces the highest cumulative gas production. Scenario B produces total gas about 21 percent for ten years simulation. Scenario A and scenario C produce total gas about 16 percent and 10.5 percent respectively.

Our reservoir model is square anisotropic system with 80 acres area. From the transformation of anisotropic system to isotropic system, we know that the square anisotropic system can be transformed to a rectangular isotropic system. For this reservoir simulation, the following **Fig. 6.13** describes the transformation into isotropic system.

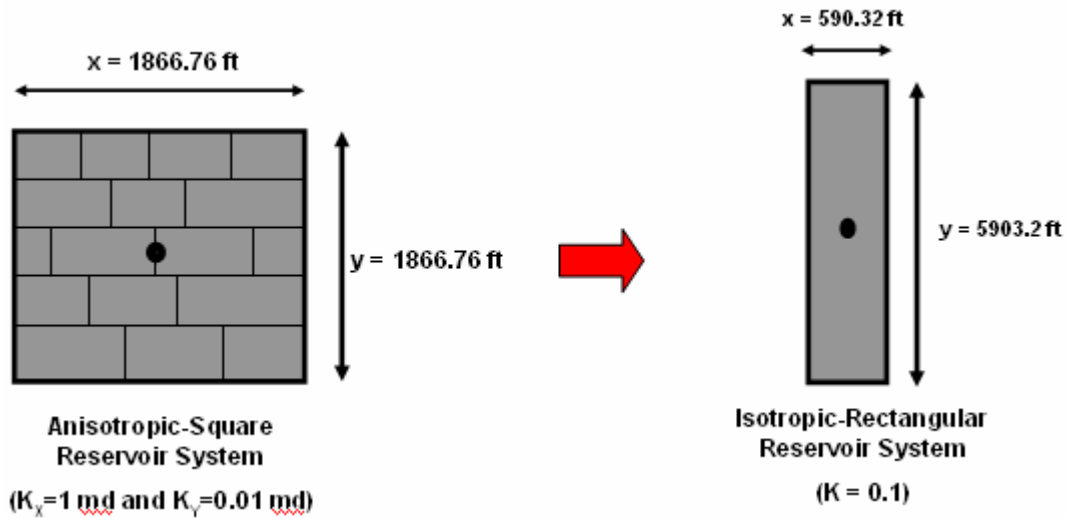


Fig. 6.13—Schematic of reservoir model for transformation of square-anisotropic 80 acre reservoir to rectangular-isotropic 80 acre reservoir.

We can see from **Fig. 6.13** that for isotropic system the reservoir is rectangular and longer in y-axis. Therefore, to optimal production can be achieved by increasing number of wells and placing the wells along the y axis. Number of wells should be increased and placed along the minimum permeability direction to get the optimal production.

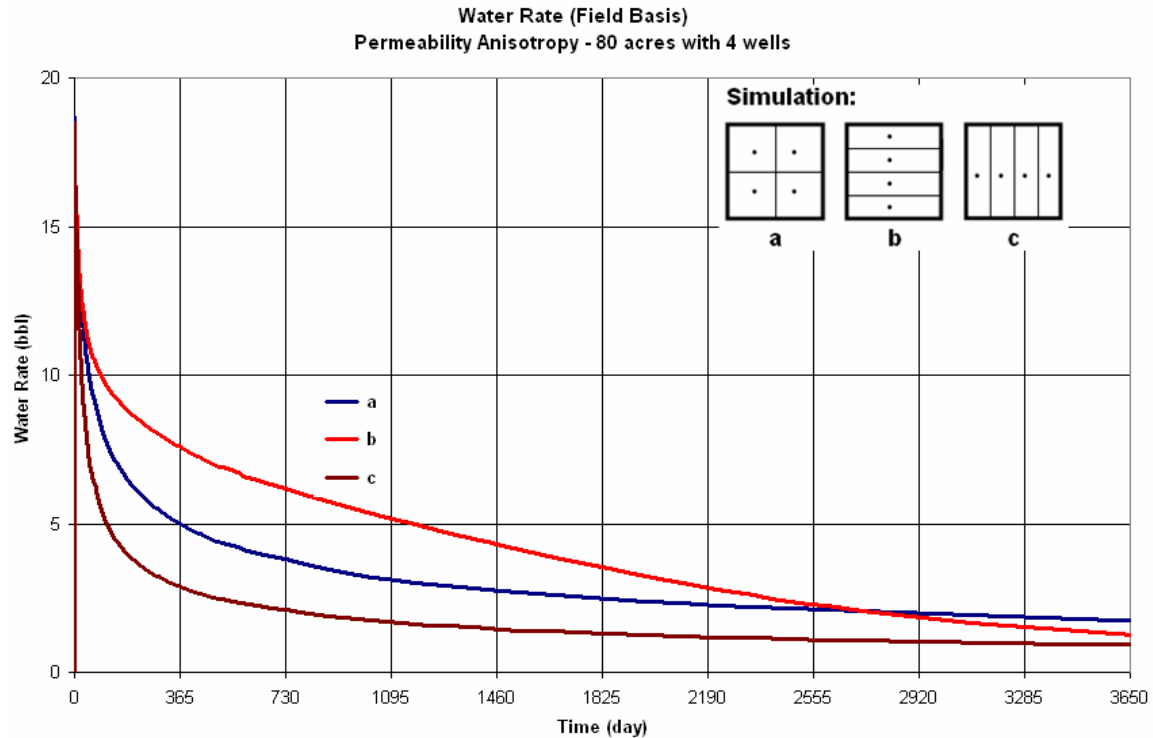


Fig. 6.14—Comparison of water rates for three types of well configurations. Configuration type b gives the highest water rate for most of ten years simulation and type c gives the lowest.

From **Fig. 6.14**, scenario B produces the highest water rate in the early seven years production followed scenario A and scenario C. It means that scenario B accelerates the dewatering stage. Scenario B produces more water compare to other scenarios, scenari A and scenario C. In the year seven the water rate for scenario B starts to be lower than scenario A.

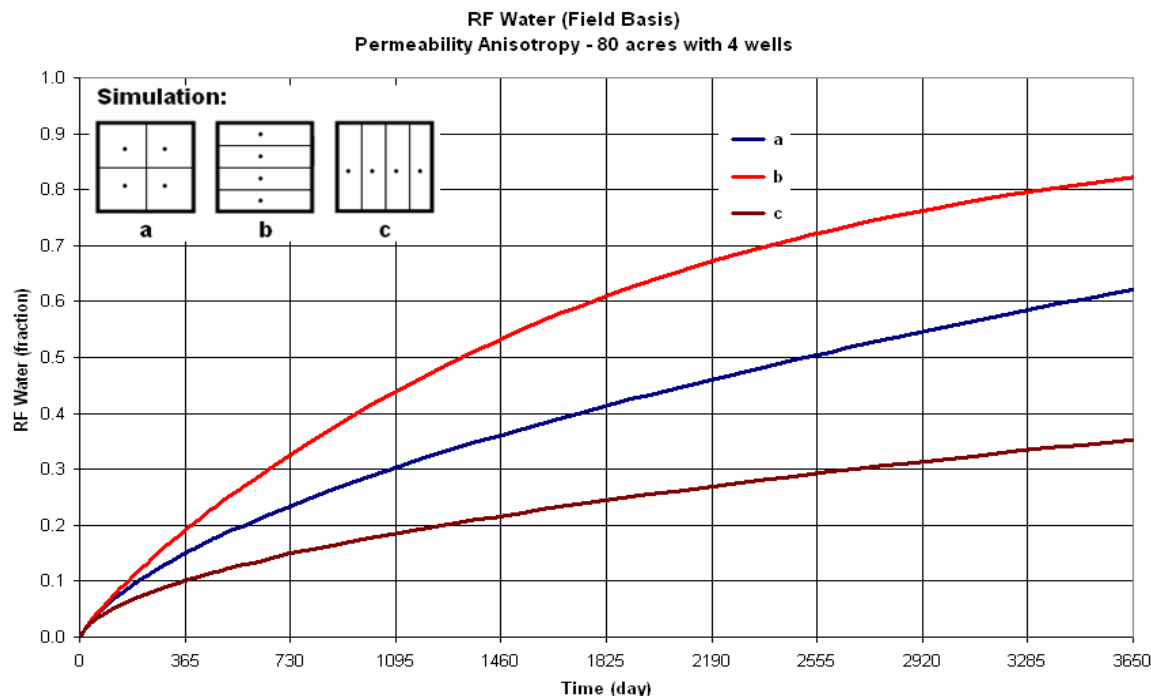


Fig. 6.15–Comparison of recovery factor of water production for three types of well configurations. Configuration type b gives the highest cumulative production for ten years simulation and type c gives the lowest. Configuration type b accelerates dewatering of the CBM reservoir.

From **Fig. 6.15**, for ten years simulation scenario B produces the highest cumulative water production. As we can see from **Fig. 6.15**, at certain year scenario B produces more water compare to other scenarios. It means that this type of well configuration dewateres the reservoir more compare to others. Therefore, it is obviously true that this type of configuration produces the highest cumulative gas production.

TABLE 6.2–COMPARISON RESULTS FOR THREE TYPES OF WELL CONFIGURATIONS					
		<i>OGIP</i> =	9.04E+08	<i>Scf</i>	
		<i>OWIP</i> =	1.79E+04	<i>Stb</i>	
No.	Type of simulation	Cum. Gas Production (<i>scf</i>)	Cum. Water Production (<i>stb</i>)	RF Gas	RF Water
1	Type A	1.44E+08	11255.9	15.92%	62.77%
2	Type B	1.95E+08	14838.3	21.58%	82.75%
3	Type C	9.48E+07	6400.76	10.49%	35.70%

Table 6.2 shows the tabulated results for ten years simulation.

6.2.4 Effect of Cleats Compression and Matrix Shrinkage (Permeability Changes) on Coalbed Methane Production

Effects of cleats compression and matrix shrinkage (permeability changes) on coal bed methane production are investigated using sensitivity analysis. In a sensitivity study, one parameter is varied while all other parameters are kept constant at some base values. The sensitivity analysis is conducted by varying the pertinent modeling parameters that affect coalbed methane gas production, using the base case model. The results of the simulation were analyzed to determine the primary performance of the coal-seam under these varying conditions for which varying these parameters would be similar to modeling different types of coal seams.

To investigate the effect of matrix shrinkage and cleats compression on gas recovery, we conduct the sensitivity analysis of the following parameters:

A. Effects of Young's modulus

To investigate the effects of Young's modulus on the production performance of coal bed methane we conduct sensitivity analysis. We are varying the Young's modulus: 500,000 psi, 750,000 psi, 1,000,000 psi, 1,500,000 psi, 2,000,000 psi, 3,000,000 psi, 4,000,000 psi, and 5,000,000 psi.

B. Effects of Poisson's ratio

To investigate the effects of Poisson's ratio on the production performance of coal bed methane we conduct sensitivity analysis. We are varying the Poisson's ratio: 0.1, 0.2, 0.3, 0.4, and 0.5.

C. Effects of strain maximum

To investigate the effects of infinite strain on the production performance of coal bed methane we conduct sensitivity analysis. We are varying the infinite strain: 0.0025, 0.0050, 0.0075, 0.01, 0.0125, 0.0150, 0.0175, and 0.02.

The sensitivity study provides a discussion of the physical production responses observed for each parameter sensitivity. Results from the simulation were obtained and analyzed, while focusing on indicators such as; gas rate and cumulative gas production.

6.2.4.1 Young's Modulus

Eqn. 6.1 describes the palmer and Mansoori theory to model the effects of cleats compression and matrix shrinkage (permeability changes) on coal bed methane production.

$$\frac{\phi}{\phi_i} = 1 + c_f(p - p_i) + \varepsilon_L \left(1 - \frac{K}{M} \right) \left(\frac{p_i}{p_i + p_L} - \frac{p}{p + p_L} \right) \dots\dots\dots 6.1$$

The pore volume compressibility (c_f) values is determined from parameters as follows, **Eqn. 6.2(a) and 6.2(b)**.

$$M = E \frac{1 - \nu}{(1 + \nu)(1 - 2\nu)} \dots\dots\dots 6.2(a)$$

where E is the Young's modulus (kPa | psia) and ν is Poisson'ratio. And

$$c_f = \frac{1}{\phi_i M} \dots\dots\dots 6.2(b)$$

Fig. 6.16 shows that the gas production rate increases with the increasing in the Young's modulus (E). It can be explained such way:

- a. From **Eqn. 6.2(a)** and **Eqn. 6.2(b)**, pore volume compressibility (c_f) increases with increasing Young's modulus (E).
- b. And from the second term of **Eqn. 6.1**, the increasing of pore volume compressibility (c_f) result in increasing of formation porosity.
- c. Increasing in the formation porosity result in increasing in the formation permeability and therefore increasing in the gas rate.

Fig. 6.17 shows that the recovery factor for cumulative gas production increases with the increasing in the Young's modulus (E). We can see that for ten years simulation, the higher the Young's modulus is the greater the cumulative production is.

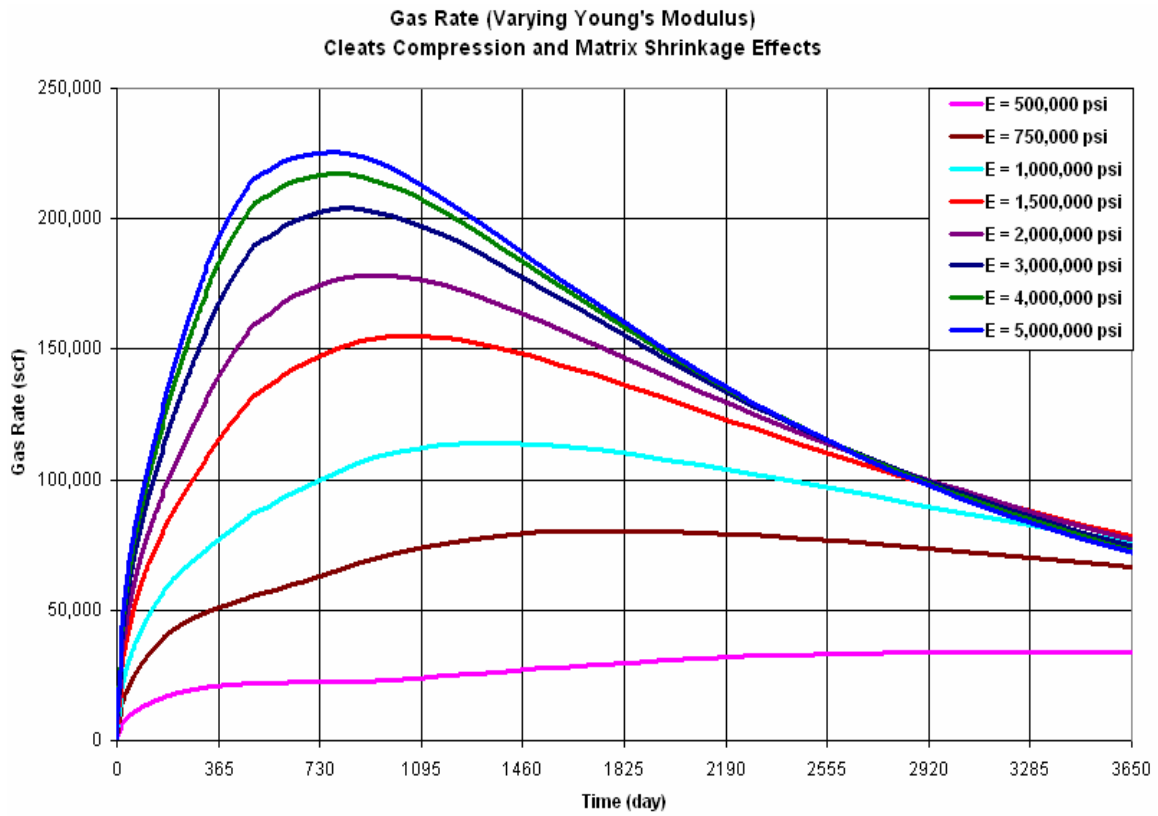


Fig. 6.16—Simulation results show that gas production rate increases with increasing magnitude in the Young's Modulus.

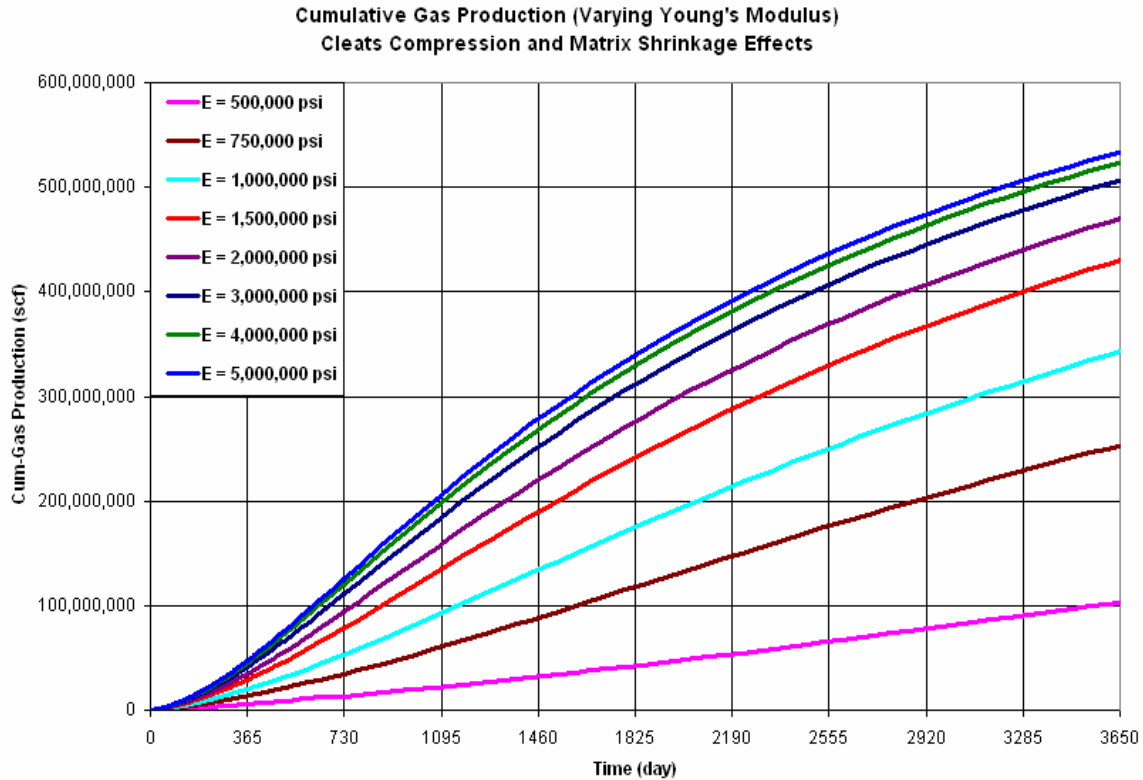


Fig. 6.17–Simulation results show that cumulative gas production increases with increasing magnitude in the Young’s Modulus.

6.2.4.2 Poisson’s Ratio

The ratio of bulk to axial modulus is represented by Poisson’s ratio as indicated by **Eqn. 6.3**.

6.3.

$$\frac{K}{M} = \frac{1}{3} \left(\frac{1+\nu}{1-\nu} \right) \dots\dots\dots 6.3$$

Fig. 6.18 shows that gas production rate increases with decreasing in the Poisson’s ratio. From **Fig. 6.18**, we also can see that the higher the Poisson’s ratio is the later and the lower peaks on gas production rate. It can be explained such way:

- a. From **Eqn. 6.3**, ratio (K/M) increases with the increasing in the Poisson’s ratio (ν).
- b. From the third term of **Eqn. 6.1**, the increasing in the (K/M) result in decreasing in the formation porosity.
- c. Decreasing in the formation porosity result in decreasing in the formation permeability and therefore decreasing in the gas rate.

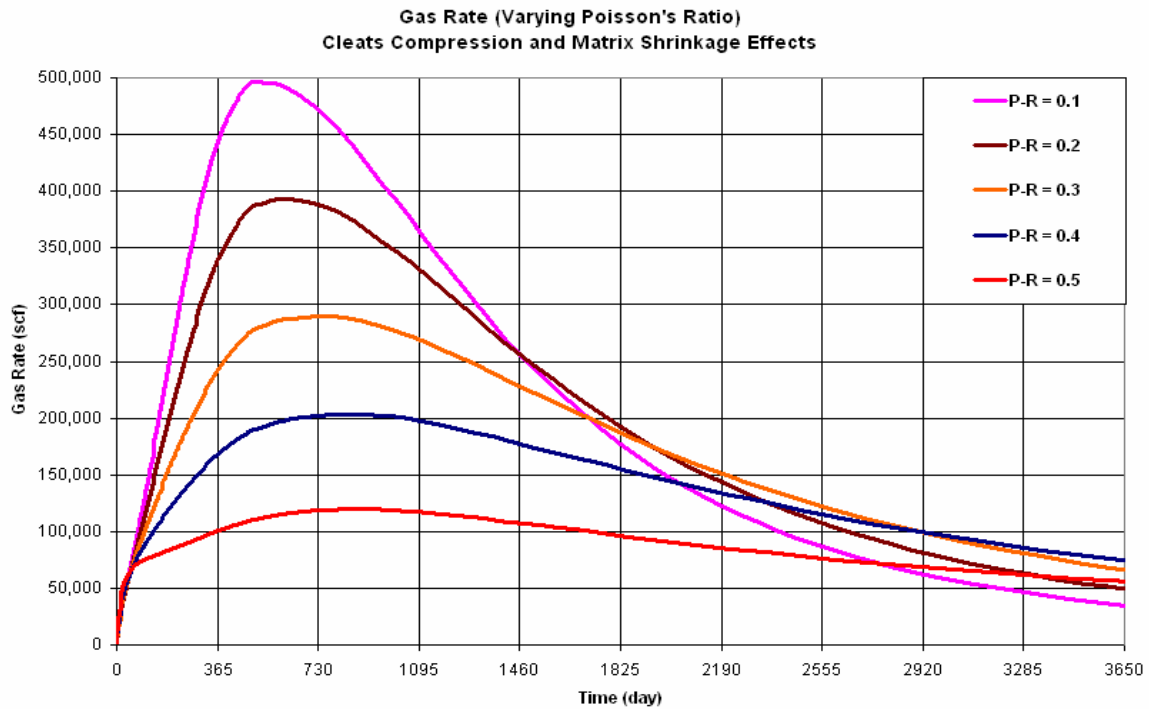


Fig. 6.18—Simulation results show that gas production rate increases with decreasing magnitude in the Poisson's ratio.

For ten years simulation runs (**Fig. 6.19**), the higher the Poisson's ratio is the lower the cumulative gas production.

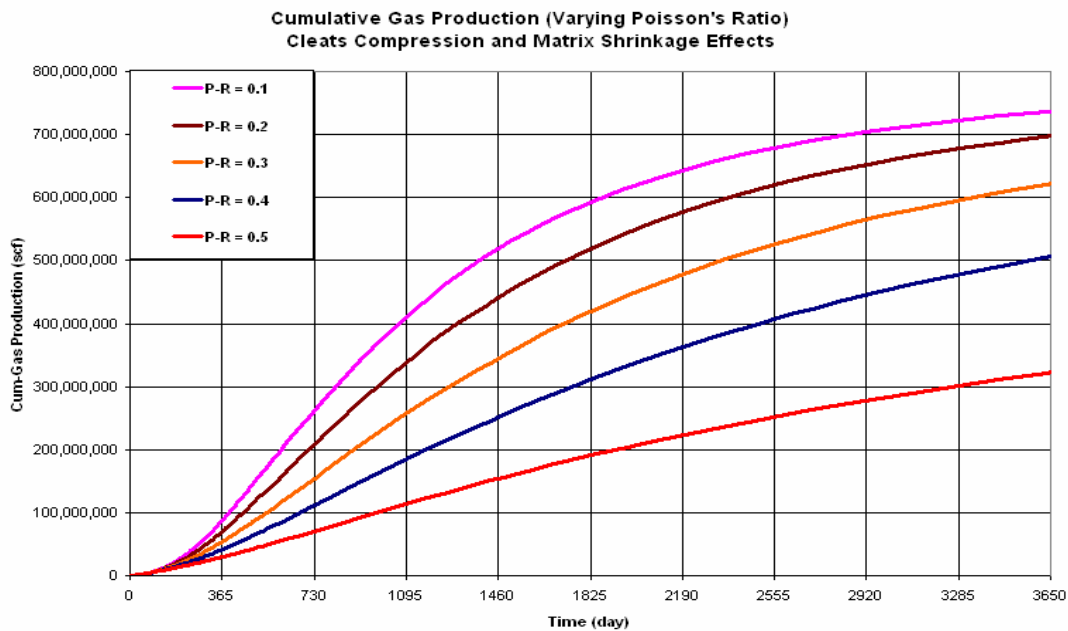


Fig. 6.18—Simulation results show that cumulative gas production increases with decreasing magnitude in the Poisson's ratio.

6.2.4.3 Strain Maximum

Strain maximum (ϵ_L) is the magnitude of strain at infinite pressure. The higher the strain maximum is the greater the deformation is.

Fig. 6.20 shows that gas rate increases with increasing in the strain maximum (strain an infinite pressure). It can be explained such way:

- From the third term of **Eqn. 6.1**, the increasing in the strain maximum (ϵ_L) result in increasing in the formation porosity.
- Increasing in the formation porosity result in increasing in the formation permeability and therefore decreasing in the gas rate.

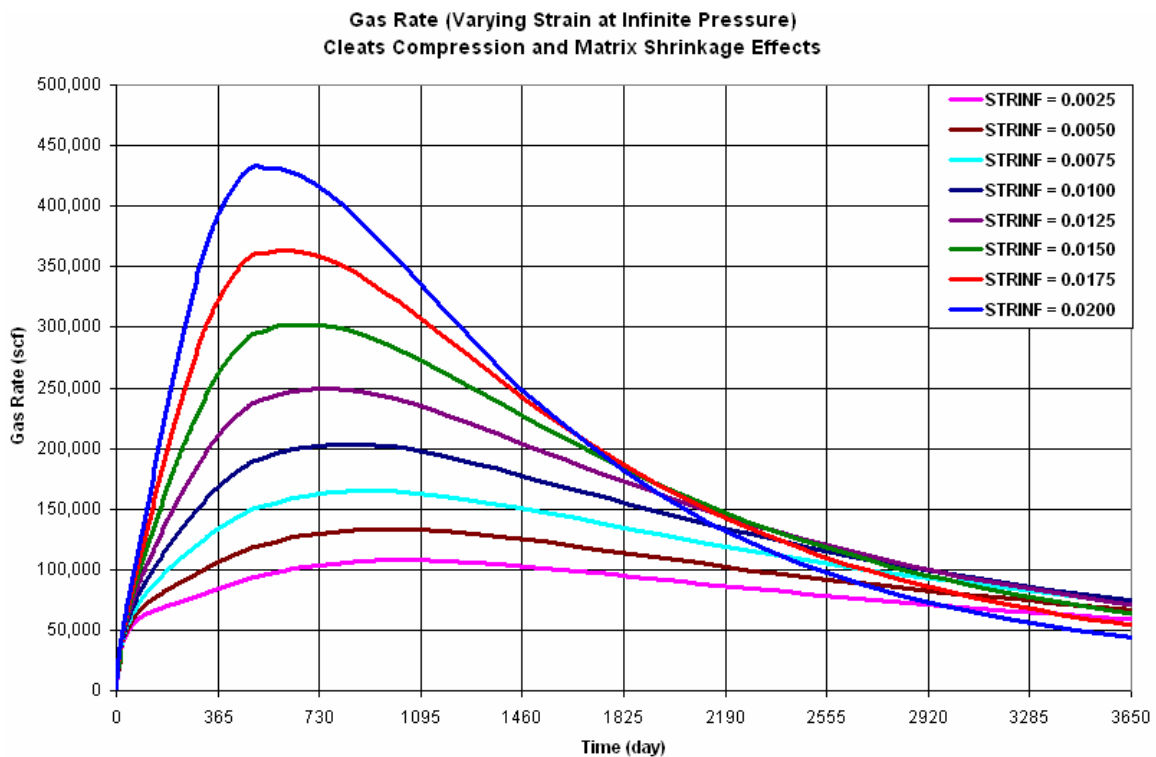


Fig. 6.20—Simulation results show that gas rate increases with increasing magnitude in the strain maximum (strain at infinite pressure).

Fig. 6.21 shows the cumulative production for ten years simulation. From the figure we can see that increasing in the maximum strain (ϵ_L) result in increasing the cumulative production.

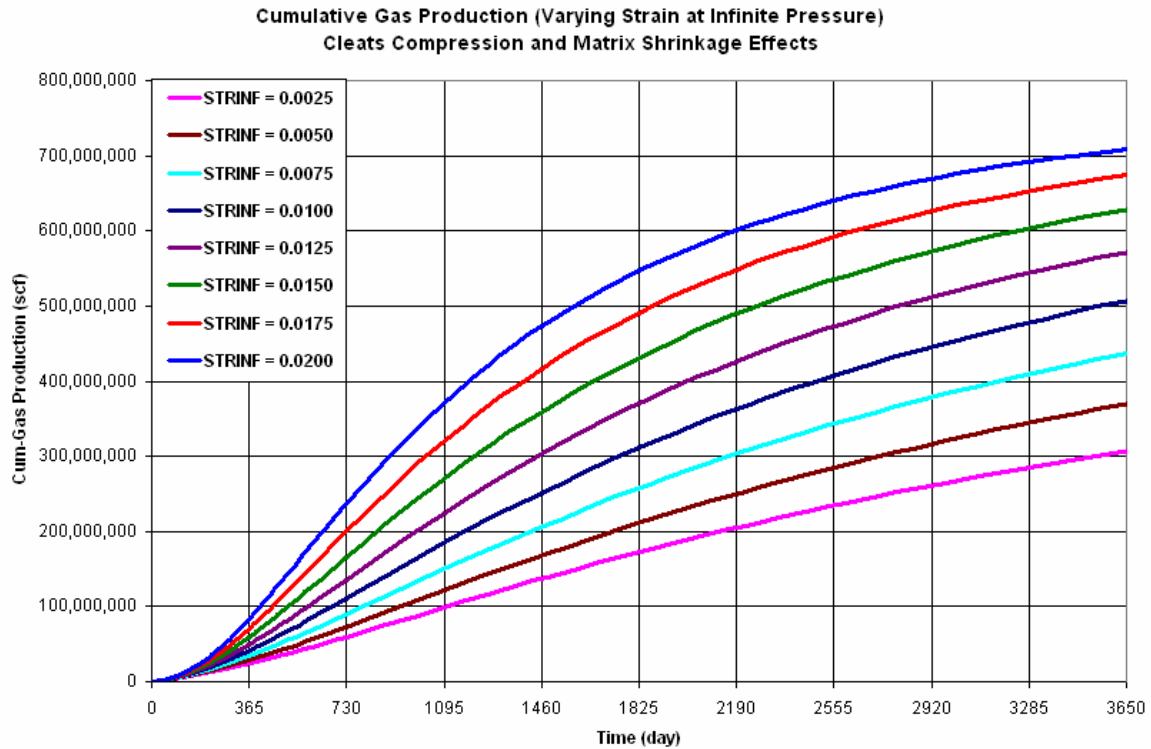


Fig. 6.21–Simulation results show that cumulative gas production increases with increasing magnitude in the maximum strain (strain at infinite pressure).

6.2.5 Formation Compressibility

Appendix D describes how the formation compressibilities are calculated in the CMG-GEM 2004 in detail. The investigation shows that in the simulation with Palmer and Mansoori model, the formation compressibilities are calculated using **Eqn. 6.2(a) and 6.2(b)**. CMG-GEM 2004 will ignore the use of CCPOR and CPRPOR as a direct input data for formation compressibilities.

In the simulation without Palmer and Mansoori model, the simulator will use the input data from CPOR and PRPOR as the formation compressibilities.

CHAPTER VII

CONCLUSIONS AND RECOMMENDATIONS

7.1 Conclusions

1. Interference between wells is beneficial for coalbed methane reservoir. It accelerates the dewatering stage and therefore accelerates and increase gas production.
2. The closer the well spacing is, the earlier and the higher peak gas rate is.
3. The cumulative gas production increases with the increasing in the well spacing.
4. Wells configuration (placement of well) has a significant effect on coalbed methane reservoir development regarding the existence of permeability anisotropy. Wells should be placed (aligned) along the lower permeability direction to optimally deplete the reservoir.
5. Gas rate increases with the increase in the Young's modulus as well as cumulative gas production.
6. Gas rate and cumulative gas rate increase with the decrease in the Poisson's ratio.
7. The greater the maximum strain is, the higher the gas rate is. Cumulative gas rate also increases with the increase in the maximum strain.
8. In the simulation with Palmer and Mansoori model, the formation compressibilities are calculated using **Eqn. 6.2(a) and 6.2(b)**. CMG-GEM 2004 will ignore the use of CCPOR and CPRPOR as a direct input data for formation compressibilities. And, in the simulation without Palmer and Mansoori model, the simulator will use the input data from CPOR and PRPOR as the formation compressibilities.

7.2 Recommendations

1. Coalbed methane reservoir simulation study should be made using other simulator, so that we can compare the results from CMG and other simulator (e.g. Eclipse).
2. Economic analysis should be made incorporated to simulation study to determine the optimal well spacing for the field development of the specific reservoir.

NOMENCLATURE

A	= Surface Area of matrix element, ft^2
a	= shape factor, ft^{-1}
b	= Langmuir coefficient, $l/psia$
C	= Coal bed gas content, scf/ft^3 or $gmole/lb$ of rock
$C(p)$	= Coal bed gas content (gas concentration) as a function of pressure only, scf/ft^3 or $gmole/lb$ of rock
\bar{C}	= Average gas concentration in the matrix, scf/ft^3 or $gmole/lb$ of rock
D	= Diffusion coefficient, cm^2/sec of Diffus(k) = Diffusivity constant
E	= Young's modulus, $psia$
f	= fraction
K	= Bulk modulus, psi
k	= permeability, md
k_o	= initial permeability, md
L	= distance, ft
M	= Axial modulud, psi
N_e	= Number of matrix elements within a grid block
p	= reservoir pressure, $psia$
p_L	= Langmuir pressure, $psia$
Q_{gas}	= Diffusion rate, scf/day
q	= gas flow rate, scf/day
S_w	= water saturation, fraction
S_g	= gas saturation, fraction
V	= adsorbed gas in the matrix, scf/ton
V_m	= maximum adsorbed gas in the matrix, scf/ton
V_L	= Langmuir volume, scf/ft^3 or $gmole/lb$ of rock
β	= grain compressibility
ρ_B	= Bulk density of coal deposit, $gram/cm^3$
μ	= viscosity, cp
ϕ	= porosity, fraction

ϕ_o = porosity, fraction
 ν = Poisson's ratio, fraction

Subscript

o = original
 i = initial
 f = fracture
 g = gas
 m = matrix
 w = water

Units

rcf = reservoir cubic feet
 $res.bbl$ = reservoir barrel
 scf = standard cubic feet
 $Mscf$ = 1000 scf
 $MMscf$ = 1000000 scf
 stb = stock tank barrel

REFERENCES

1. Nelson, C.R., Mavor, M.J., Pratt, T.J., and Casey, T.A.: "Protocol Ups Coal Seam Gas Analysis," *The American Oil and Gas Report* (October 1997) **40**, No. 10, 86.
2. Puri, R. and Yee, D.: "Enhanced Coalbed Methane Recovery." paper SPE 20732 presented at the Annual Technical Conference and Exhibition, New Orleans, Louisiana, 23-26 September 1990.
3. Patching, T. H.: "The Retention and Release of Gas in Coal," *Cdn. Mining and Metallurgical Bulletin* (1970) **8**, No. 1302, 63.
4. Darton, N. H.: "Occurrence of Explosive Gases in Coal Mines," *United States Bureau of Mines Bulletin* (1915) **10**, No.101, 72.
5. Wold, M. B., Choi, S. K., Koenig, R. A., and Davidson, S. C.: "Anisotropic Seam Response to Two-Phase Fluid Injection into a Coalbed Methane Reservoir-Measurement and Simulation," paper SPE 36984 presented at SPE Asia Pacific Oil and Gas Conference, Adelaide, Australia, 28-31 October 1996.
6. Harpalani, S. and Schraufnagle, R. A.: "Influence of Matrix Shrinkage and Compressibility on Gas Production from Coalbed Methane Reservoirs", paper SPE 20729 presented at the Annual Technical Conference and Exhibition, New Orleans, Louisiana, 23-26 September 1990.
7. Palmer, I. and Mansoori, J.: "How Permeability Depends on Stress and Pore Pressure in Coalbeds: A New Model," paper SPE 36737 presented at the Annual Technical Conference and Exhibition, Denver, Colorado, 6-9 October 1996.
8. Remner D. J., Ertekin. T., Sung, W., and King, G.R.: "A Parametric Study of the Effects of Coal Seam Properties on Gas Drainage Efficiency," paper SPE 13366 presented at the SPE Eastern Regional Meeting, Charleston, West Virginia, 31 October- 2 November 1986.
9. Wicks, D.E., Schewerer, F. C., Militzer, M.R., and Zuber, M.D.: "Effective Production Strategies for Coalbed Methane in the Warrior Basin," paper SPE 15234 presented at the Unconventional Gas Technology Symposium, Louisville, Kentucky, 18-21 May 1986.

10. Young, G.B.C., McElhiney, J.E., Paul, G.W., and McBane, R.A.: "An Analysis of Fruitland Coalbed Methane Production, Cedar Hill Field, Northern San Juan Basin," paper SPE 22913 presented at the Annual Technical Conference and Exhibition, Dallas, Texas, 6-9 October 1991.
11. Young, G.B.C., McElhiney, J.E., Paul, G.W., and McBane, R.A.: "A Parametric Analysis of Fruitland Coalbed Methane Producibility," paper SPE 24903 presented at the Annual Technical Conference and Exhibition, Washington, DC, 4-7 October 1992.
12. Chaianansutcharit, T. Her-Yuan Chen, and Teufel, L.W.: "Impacts of Permeability Anisotropy and Pressure Interference on Coalbed Methane (CBM) Production," paper SPE 71069 presented at the SPE Rocky Mountain Petroleum Technology Conference, Keystone, Colorado, 21-23 May 2001.
13. Bumb, A.C. and McKee, C.R.: "Use of a Computer Model to Design Optimal Well for Dewatering Coal Seams for Methane Production," paper SPE 12859 presented at the Unconventional Gas Technology Symposium, Pittsburgh, Pennsylvania, 13-15 May 1984.
14. Sung, W., Ertekin, T., and Schewerer, F. C.: "An Analysis of Field Development Strategies for Methane Production from Coal Seams," paper SPE 16858 presented at the Annual Technical Conference and Exhibition, Dallas, Texas, 27-30 September 1987.
15. Gray, I.: "'Reservoir Engineering in Coal Seams: Part I – The Physical Process of Gas Storage and Movement in Coal Seams", *SPE Reservoir Engineering* (February 1987) **2**, 28.
16. Sawyer, W. K., Paul, G. W., and Schraufnagle, R. A.: "Development and Application of a 3D Coalbed Methane Simulator", paper SPE 12316 presented at the International Technical Meeting CIM/SPE, Calgary, Canada, 10-13 June 1990.
17. Wise, R. L.: "Methane Recovery and Utilization from Coalbeds," paper SPE 8357 presented at the Annual Technical Conference and Exhibition, Las Vegas, Nevada, 23-26 September 1979.
18. Cervik, J.: "Behavior of Coal-Gas Reservoirs," paper SPE 1973 presented at the Annual Eastern Regional Meeting, Pittsburgh, Pennsylvania, 2-3 November 1967.

19. Saghafi, A.: "Coal Seam Gas Reservoir Characterization," presented at the Coal Symposium, Brisbane, Australia, 27 March 2001.
20. Seidle, J. P. and Arri, L. E., "Use of Conventional Reservoir Models for Coalbed Methane Simulation," paper SPE 21599 presented at the International Technical Meeting CIM/SPE, Calgary, Canada, 10-13 June 1990.
21. Warren, J. E. and Root, P. S.: "The Behavior of Naturally Fractured Reservoirs," paper SPE 426 presented at the Fall Meeting of Society of the Petroleum Engineers, Los Angeles, California, 7-10 October 1965.
22. Zuber, M. D., Sawyer, W. K., Schrufnagel, R. A., and Kuuskraa, V. A.: "The Use of Simulation and History Matching to Determine Critical Coalbed Methane Reservoir Properties," paper SPE 16420 presented at the SPE/DOE Low Permeability Reservoir Symposium, Denver, Colorado, 18-19 May 1987.
23. Kazemi, H.: "Pressure Transient Analysis of Naturally Fractured Reservoirs with Uniforms Fracture Distribution," *Society of Petroleum Engineers Journal* (December 1965) **5**, 18.
24. Villagran, J. A. A.: *Analysis of Long Term Behavior in Tight Gas Reservoir : Case Histories*, Ph.D. Dissertation, Texas A&M University, College Station (2001).
25. Okeke, A. N.: *Sensitivity Analysis of Modeling Parameters That Affect the Dual Peaking Behavior in Coalbed Methane Reservoir*, M.S. Thesis, Texas A&M University, College Station (2005).
26. Palmer, I. and Mansoori, J.: "How Permeability Depends on Stress and Pore Pressure in Coalbeds: A New Model," paper SPE 52607 was revised for publication from paper SPE 36737, December 1998.
27. *CMG-GEM User Manual*, Computer Modelling Group Co., Calgary (2004).

APPENDIX A

DESCRIPTION OF CMG SIMULATOR

CMG (Computer modeling Group) simulator can be used to model the coal bed methane reservoir. CMG uses a two-phase compositional simulation to model the coalbed methane reservoir. The numerical formulations and solution protocols on which this model is based can be found in the GEM 2004.10 user manual²⁷.

CMG-GEM 2004.10 is a two-phase compositional simulator that has the ability of modeling coalbed methane reservoir including Palmer and Mansoori Theory. CMG-GEM 2004.10 models the coalbed methane reservoir using the dual porosity model (DUALPOR) and the sorption isotherms using the Langmuir's sorption isotherm. The flow of gas in the fractures is modeled by the standard Darcy's Law and the flow of gas in the matrix is modeled by Fick's Law.

A.1 Dual Porosity Formulations in CMG

Dual porosity option is activated using DUALPOR keyword. The dual porosity option in CMG-GEM 2004.10 models each reservoir grid block to have up to two porosity systems; matrix system and fracture system. Matrix properties are denoted by the use of the *MATRIX keyword and fracture properties are denoted by the use of *FRACTURE keyword.

For the dual porosity modeling, CMG uses the finite difference equation for dual porosity developed by Gilman and Kazemi²³.

Fracture porosity is required to indicate the reservoir volume that the cleats occupy, while matrix porosities should be set to small positive values to allow for the modeling of a small amount of free gas within the matrix porosity. Similarly, fracture permeability is required to describe the permeability of the cleat system. Value must also be entered for matrix permeability as well, but since the simulator disables all matrix-to-fracture Darcy flow when coal bed modeling is being used, a positive value is only used to indicate that there is a pathway for diffusion to occur between matrix (coal) and fracture (cleats), while a

zero value indicates that no connection of any kind is to be made between the matrix and fracture for that cell.

A.2 Adsorption and Diffusion

The LANG-DIFFUSION-COAL keyword specifies gas concentrations based on Langmuir desorption are used to calculate concentration gradients for diffusive flow calculations. The concentration of gas on the surface of the coal is assumed to be a function of pressure only.

The Langmuir isotherm can be defined in two ways;

- 1) input the maximum gas concentration using the *ADSORBTMAX keyword and also inputting a keyword *ADSTAB followed by a two column table. The first column is for pressure and the second column is for the gas concentration.
- 2) input just the maximum gas concentration V_L , using the *ADGMAXC and the Langmuir pressure constant $1/p_L$, using the *ADGCSTC.

The LANG-DIFFUSION-COAL model can be described by the following equation²⁷

$$q(Lang,k) = Vol * [Shape * Diffus(k)] * F(Sg) * (Lang(k,m) - Lang(k,f)) \dots\dots\dots A.1$$

Where,

- Vol = Cell volume;
- $Shape$ = Inverse area;
- $Diffus(k)$ = Diffusion value;
- $F(Sg)$ = Function of fracture gas saturation modelling water blocking;
- $C(k,f)$ = Mass concentration of species k in the free gas phase in the cleats;
- $C(k,m)$ = Mass concentration of species k in the free gas phase in the micro-pore space within the matrix system.

As regards gas diffusion between the matrix (coal) and the fracture (cleat) system, the gas phase mass transfer rate for component "k" (Equation 3.16) can be written as follows:

$$Rate_{block-basis} = Vol * Shape * Diffus(k) * Sg^{A-mod} * (C(k,gas,m) - C(k,gas,f)) \dots\dots\dots A.2$$

Where,

Vol = Bulk Volume

$Shape$ = Shape factor (matrix-fracture interface area per unit volume)
 $= Shape = 4 * \sum (1 / FracSpacing)^2$

$Diffus(k)$ = Diffusion value (COAL-DIF-COMP)

Sg^{A-mod} = gas saturation in the matrix (default = 1)

$C(k, gas, m)$ = Concentration of component 'k' in gas phase of matrix cell "m"

$C(k, gas, f)$ = Concentration of component 'k' in gas phase of fracture cell "f"

In the **Eqn. A.2**, $C(k, gas, m)$ is the concentration of component "k" in the gas phase of matrix cell "m" and $C(k, gas, f)$ is the same for fracture cell "f". $C(k, gas, m)$ is evaluated using standard material balance method while $C(k, gas, f)$ is evaluated using Langmuir desorption isotherm model. $Diffus(k)$ is the diffusion value given by COAL-DIF-COMP keyword for component "k" (input in units of cm^2/sec , but converted internally by the simulator for use in the formula here). Finally, the presence of water in the fracture can affect diffusive flows. When net diffusion is from the matrix to the fracture, Sg^{A-mod} is taken to be 1 (which is the assumed gas saturation in the matrix), and fracture water has no effect. But, when net diffusion is from the fracture to the matrix, water in the fracture is expected to reduce the contact area for diffusive flow. Thus, Sg^{A-mod} is taken to be the gas saturation in the fracture (that is, $1-S_w$) when the gas (molar) density in the fracture exceeds that of the co-located matrix.

If COAL-DIF-COMP is not used to set " $Diffus(k)$ ", then COAL-DIF-TIME can be used to define $1/(Shape * Diffus(k))$ in units of days. COAL-DIF-TIME is the parameter that can be used to measure how fast the diffusion of gas is (τ). The higher the COAL-DIF-TIME is, the slower the diffusion rate is. **Eqn A.3** describes the COAL-DIF-TIME keyword.

$$\tau = COAL - DIF - TIME = \frac{1}{Shape * Diffus(k)} \dots \dots \dots A.3$$

$$shape = 4 * \sum \left[\left(\frac{1}{DIFRAC^2} \right) + \left(\frac{1}{DJFRAC^2} \right) + \left(\frac{1}{DKFRAC^2} \right) \right] \dots \dots \dots A.4$$

A.3 Palmer and Mansoori Theory

Flow in the fracture system in coal is described by Darcy flow. The absolute permeability appearing in Darcy's Law is not constant but varies in situ with the change in the net overburden stress (overburden pressure – pore pressure) and with effects associated with desorption/adsorption of gas in the matrix. As the pressure is reduced therefore there are two competing effects, pore closure due compressibility effects and pore enlargement due to matrix shrinkage. The Palmer and Mansoori model determines for both effects and allows for changes in porosity and absolute permeability to be calculated as a function of changes in fracture pressure and matrix shrinkage/swelling. **Eqn. A.5** below reproduces the Palmer and Mansoori relationship.

$$\frac{\phi}{\phi_i} = 1 + c_f(p - p_i) + \varepsilon_L \left(1 - \frac{K}{M} \right) \left(\frac{p_i}{p_i + p_L} - \frac{p}{p + p_L} \right) \dots\dots\dots \text{A.5}$$

where:

- ϕ_i = initial natural fracture porosity
- ϕ = fracture porosity at pressure p
- c_f = pore volume compressibility (1/kPa | 1/psia)
- p_i = initial pressure (kPa | psia)
- p = pressure (kPa | psia)
- ε_L = strain at infinite pressure
- K = bulk modulus (kPa | psia)
- M = axial modulus (Kpa | psia)
- p_L = Langmuir pressure (kPa | psia)

The ratio of bulk to axial modulus is related to the Poisson's ratio as indicated by **Eqn. A.6**.

$$\frac{K}{M} = \frac{1}{3} \left(\frac{1 + \nu}{1 - \nu} \right) \dots\dots\dots \text{A.6}$$

Where, ν is the Poisson's ratio (dimensionless).

The pore volume compressibility values can be entered directly using the *CCPOR keyword or calculated from entered parameters as follows, **Eqn. A.7 (a) and A.7 (b)**.

$$M = E \frac{1 - \nu}{(1 + \nu)(1 - 2\nu)} \dots\dots\dots \text{A.7 (a)}$$

Where E is the Young's modulus (kPa | psia) and

$$c_f = \frac{1}{\phi_i M} \dots\dots\dots \text{A.7 (b)}$$

The Palmer and Mansoori model relates the absolute permeability ratio to the porosity ratio in the following manner, **Eqn. A.8:**

$$\frac{k}{k_o} = \left(\frac{\phi}{\phi_o} \right)^3 \dots\dots\dots \text{A.8}$$

The Palmer and Mansoori⁷ theory can be activated using the following keywords:

- 2) *POISSR, this keyword indicating that a value for the (dimensionless) Poisson's ratio used in calculating the ratio of bulk to axial modulus required for the Palmer and Mansoori model. Poisson's ratio is dimensionless.
- 3) *YOUNGM, this keyword used to specify a value for the Young's modulus used in calculating the pore compressibility. The unit of Young's Modulus is psia.
- 4) *STRINF, this keyword indicating that a value for the strain at infinite pressure required in the Palmer and Mansoori equation. The strain is the fractional change in volume divided by the initial volume and therefore is dimensionless.
- 5) *PRESLN, this keyword indicating that a value for the Langmuir pressure required in the Palmer and Mansoori equation. The unit of this parameter is psia.
- 6) *EXPPM, this keyword indicating that a value for the Palmer and Mansoori (dimensionless) exponent used in calculating the change in fracture permeability as a function of the change in fracture porosity.

APPENDIX B

CMG BASE CASE DATA FILE

B.1 Reservoir Simulation Data (Base Case)

Schematic diagram of reservoir grid system is illustrated by **Fig. B.1**.

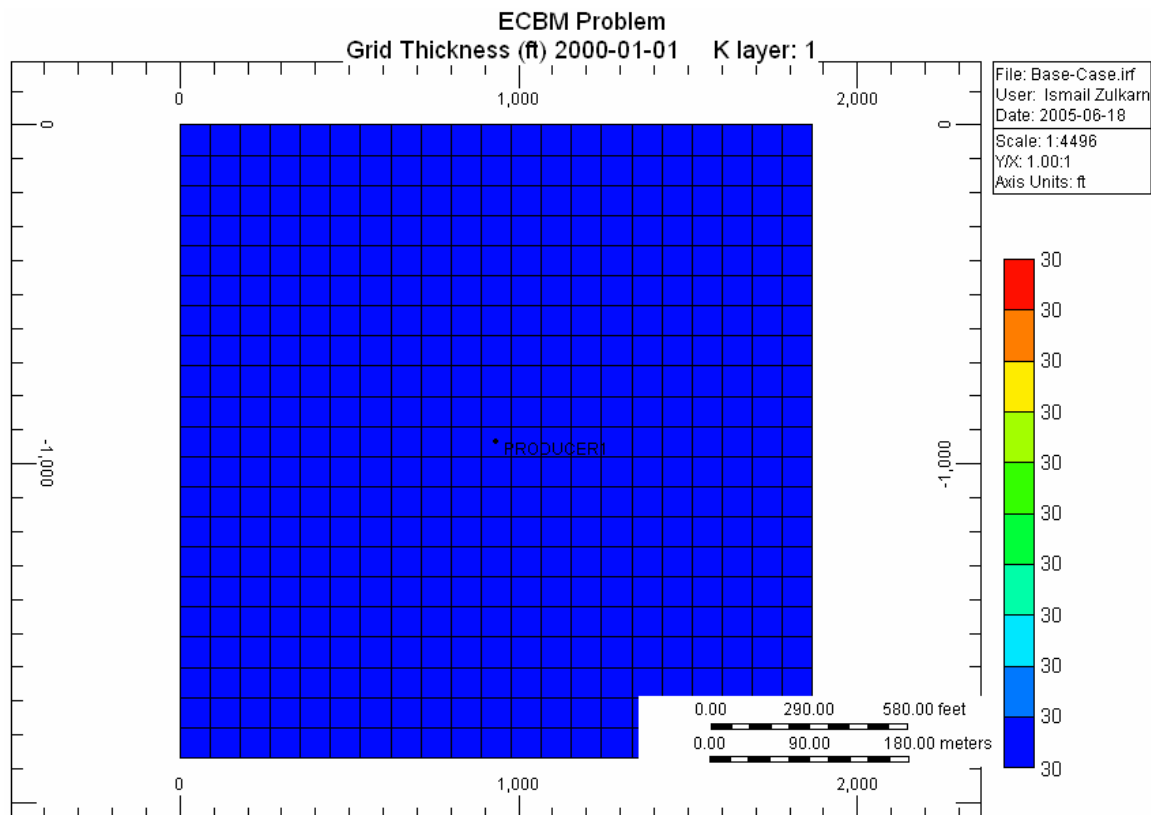


Fig. B.1—21*21 simulation model grid model. Reservoir thickness is 30 ft and drainage area is 80 acre (square).

B.2 Reservoir Data

```

RESULTS SIMULATOR GEM
RESULTS SECTION INOUT
*DIM *MAXPERCENT_OF_FULLYIMPLICITBLOCKS 100
*TITLE1 'ECBM Problem'
*INUNIT *FIELD
*INTERRUPT *INTERACTIVE
*RANGECHECK *ON
*XDR *ON
*MAXERROR 20
*WRST 0
*WPRN *WELL 5
*WPRN *GRID *TIME
*WSRF *WELL 5
*WSRF *GRID 1

```

*OUTPRN *WELL *ALL
 *OUTPRN *GRID PRES SW SG DENW DENG VISG ADS 'C1' Y 'C1'
 *OUTPRN *RES *ALL
 *OUTSRF *GRID PRES SW SG DENW DENG VISG ADS 'C1' Y 'C1'
 *OUTSRF *RES *ALL

****Reservoir Dimension:**

GRID CART 21 21 1
 KDIR DOWN
 *DI *CON 88.89342392
 *DJ *CON 88.89342392
 DK CON 30
 PAYDEPTH ALL
 441*3280.84

****Dual porosity option:**

DUALPOR
 NULL MATRIX CON 1.
 NULL FRACTURE CON 1.
 PINCHOUTARRAY CON 1.
 RESULTS SECTION GRID
 RESULTS SECTION NETPAY
 RESULTS SECTION NETGROSS
 RESULTS SECTION POR

****Porosity data :**

POR MATRIX CON 0.005
 POR FRACTURE CON 0.001
 RESULTS SECTION PERMS

****Permeability data:**

PERMI MATRIX CON 0.0001
 PERMI FRACTURE CON 1
 PERMJ MATRIX CON 0.0001
 PERMJ FRACTURE CON 1
 PERMK MATRIX CON 0.0001
 PERMK FRACTURE CON 1
 RESULTS SECTION TRANS
 RESULTS SECTION FRACS

****Fracture spacing data**

DIFRAC CON 0.042
 DJFRAC CON 0.042
 DKFRAC CON 0.042
 RESULTS SECTION GRIDNONARRAYS

****Compressibility data (matrix)**

CPOR MATRIX 100E-06
 PRPOR MATRIX 1109.54

****Compressibility data (fracture)**

CPOR FRACTURE 100E-06
 PRPOR FRACTURE 1109.54
 RESULTS SECTION VOLMOD
 RESULTS SECTION SECTORLEASE
 RESULTS SECTION ROCKCOMPACTION

RESULTS SECTION GRIDOTHER

RESULTS SECTION MODEL

****Methane and water data:**

```

*MODEL      *PR
*NC         1 1
*COMPNAME   'C1'
*HCFLAG     0
*VISCOR     *HZYT
*VISCOEFF   0.1023
            0.023364
            0.058533
            -0.040758
            0.0093324
*MIXVC      1
*TRES       113.**F
*PCRIT      45.400000
*TCRIT      190.60000
*AC         0.008000
*VCRIT      0.099000
*MW         16.04300
*PCHOR      77.00000
*SG         0.300000
*TB         -258.61000
*VISVC      0.099000
*VSHIFT     0.000000
*OMEGA      0.457235530
*OMEGB      0.077796074
**PVC3      1.2
*PHASEID    *DEN
**BIN
**          0.103
*DENW       62.4
*CW         3.99896E-06
*REFPW      14.69595
*VISW       0.607

```

RESULTS SECTION MODELARRAYS

RESULTS SECTION ROCKFLUID

****Rock fluid data**

```
*ROCKFLUID
```

****Matrix data:**

```
*RPT 1 *DRAINAGE
```

****Relative permeability of oil and water**

```

*SWT
** Sw      Krw      Krow
0.000000  0.000000  0.000010  0.000000
0.050000  0.000600  0.0000095  0.000000
0.100000  0.001300  0.000009  0.000000
0.150000  0.002000  0.0000085  0.000000
0.200000  0.007000  0.000008  0.000000
0.250000  0.015000  0.0000075  0.000000
0.300000  0.024000  0.000007  0.000000
0.350000  0.035000  0.0000065  0.000000
0.400000  0.049000  0.000006  0.000000

```

0.450000	0.067000	0.0000055	0.000000
0.500000	0.088000	0.000005	0.000000
0.550000	0.116000	0.0000045	0.000000
0.600000	0.154000	0.000004	0.000000
0.650000	0.200000	0.0000035	0.000000
0.700000	0.251000	0.000003	0.000000
0.750000	0.312000	0.0000025	0.000000
0.800000	0.392000	0.000002	0.000000
0.850000	0.490000	0.0000015	0.000000
0.900000	0.601000	0.000001	0.000000
0.950000	0.731000	0.0000005	0.000000
0.975000	0.814000	0.0000002	0.000000
1.000000	1.000000	0.000000	0.000000

****Relative permeability of oil and gas**

*SLT

** SI	Krg	Krog	
0.000000	1.000000	0.000000	0.000000
0.050000	0.835000	0.0000005	0.000000
0.100000	0.720000	0.000001	0.000000
0.150000	0.627000	0.0000015	0.000000
0.200000	0.537000	0.000002	0.000000
0.250000	0.466000	0.0000025	0.000000
0.300000	0.401000	0.000003	0.000000
0.350000	0.342000	0.0000035	0.000000
0.400000	0.295000	0.000004	0.000000
0.450000	0.253000	0.0000045	0.000000
0.500000	0.216000	0.000005	0.000000
0.550000	0.180000	0.0000055	0.000000
0.600000	0.147000	0.000006	0.000000
0.650000	0.118000	0.0000065	0.000000
0.700000	0.090000	0.000007	0.000000
0.750000	0.070000	0.0000075	0.000000
0.800000	0.051000	0.000008	0.000000
0.850000	0.033000	0.0000085	0.000000
0.900000	0.018000	0.000009	0.000000
0.950000	0.007000	0.0000095	0.000000
0.975000	0.003500	0.0000097	0.000000
1.000000	0.000000	0.000010	0.000000

****Langmuir adsorption isotherm data**

*ADSORBTMAX 'C1' 0.2268

*ADSTAB 'C1'

** Press Adsorp

0	0
29.00755	0.00872294
58.0151	0.0167997
87.0226	0.0242996
116.0302	0.0312822
145.0377	0.03779935
174.0453	0.043896
203.053	0.0496117
232.0604	0.0549808
261.068	0.0600343
290.0755	0.0647988
319.083	0.0692988

348.090	0.0735555
377.098	0.0775882
406.106	0.081414
435.113	0.0850486
464.121	0.0885059
493.128	0.0917985
522.136	0.094938
551.143	0.0979347
580.151	0.1007982
609.159	0.1035375
638.166	0.10616
667.174	0.1086732
696.181	0.111084
725.189	0.113398
754.196	0.1156216
783.204	0.1177596
812.211	0.119817
841.219	0.121798
870.226	0.123707
899.234	0.125548
928.242	0.1273243
957.25	0.1290393
986.257	0.130696
1015.26	0.1322978
1044.27	0.133847
1073.28	0.135346
1102.287	0.1367976
1131.29	0.138204
1160.30	0.1395668
1189.31	0.1408885
1218.31	0.1421708
1247.32	0.1434153
1276.33	0.144624
1305.34	0.1457978
1334.34	0.1469385
1363.35	0.1480476
1392.36	0.1491262
1421.37	0.1501758
1450.37	0.1511973

****Fracture data:**

*RPT 2 *DRAINAGE

****Relative permeability of oil and water**

*SWT

0.000000	0.000000	1.000000	0.000000
1.000000	1.000000	0.000000	0.000000

****Relative permeability of gas and water**

*SGT

0.010000	0.000000	1.000000	0.000000
1.000000	1.000000	0.000000	0.000000

****Relative permeability option**

*KROIL *STONE2 *SWSG

RESULTS SECTION ROCKARRAYS

****Specifying rock fluid data**

RTYPE MATRIX CON 1.
RTYPE FRACTURE CON 2.

****Rock density data**

ROCKDEN MATRIX CON 89.5841
ROCKDEN FRACTURE CON 89.5841

****Diffusion data**

COAL-DIF-TIME 'C1' MATRIX CON 100
RESULTS SECTION INIT

****Initial condition**

*INITIAL
*VERTICAL *BLOCK_CENTER *COMP
*NREGIONS 2
*REFDEPTH 3280.84 3280.84
*REFPRES 1109.54 725.189
*DWOC 328.084 328.084
*SWOC 0.9999 0.2
*CDEPTH 3.28051E+04 3.28051E+04
*ZDEPTH
1 3280.84 1
2 3280.84 1
*SEPARATOR
14.69595 59
RESULTS SECTION INITARRAYS
ITYPE MATRIX CON 2.
ITYPE FRACTURE CON 1.
RESULTS SECTION NUMERICAL

****Numerical data**

*NUMERICAL
*DTMAX 365.
*DTMIN 0.01
*CONVERGE *PRESS 0.514884
RESULTS SECTION NUMARRAYS
RESULTS SECTION GBKEYWORDS
RUN

****Simulation******start date**

DATE 2000 01 01
DTWELL 1.E-06
*DTMIN 1.E-07

**\$ RESULTS PROP AIMSET FRACTURE Units: Dimensionless
**\$ RESULTS PROP Minimum Value: 3 Maximum Value: 3
AIMSET FRACTURE CON 3.
**\$ RESULTS PROP AIMSET MATRIX Units: Dimensionless
**\$ RESULTS PROP Minimum Value: 3 Maximum Value: 3
AIMSET MATRIX CON 3.

****Well data**

WELL 1 'PRODUCER1'
PRODUCER 'PRODUCER1'

****Production constraint**

OPERATE MAX STW 512 CONT
OPERATE MIN BHP 50.650377 CONT

****Well description**

GEOMETRY K 0.11975 0.37 1.0 0.
PERF GEO 'PRODUCER1'
11 11 1 1. OPEN FLOW-TO 'SURFACE'

****Time step**

TIME 0.1
TIME 3750
STOP

***** TERMINATE SIMULATION*****

RESULTS SECTION WELLDATA
RESULTS SECTION PERFS

APPENDIX C

MODULI DEFINITIONS

C.1. Young's Modulus of Elasticity

Young's modulus is defined as the ratio between axial stress and strain. It describes the elastic nature of a given substance and can conveniently describe the amount of deformation of a given object when a given stress is applied. Often this is referred to as the "stiffness" of a material. The greater the value of the modulus, the less deformation occurs at a given pressure. Several examples of different moduli values are = high strength concrete is (4.5E6 psi) and a more ductile material such as polystyrene (0.45E6 psi).

Where:

E = Young's Modulus (psia)

ϵ = strain (dimensionless)

σ = stress (psia)

C.2. Constrained Axial Modulus

Constrained axial modulus is defined as the ratio between axial stress and strain, but strain in only one axis is allowed. The compressed material is bounded on the sides, but not in the direction force is applied, as in the following diagram.

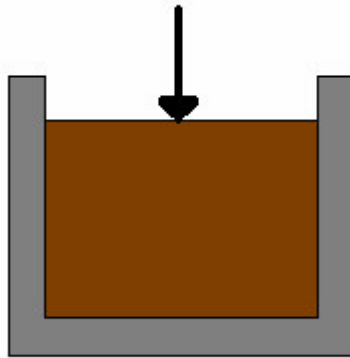


Fig. C.1—Schematic of axial modulus.

C.3. Bulk Modulus

Bulk modulus is the ratio of the change in pressure to the fractional volume compression of the material. For example the bulk modulus for steel is 160E9 Pa while water is at 2.2E9 Pa. Therefore in an environment where the pressure is 2.2E7 Pa, we would expect the fractional change in water to be 1.0%.

C.4. Poisson's Ratio (ν)

Poisson's ratio relates changes in size of an object along different axes. When compressive force is applied to a particular axis of a material, there will be tensile deformation along a different axis than from which the force was applied. Poisson's ratio is the ratio of contraction strain to extension strain. To give the value a direction, positive is said to be when strain occurs in the direction of a stretching force.



Fig. C.2—Schematic of Poisson's ratio.

APPENDIX D
INPUT DATA FOR CLEATS COMPRESSION AND MATRIX SHRINKAGE
MODEL (PALMER AND MANSOORI THEORY)

D.1 Input Data

Palmer and Mansoori model is a built in feature of coal bed methane simulation on CMG-GEM. It needs no specific keyword to activate this feature.

The following input data should be added to the CMG input data previously mentioned in the Appendix B.2.

****Input data for matrix system**

*CROCKTYPE 1
 *CCPOR *MATRIX 10E-07
 *CPRPOR *MATRIX 1109.54

****Palmer and Mansoori Model input data**

*POISSR 0.39
 *YOUNGM 3000000
 *STRINF 0.01
 *PRESLN 725.189
 *EXPPM 3.0

****Input data for Fracture system**

*CROCKTYPE 2
 *CCPOR *MATRIX 10E-07
 *CPRPOR *MATRIX 1109.54

****There is no Palmer and Mansoori input data for fracture system**

****Specifying Input data for fracture system and matrix system**

*CTYPE *FRACTURE *IJK 1:21 1:21 1:1 1
 *CTYPE *MATRIX *IJK 1:21 1:21 1:1 2

There are two ways to input the formation compressibility in the CMG input data, they are:

1. Using CPOR keyword and PRPOR keyword. CPOR is the input data for formation compressibility and PRPOR is the input data for reference pressure of the formation compressibility.
2. Using CROCKTYPE keyword. This keyword must be followed by CCPOR keyword for the formation compressibility and CPRPOR keyword for the reference pressure of the formation compressibility.

If *CROCKTYPE does appear, settings for *CPOR and *PRPOR will be mostly ignored. Therefore, blocks that are not assigned compressibilities using the *CCPOR/*CPRPOR subkeywords of *CROCKTYPE will end up with no compressibility values at all.

In the case we activate the Palmer and Mansoori model using POISSR, YOUNGM, STRINF, PRESLN, and EXPPM the use of CCPOR and CPRPOR are ignored. The formation compressibility will depend on the Palmer and Mansoori model. The formation compressibility will be calculate using the following equations.

$$M = E \frac{1 - \nu}{(1 + \nu)(1 - 2\nu)} \dots\dots\dots D.1$$

Where E is the Young's modulus (kPa or psia) and

$$c_f = \frac{1}{\phi_i M} \dots\dots\dots D.2$$

In the situation when we activate the Palmer and Mansoori model, CCPOR and CPRPOR keyword will be ignored but these keywords still required. We can input any number for the CCPOR and CPRPOR.

D.2 Effect of Formation Compressibility

D.2.1 Case With Palmer and Mansoori Model

In the case we activate the Palmer and Mansoori model using POISSR, YOUNGM, STRINF, PRESLN, and EXPPM the use of CCCPOR and CPRPOR are ignored. The formation compressibility will depend on the Palmer and Mansoori model. The formation compressibility will be calculated using the following equations instead of using the input data from CCPOR and CPRPOR.

$$M = E \frac{1 - \nu}{(1 + \nu)(1 - 2\nu)} \dots\dots\dots D.1$$

Where E is the Young's modulus (kPa or psia) and

$$c_f = \frac{1}{\phi_i M} \dots\dots\dots D.2$$

In the situation when we activate the Palmer and Mansoori model, CCPOR and CPRPOR keyword will be ignored but these keywords still required. We can input any number for the CCPOR and CPRPOR.

The following figures show that the changes in the formation permeability will have no effect on production performance. The figures prove that the use of CCPOR and CPRPOR are ignored.

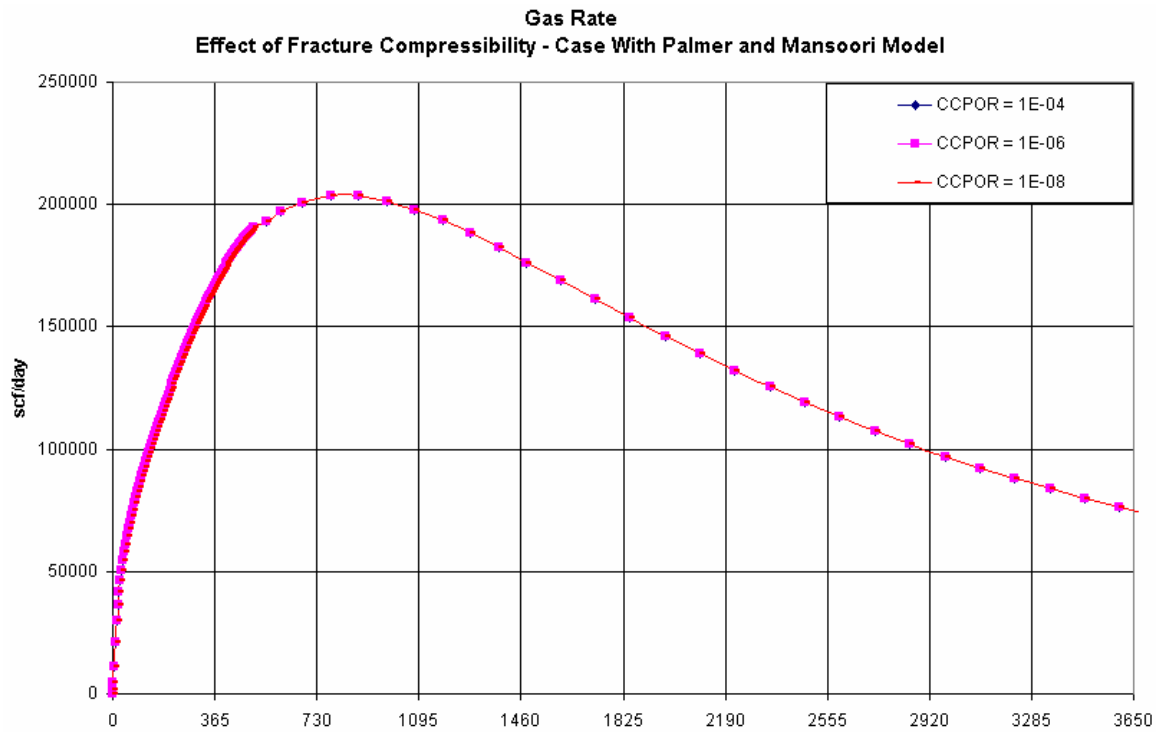


Fig. D.1—For cases with Palmer and Mansoori model, changes in fracture compressibility result in no changes in gas production rate.

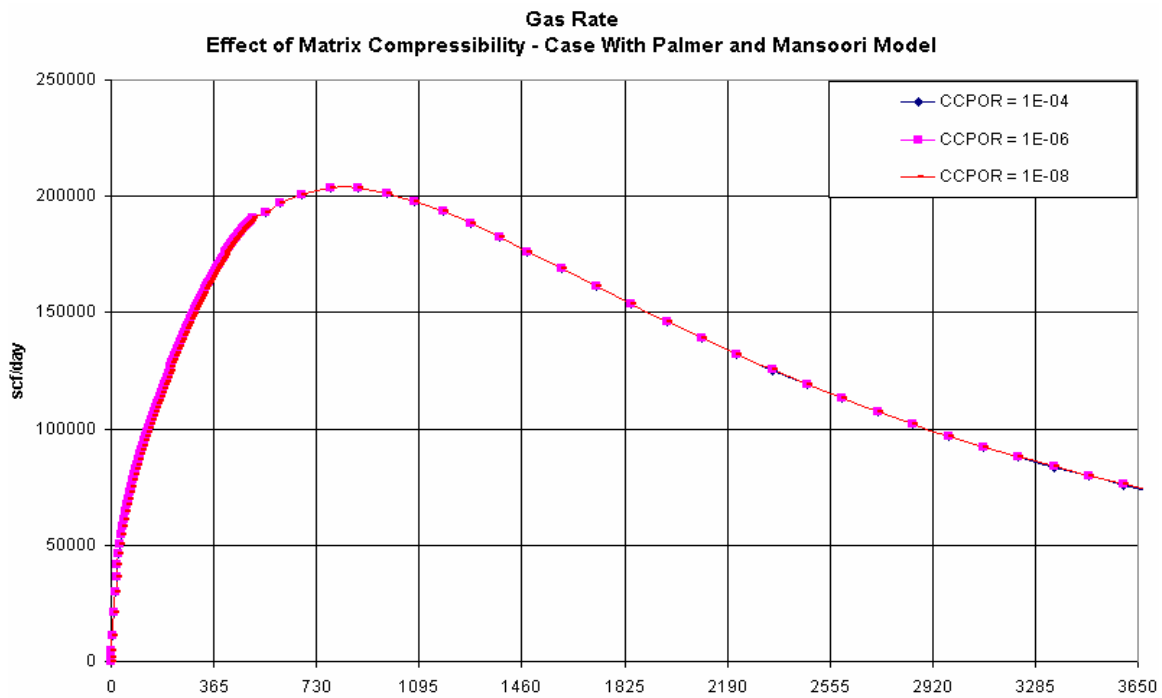


Fig. D.2—For cases with Palmer and Mansoori model, changes in matrix compressibility result in no changes in gas production rate.

D.2.1 Case Without Palmer and Mansoori Model

For cases without Palmer and Mansoori model, changes in matrix compressibilities result in no effect on gas production rate. However, changes in fracture compressibility result in a small effect on gas production rate.

The following figures show the effect of formation compressibility on production performance.

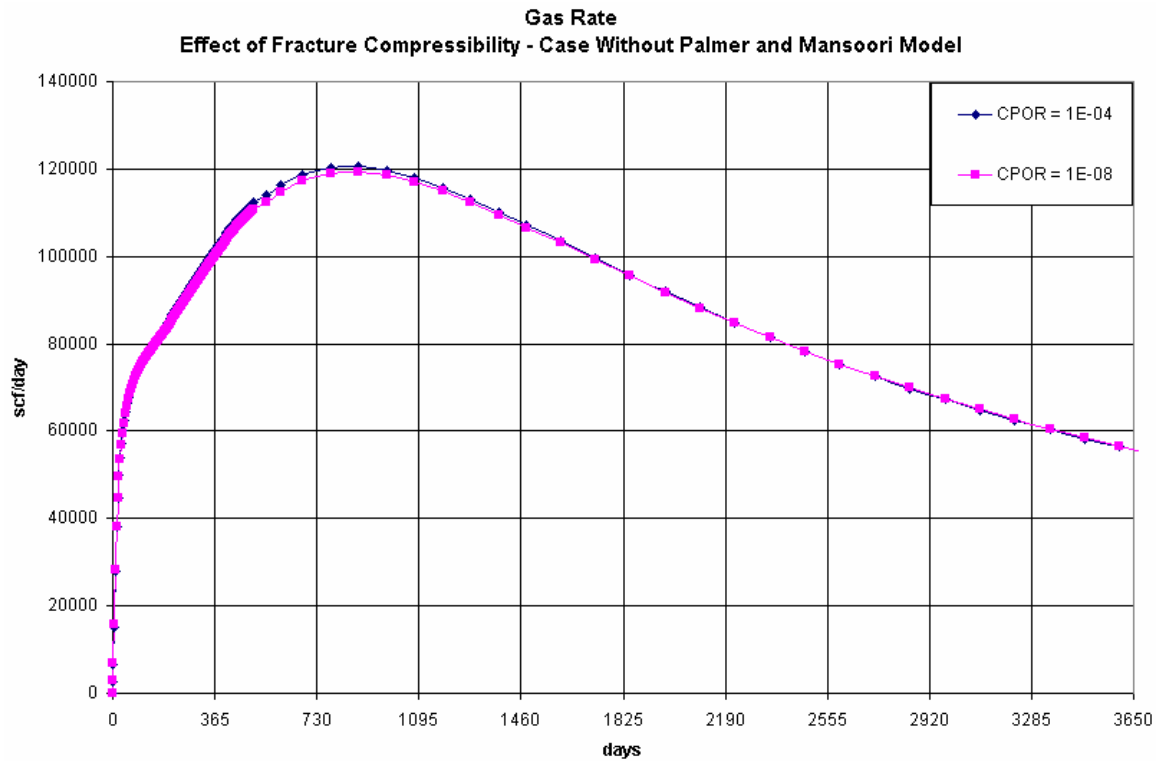


Fig. D.3—For cases without Palmer and Mansoori model, changes in fracture compressibility result in small changes in gas production rate.

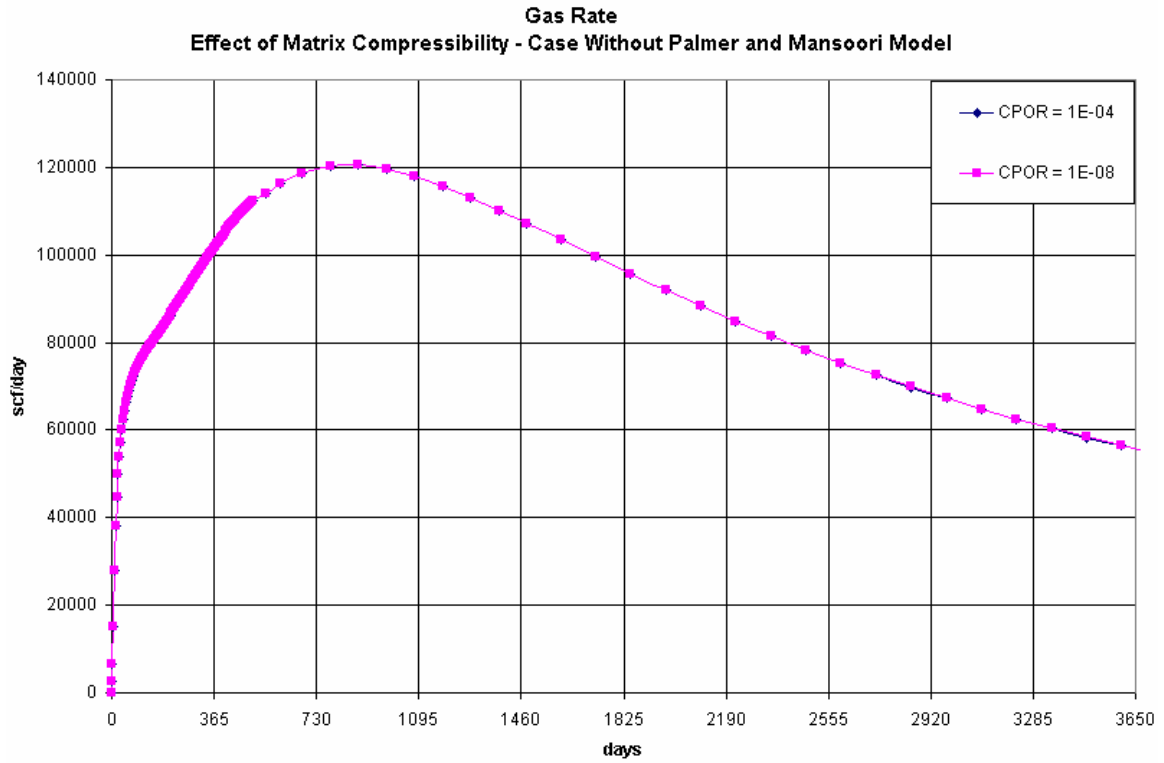


Fig. D.4—For cases without Palmer and Mansoori model, changes in matrix compressibility result in no changes in gas production rate.

APPENDIX E
SIMULATION RESULTS

E.1 Interference Effects

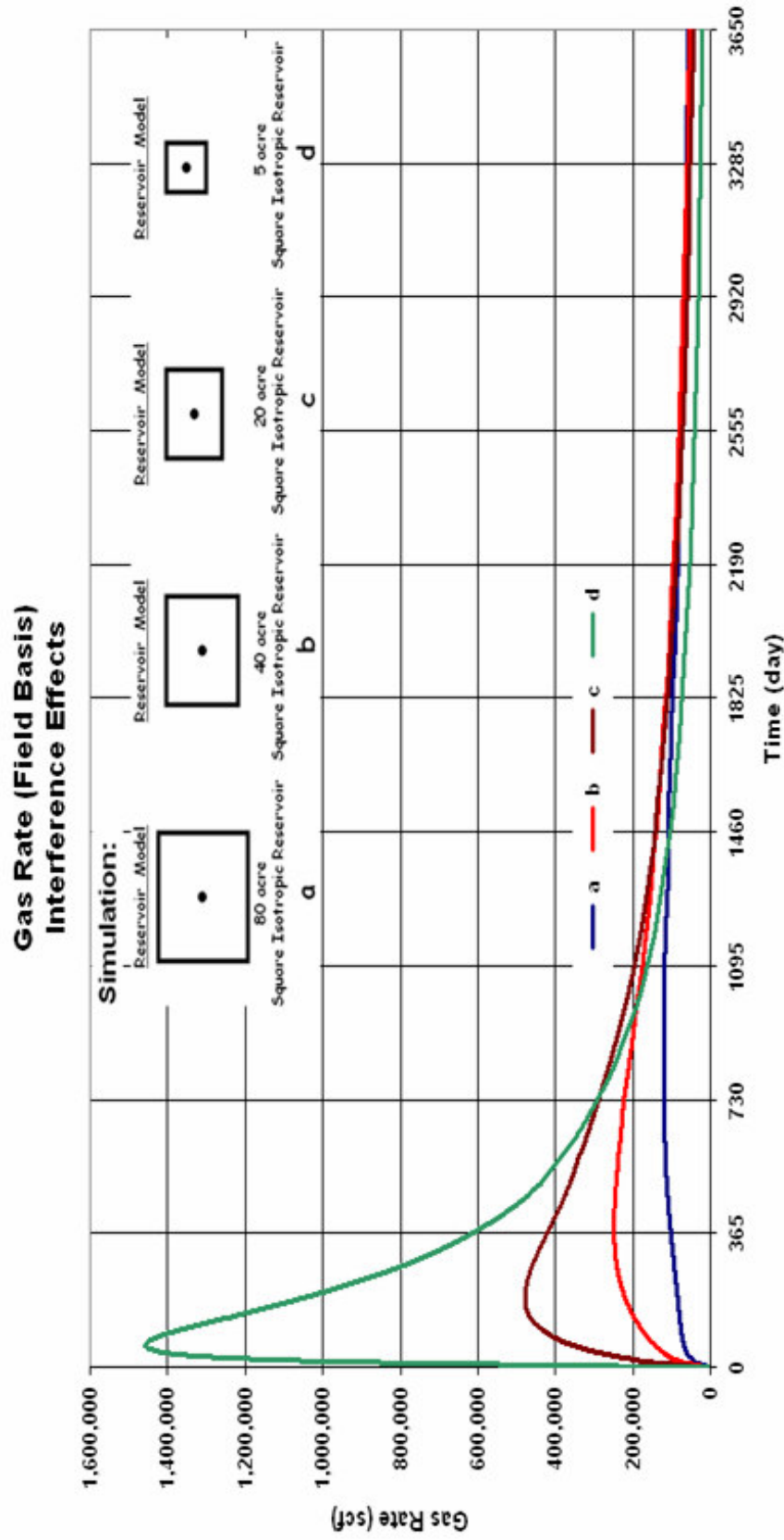


Fig. E.1—Comparison of total gas rates for various well spacings in an 80 acre reservoir. Each well is centered in its square drainage area. More wells (closer spacing) give higher early rates but then their rates become lower after a 2 to 4 years.

Water Rate (Field Basis) Interference Effects

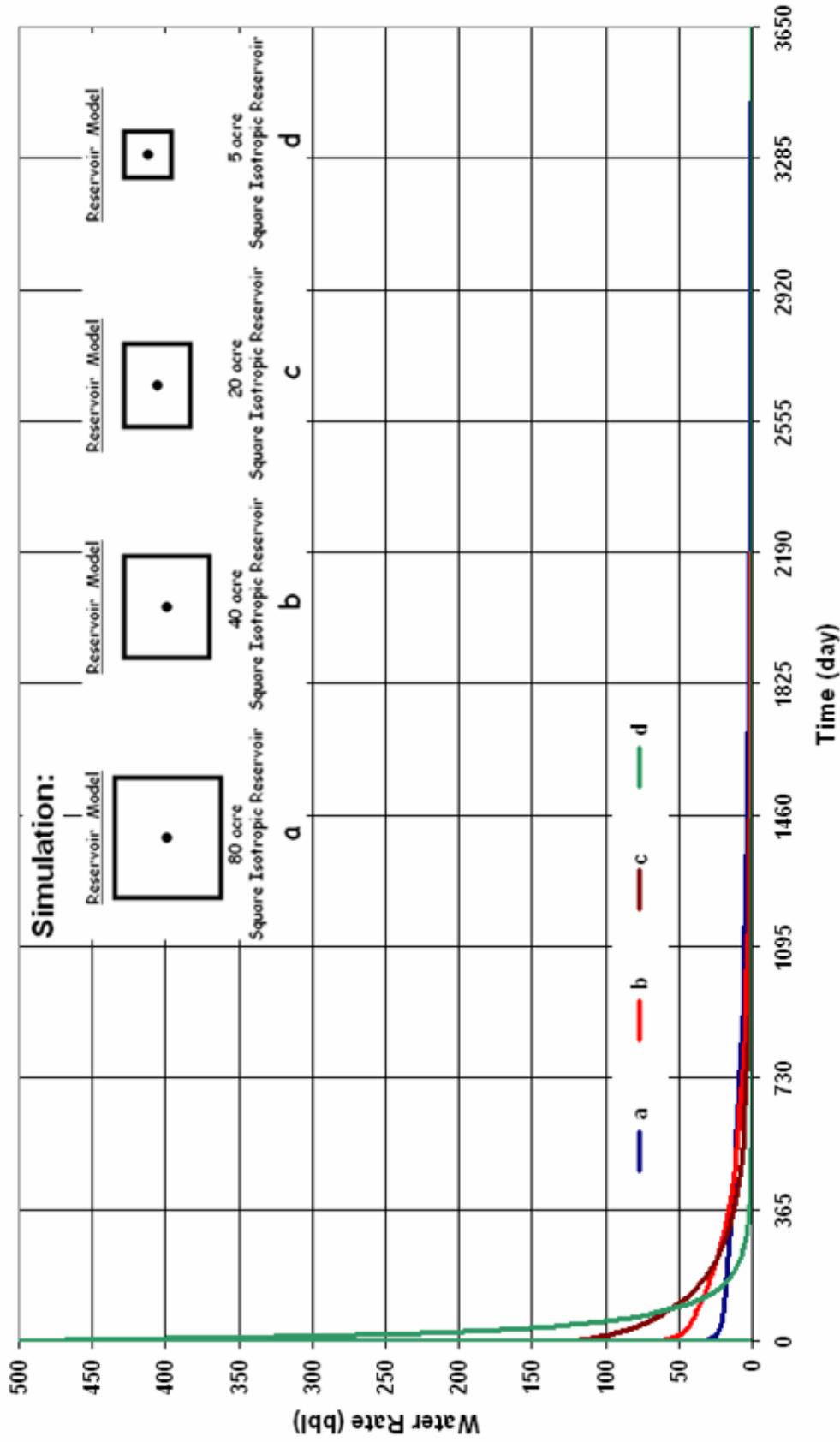


Fig. E.2—Comparison of total water rates for various well spacings in an 80 acre reservoir. Each well is centered in its square drainage area. More wells (closer spacing) give higher early rates but then their rates become lower after a half to 2 years.

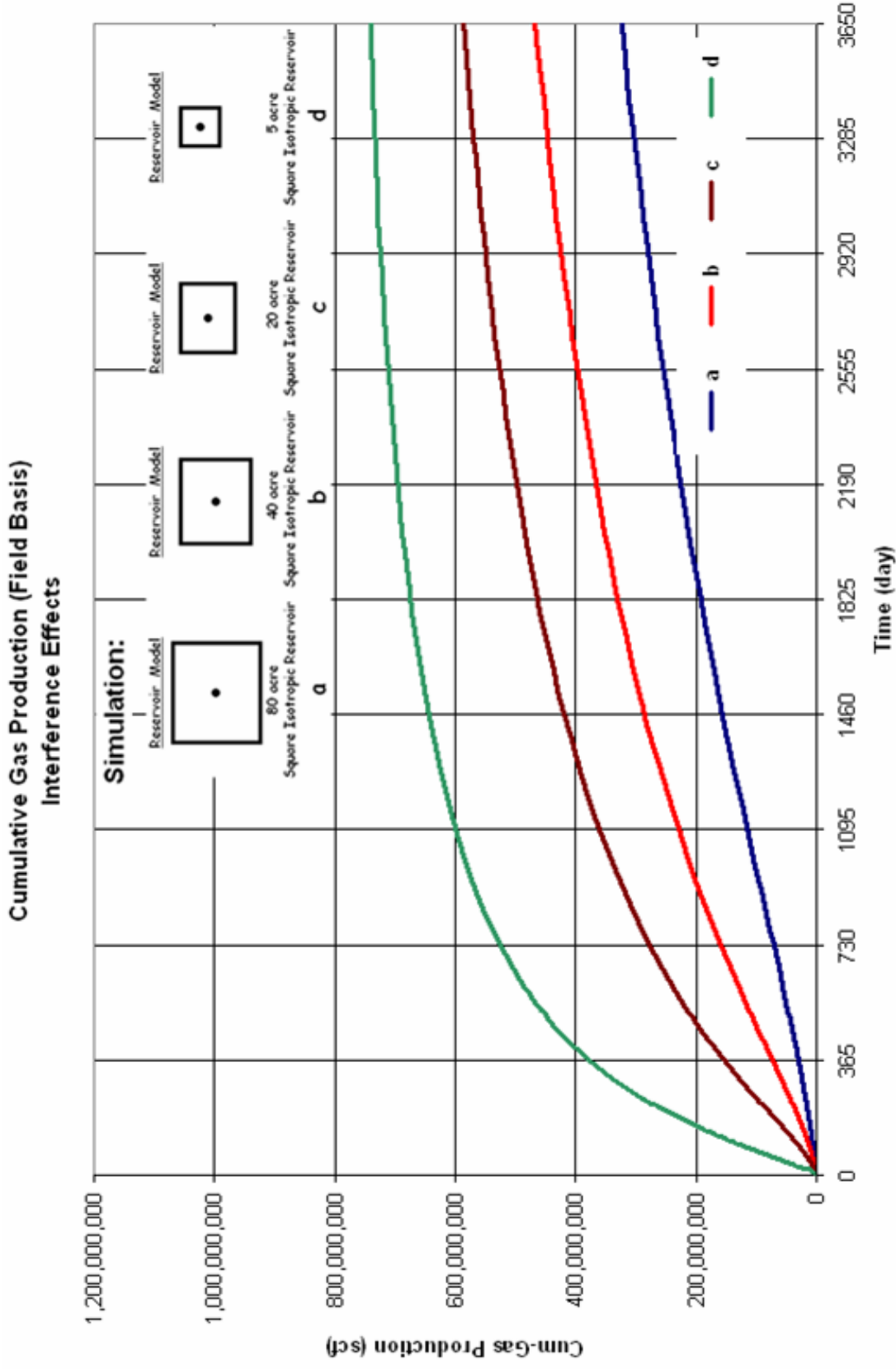


Fig. E.3—Comparison of cumulative gas production for various well spacings in an 80 acre reservoir. Each well is centered in its square drainage area. More wells (closer spacing) accelerates gas production. Closer spacing also produces higher cumulative recovery factor in the ten years simulation.

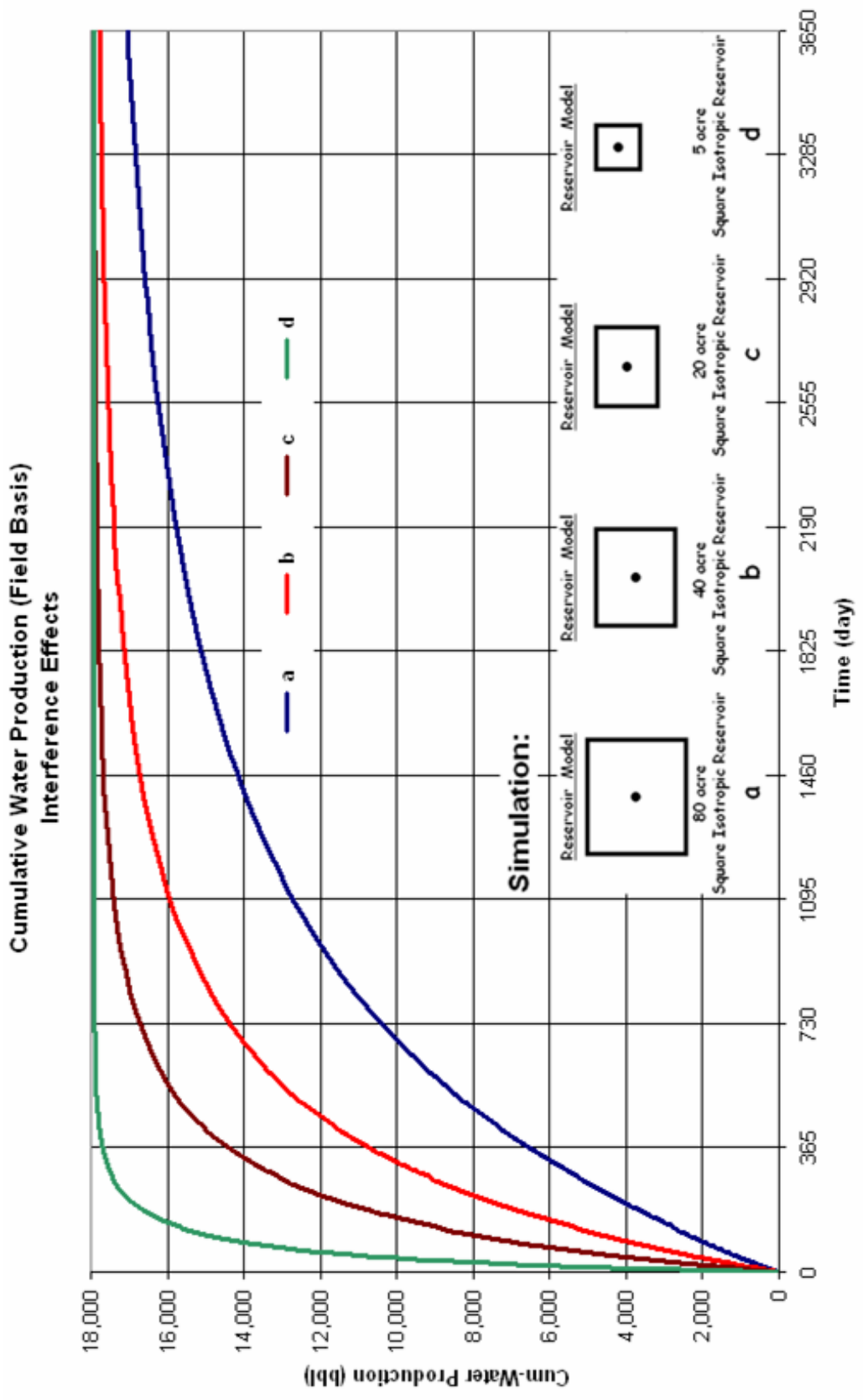


Fig. E.4—Comparison of cumulative water production for various well spacings in an 80 acre reservoir. Each well is centered in its square drainage area. More wells (closer spacing) accelerates water production but eventually three of various well-spacings produce the same recovery factor in the tenth years simulation.

RF Gas (Field Basis) Interference Effects

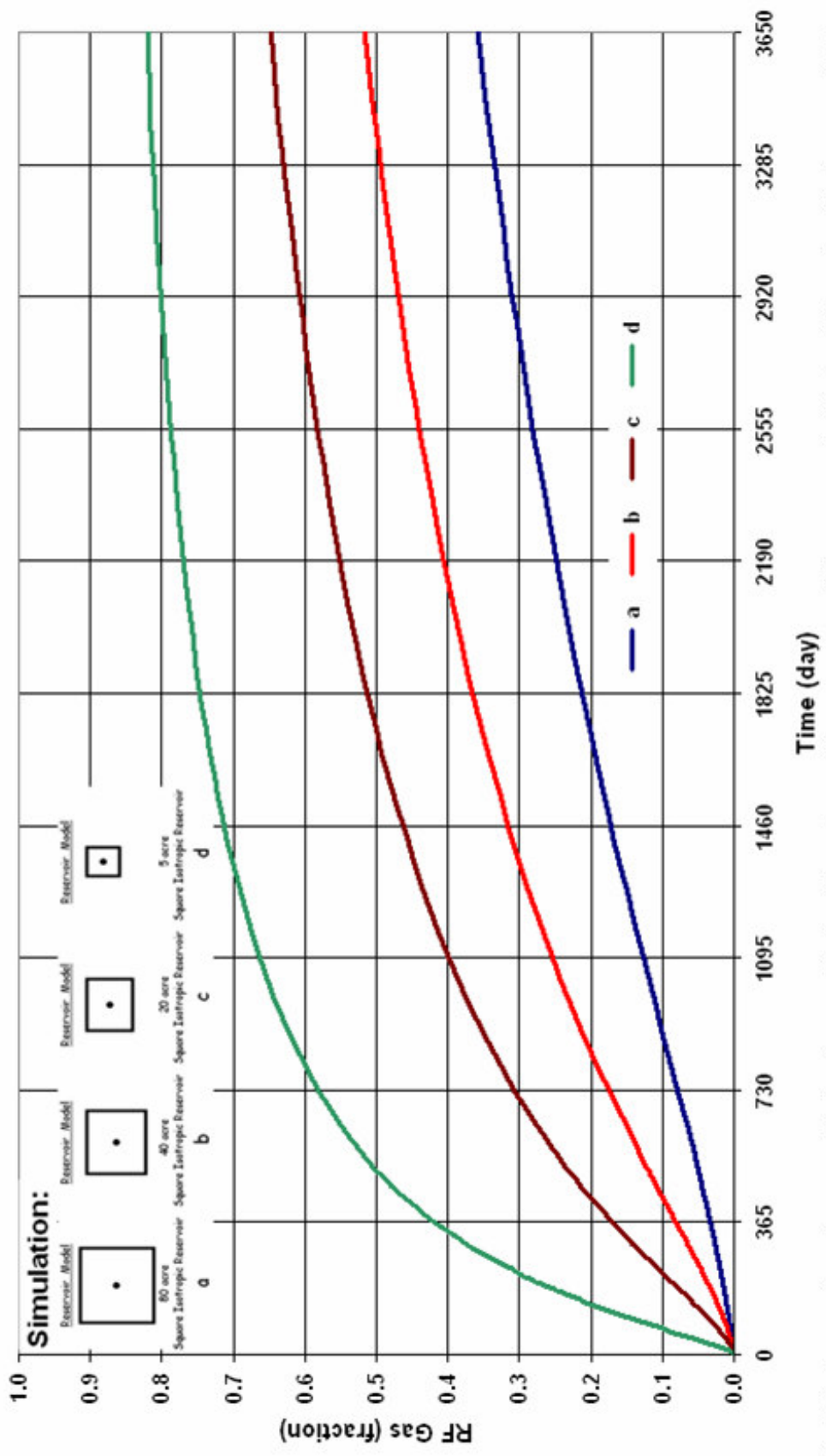


Fig. E.5—Comparison of recovery factor for various well spacings in an 80 acre reservoir. Each well is centered in its square drainage area. More wells (closer spacing) accelerates gas production. Closer spacing also produces higher cumulative recovery factor in the ten years simulation.

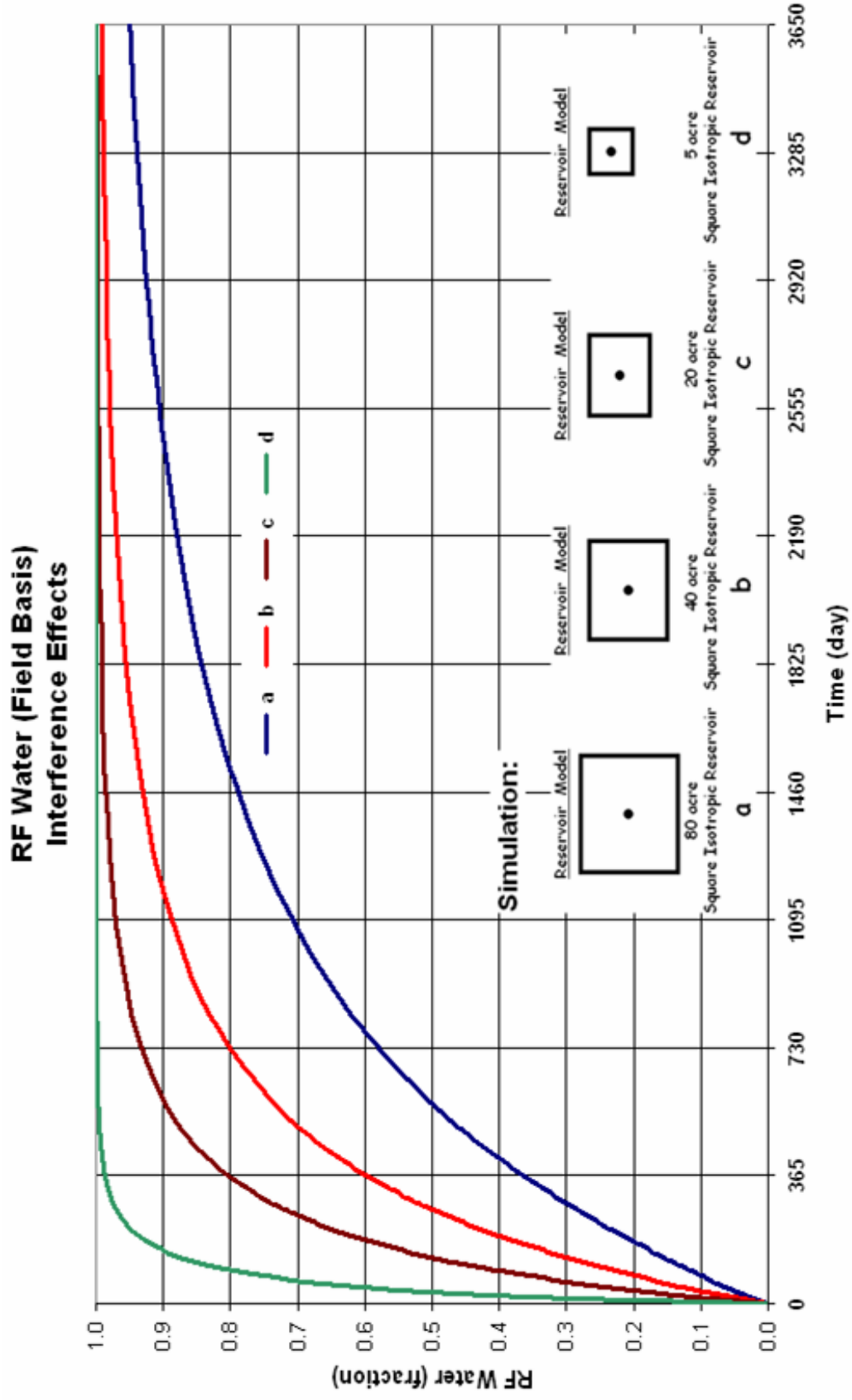


Fig. E.6—Comparison of recovery factor of water production for various well spacings in an 80 acre reservoir. Each well is centered in its square drainage area. More wells (closer spacing) accelerates water production but eventually three of various well-spacings produce the same recovery factor in the tenth years simulation.

TABLE E.1 - COMPARISON OF RESULTS FOR VARIOUS WELL SPACINGS					
		<i>OGIP</i> =	9.04E+08		<i>scf</i>
		<i>OWIP</i> =	1.79E+04		<i>stb</i>
No.	Type of simulation	Cum. Gas Production (scf)	Cum. Water Production (stb)	RF Gas	RF Water
1	80 acre	3.28E+08	17077.5	36.27%	95.24%
2	40 acre	4.71E+08	17783.3	52.09%	99.17%
3	20 acre	5.89E+08	17914.2	65.15%	99.90%
4	5 acre	7.43E+08	17931.7	82.23%	100.00%

E.2 Permeability Anisotropy
 E.2.1 20 Acre Spacing

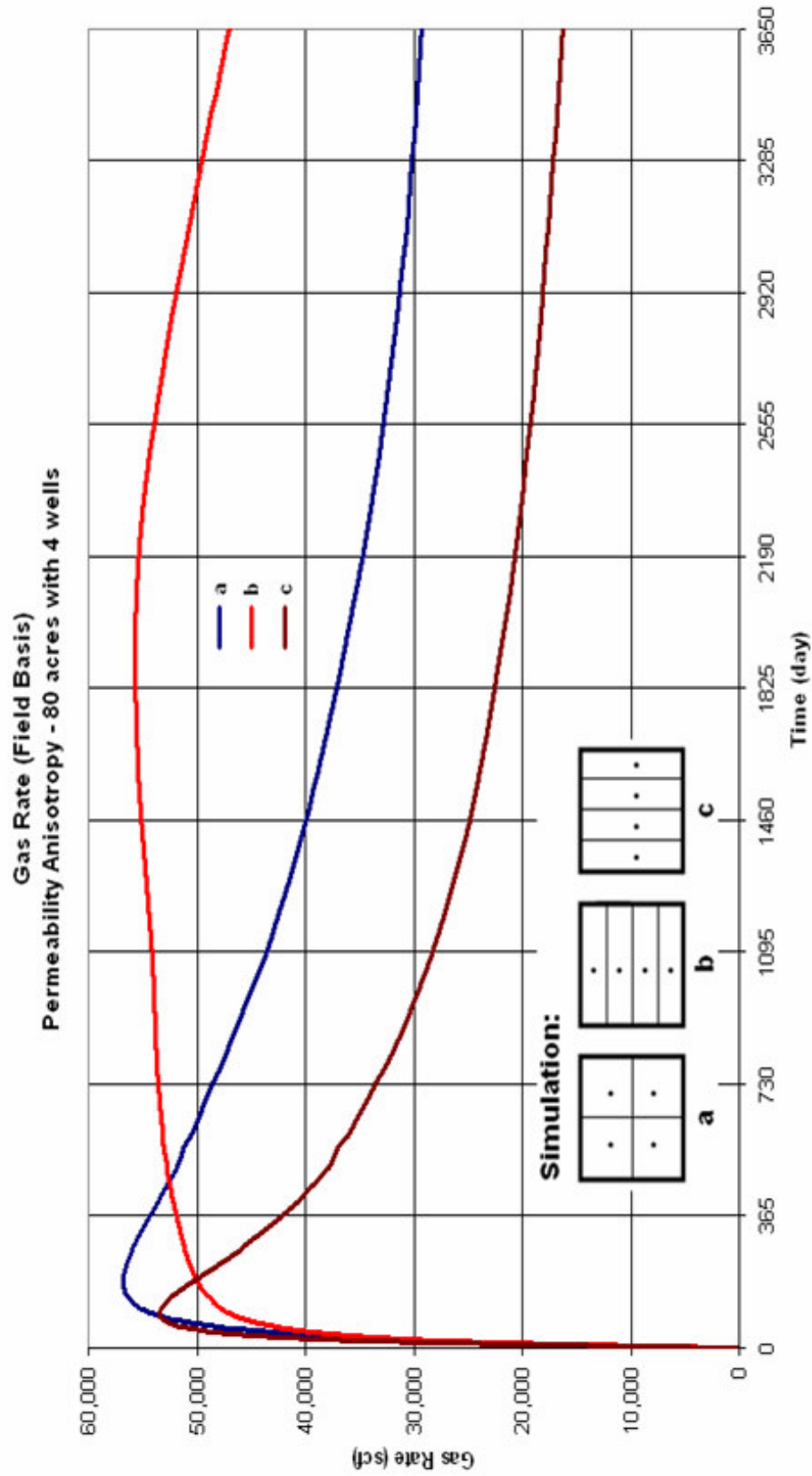


Fig. E.7—Comparison of gas rates for three types of well configurations for wells with 20 acre drainage area. Reservoir is anisotropic, $k_x = 1 \text{ md}$ and $k_y = 0.01 \text{ md}$. Configuration type b gives the highest gas rate for most of ten years simulation and type c gives the lowest.

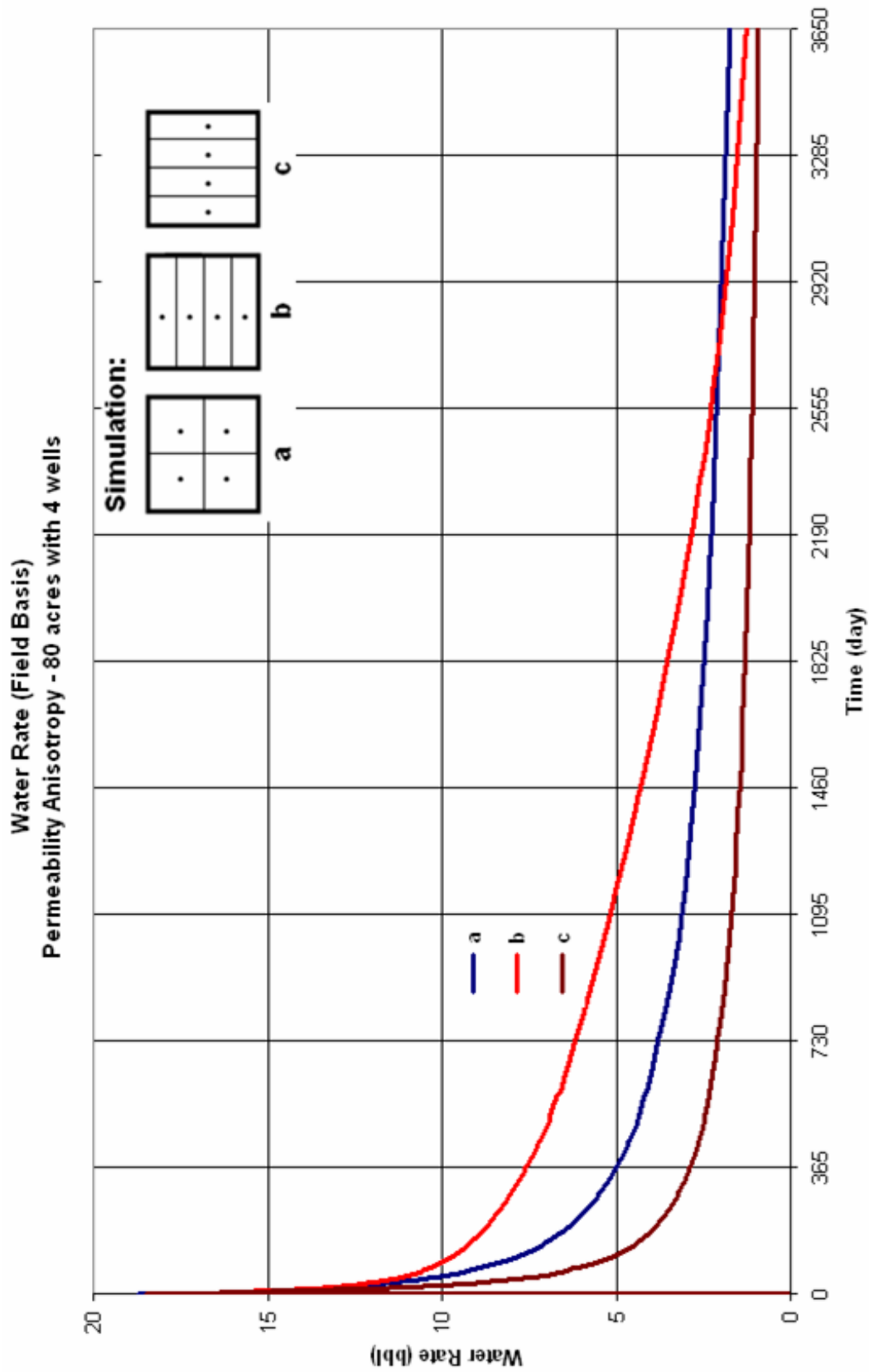


Fig. E.8—Comparison of water rates for three types of well configurations for wells with 20 acre drainage area. Configuration type b gives the highest water rate for most of ten years simulation and type c gives the lowest.

RF Gas (Field Basis)
Permeability Anisotropy - 80 acres with 4 wells

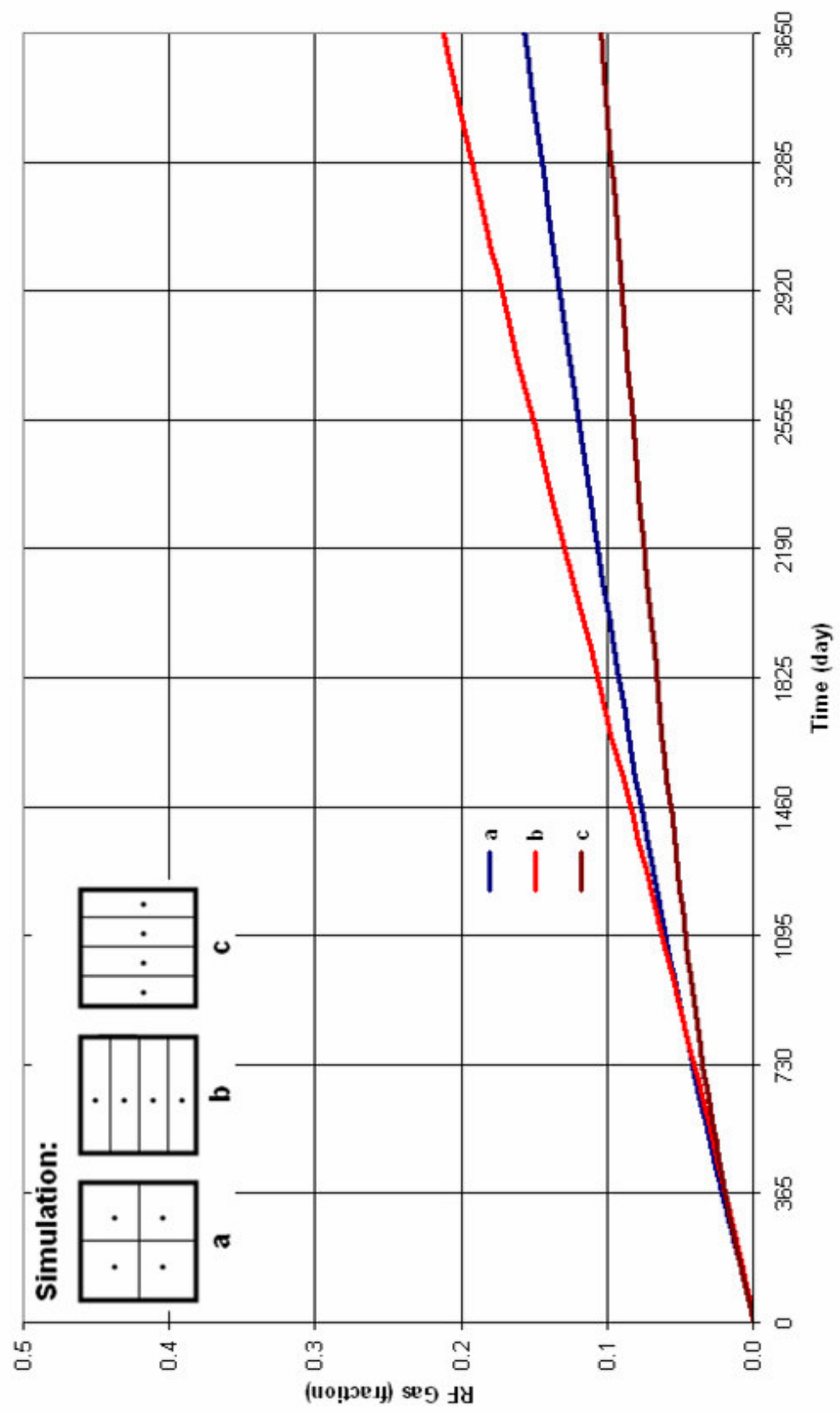


Fig. E.9—Comparison of recovery factor of gas production for three types of well configurations for wells with 20 acre drainage area. Configuration type b gives the highest cumulative production for ten years simulation and type c gives the lowest.

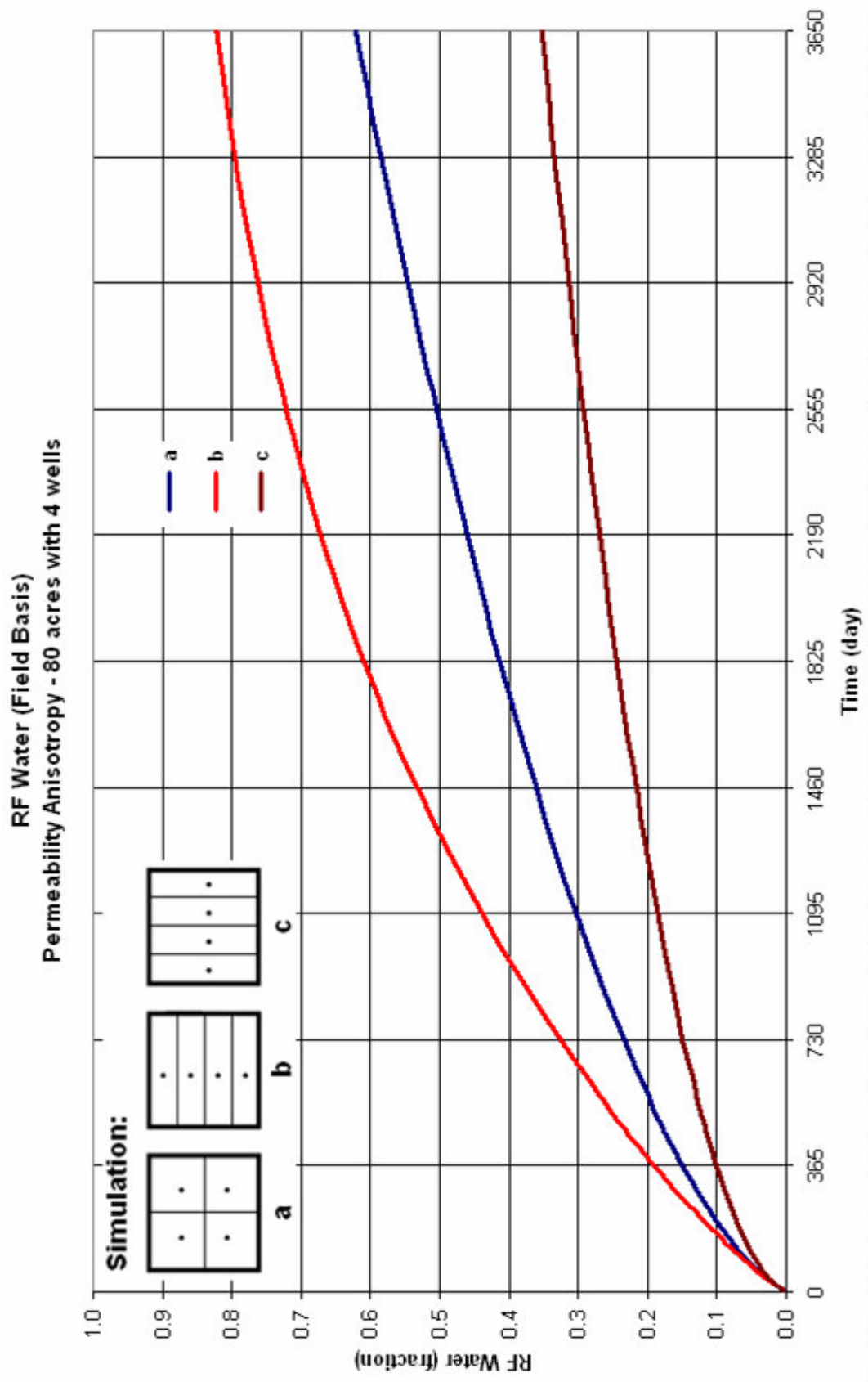


Fig. E.10—Comparison of recovery factor of water production for three types of well configurations for wells with 20 acre drainage area. Configuration type b gives the highest cumulative production for ten years simulation and type c gives the lowest. Configuration type b accelerates dewatering of the CBM reservoir.

TABLE E.2 COMPARISON RESULTS FOR VARIOUS WELL CONFIGURATIONS – 20 ACRE SPACING					
<i>OGIP</i> = 9.04E+08 <i>Scf</i> <i>OWIP</i> = 1.79E+04 <i>Stb</i>					
No.	Type of simulation	Cum. Gas Production (scf)	Cum. Water Production (stb)	RF Gas	RF Water
1	Type A	1.44E+08	11255.9	15.92%	62.77%
2	Type B	1.95E+08	14838.3	21.58%	82.75%
3	Type C	9.48E+07	6400.76	10.49%	35.70%

E.2.2 5 Acre Spacing

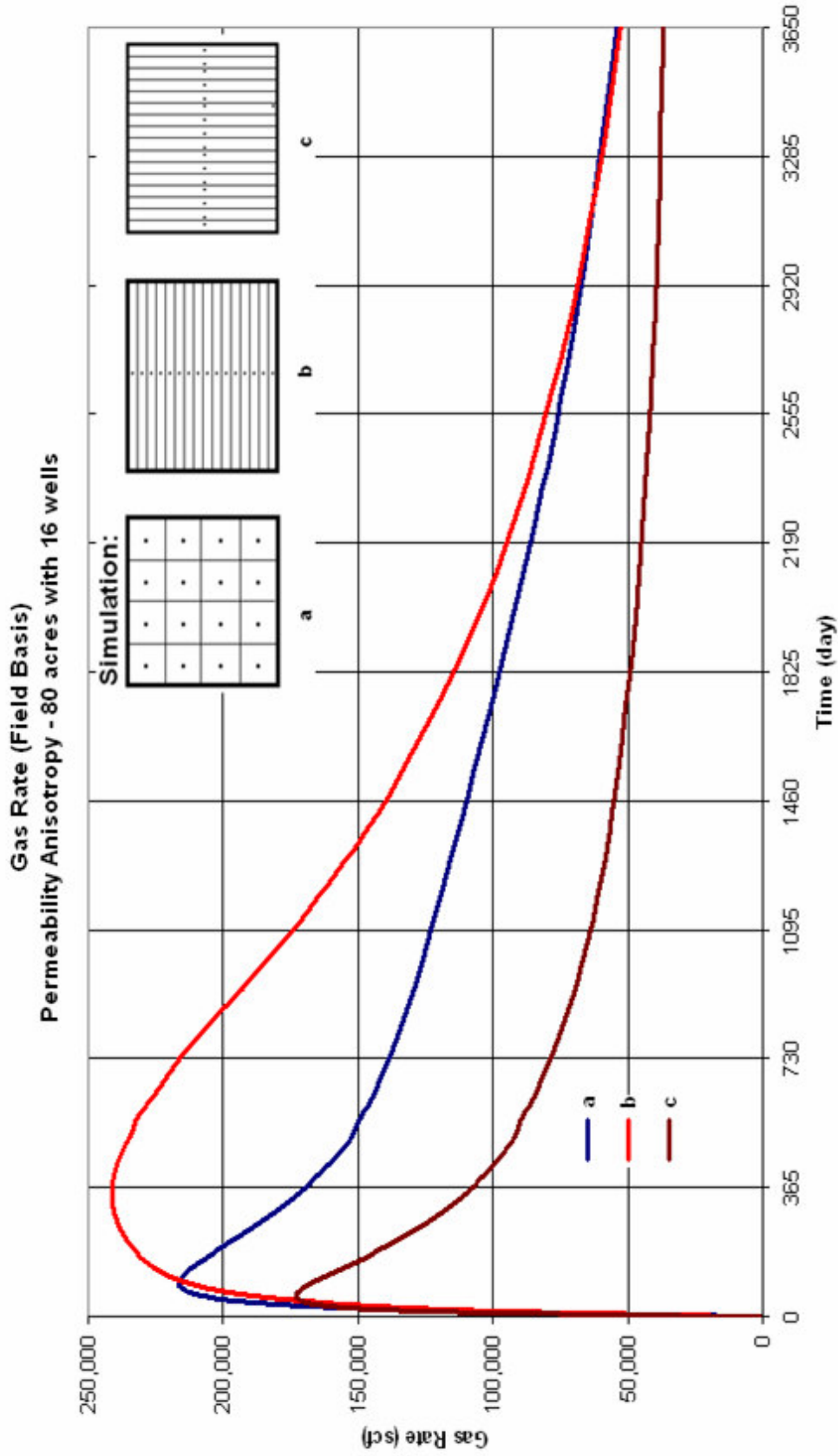


Fig. E.1.1—Comparison of gas rates for three types of well configurations for wells with 5 acre drainage area a. Reservoir is anisotropic, $k_x = 1 \text{ md}$ and $k_y = 0.01 \text{ md}$. Configuration type b gives the highest gas rate for most of ten years simulation and type c gives the lowest.

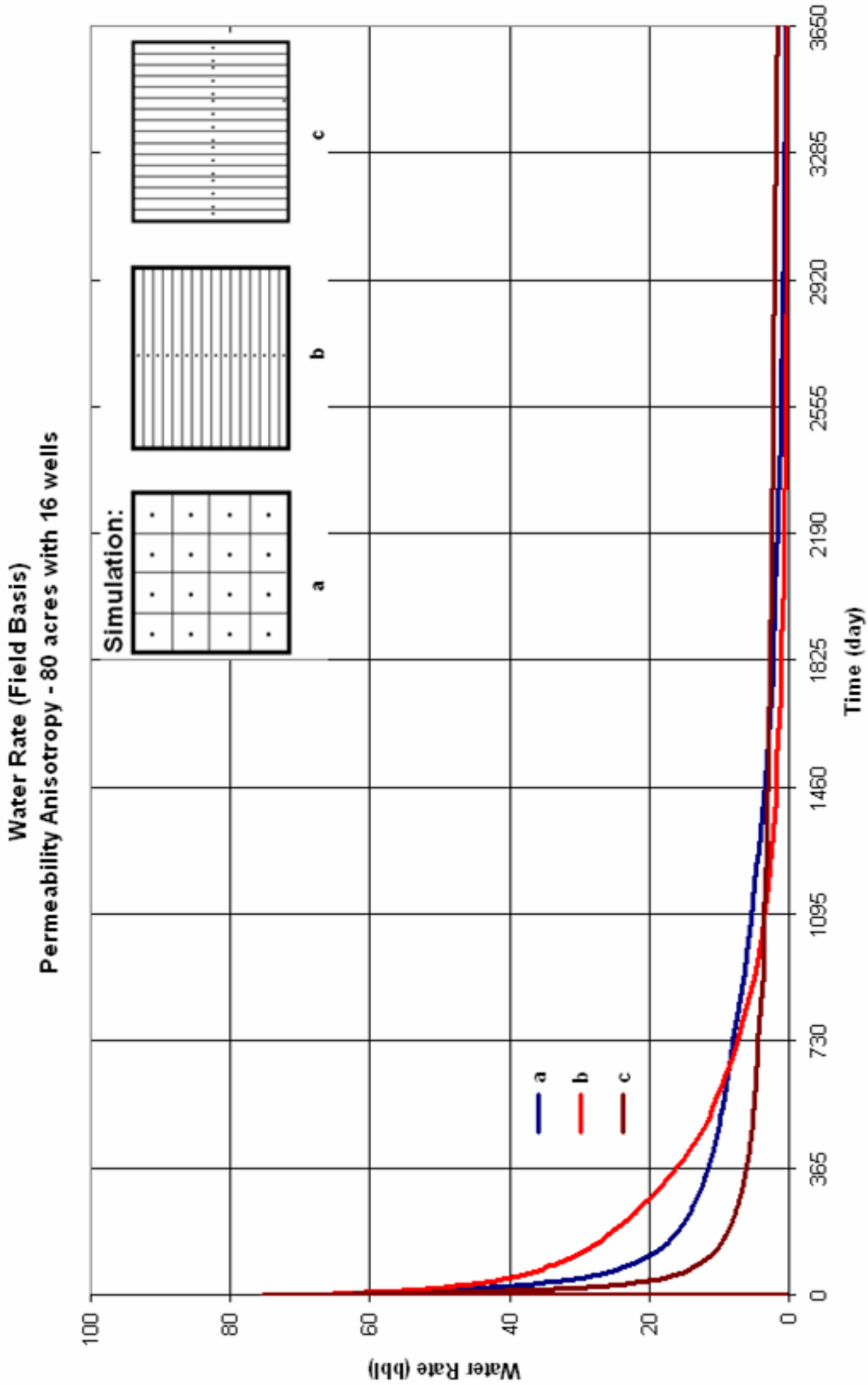


Fig. E.12—Comparison of water rates for three types of well configurations for wells with 5 acre drainage area. Configuration type b gives the highest water rate for most of ten years simulation and type c gives the lowest.

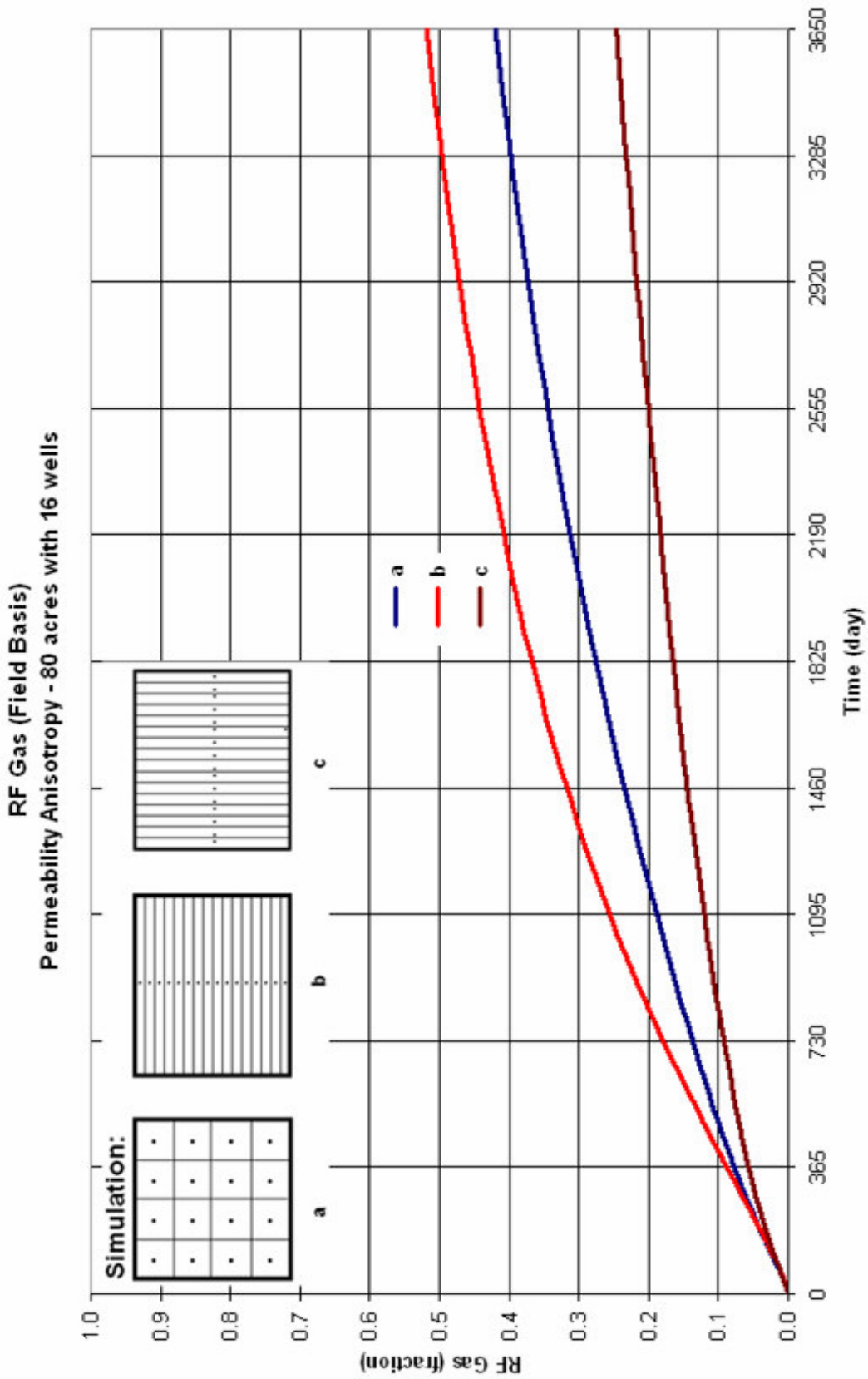


Fig. E.13—Comparison of recovery factor of gas production for three types of well configurations for wells with 5 acre drainage area. Configuration type **b** gives the highest cumulative production for ten years simulation and type **c** gives the lowest.

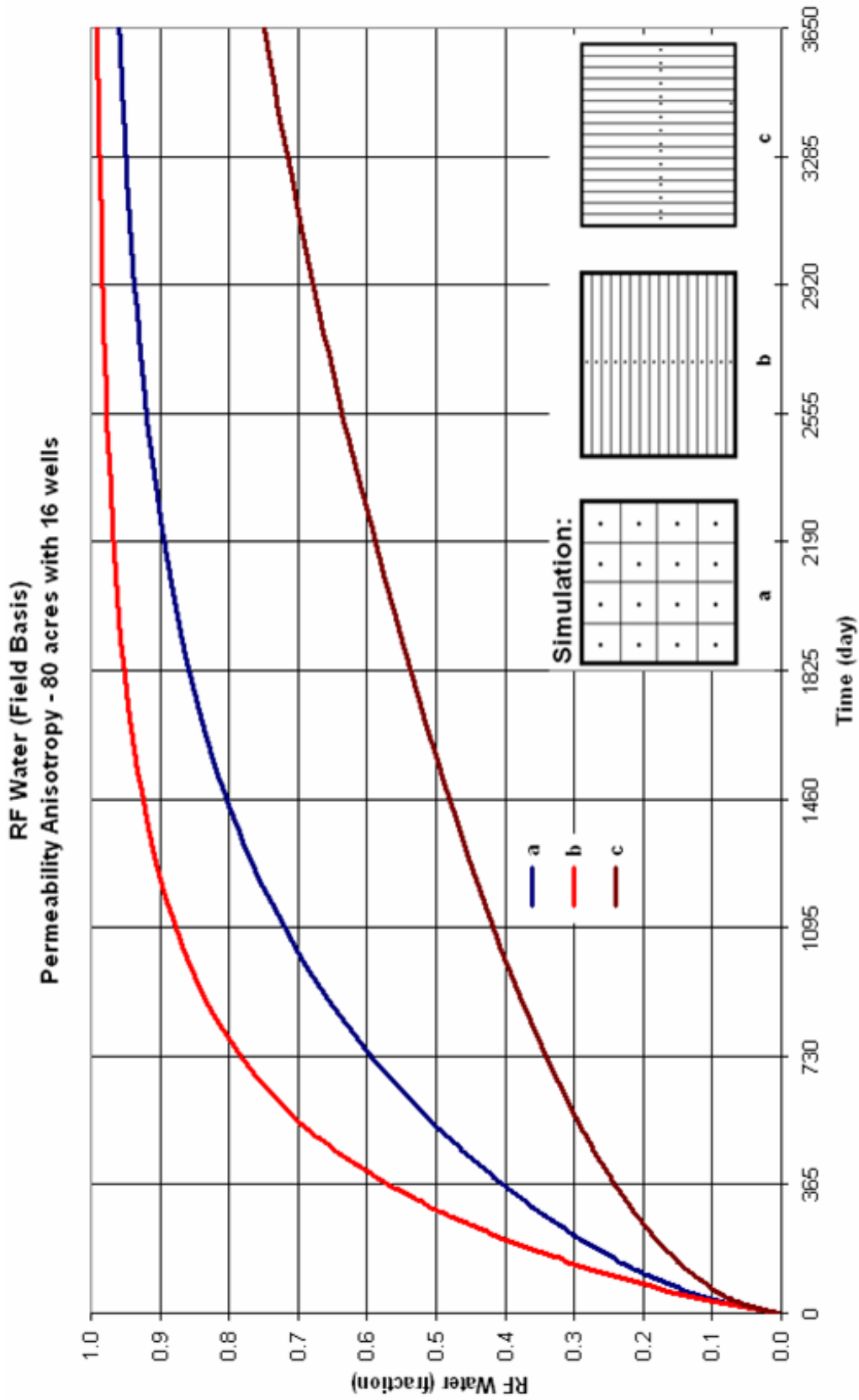


Fig. E.14—Comparison of recovery factor of water production for three types of well configurations for wells with 5 acre drainage area. Configuration type b gives the highest cumulative production for ten years simulation and type c gives the lowest. Configuration type b accelerates dewatering of the CBM reservoir.

TABLE E.3 - COMPARISON RESULTS FOR VARIOUS WELL CONFIGURATIONS - 5 ACRE SPACING					
		<i>OGIP</i> =	9.04E+08		<i>scf</i>
		<i>OWIP</i> =	1.79E+04		<i>stb</i>
No.	Type of simulation	Cum. Gas Production (scf)	Cum. Water Production (stb)	RF Gas	RF Water
1	Type A	3.84E+08	17236.40	42.48%	96.12%
2	Type B	4.73E+08	17768.00	52.29%	99.09%
3	Type C	2.26E+08	13548.00	24.99%	75.55%

E.3 Transformation of Anisotropic System to Isotropic System

E.3.1 Transformation for Permeability Anisotropy 1:0.1

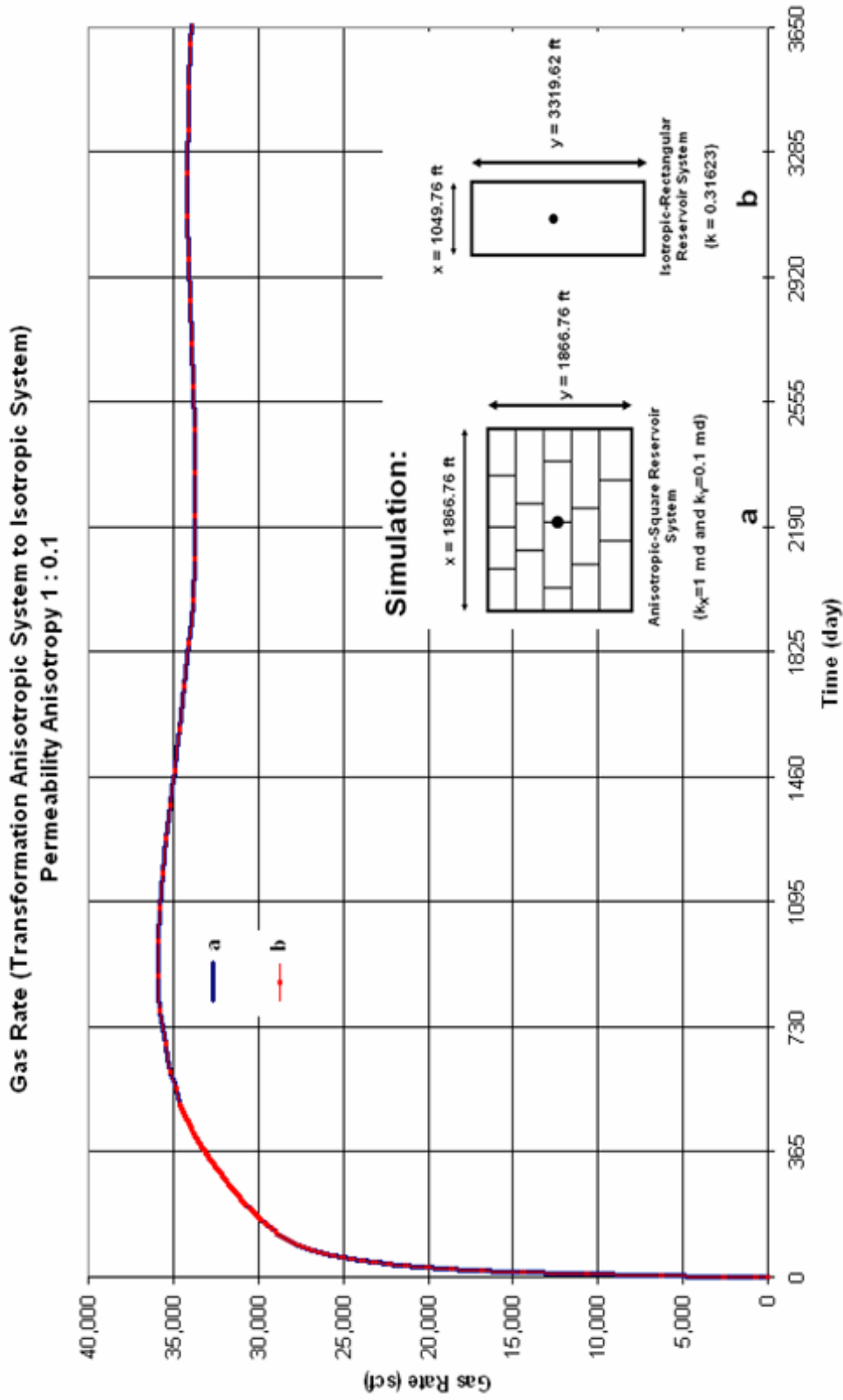


Fig. E.15—Gas rates for transformation of square-anisotropic 80 acre reservoir to rectangular-isotropic 80 acre reservoir with permeability anisotropy 1:0.1. Both of reservoir system show similar performance for gas production rate.

Cumulative Gas Production (Transformation Anisotropic System to Isotropic System)
Permeability Anisotropy 1 : 0.1

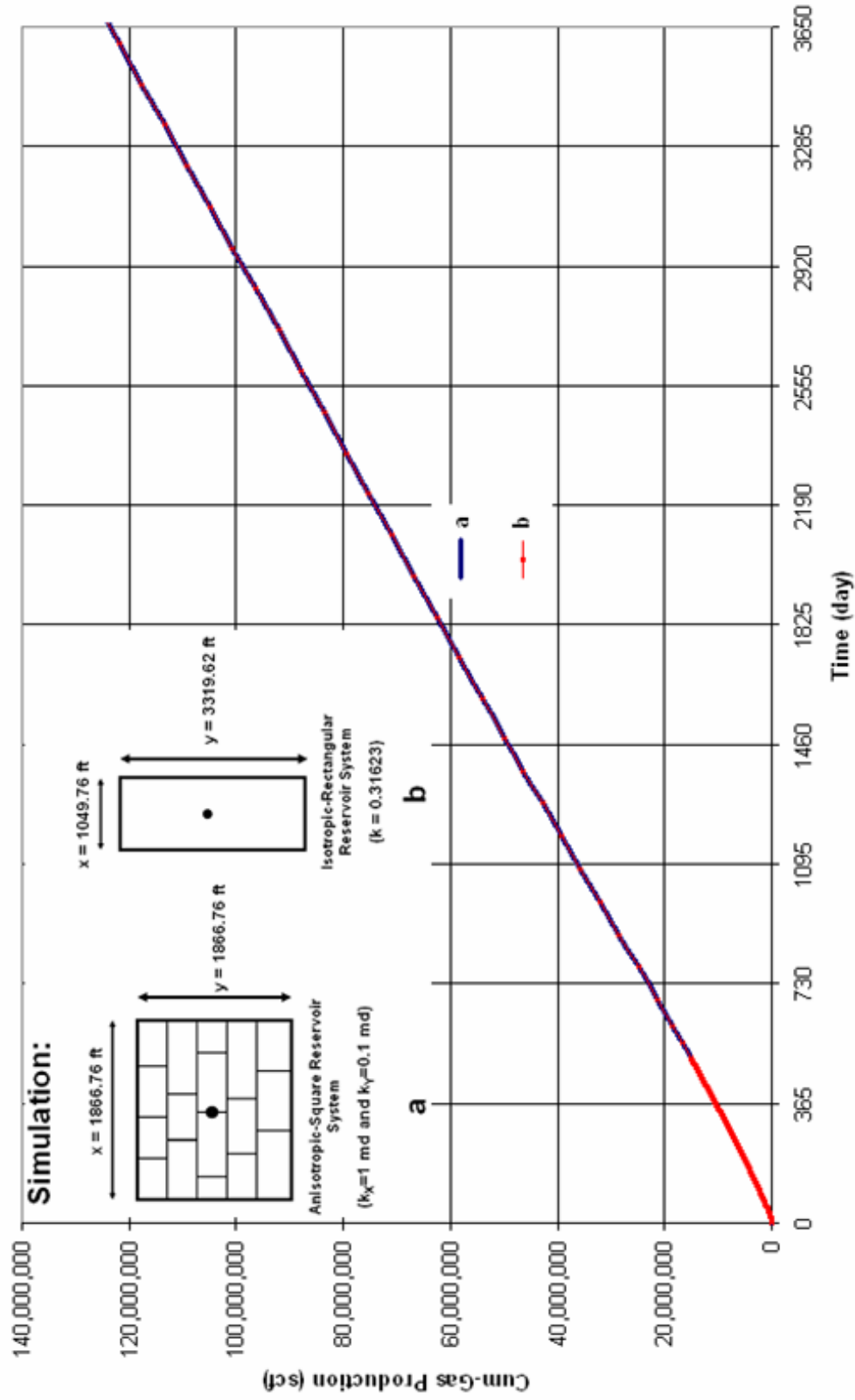


Fig. E.16—Cumulative gas production rates for transformation of square-anisotropic 80 acre reservoir to rectangular-isotropic 80 acre reservoir with permeability anisotropic 1:0.1. Both of reservoir system show similar performance for gas production rate.

E.3.2 Transformation for Permeability Anisotropy 1:0.01

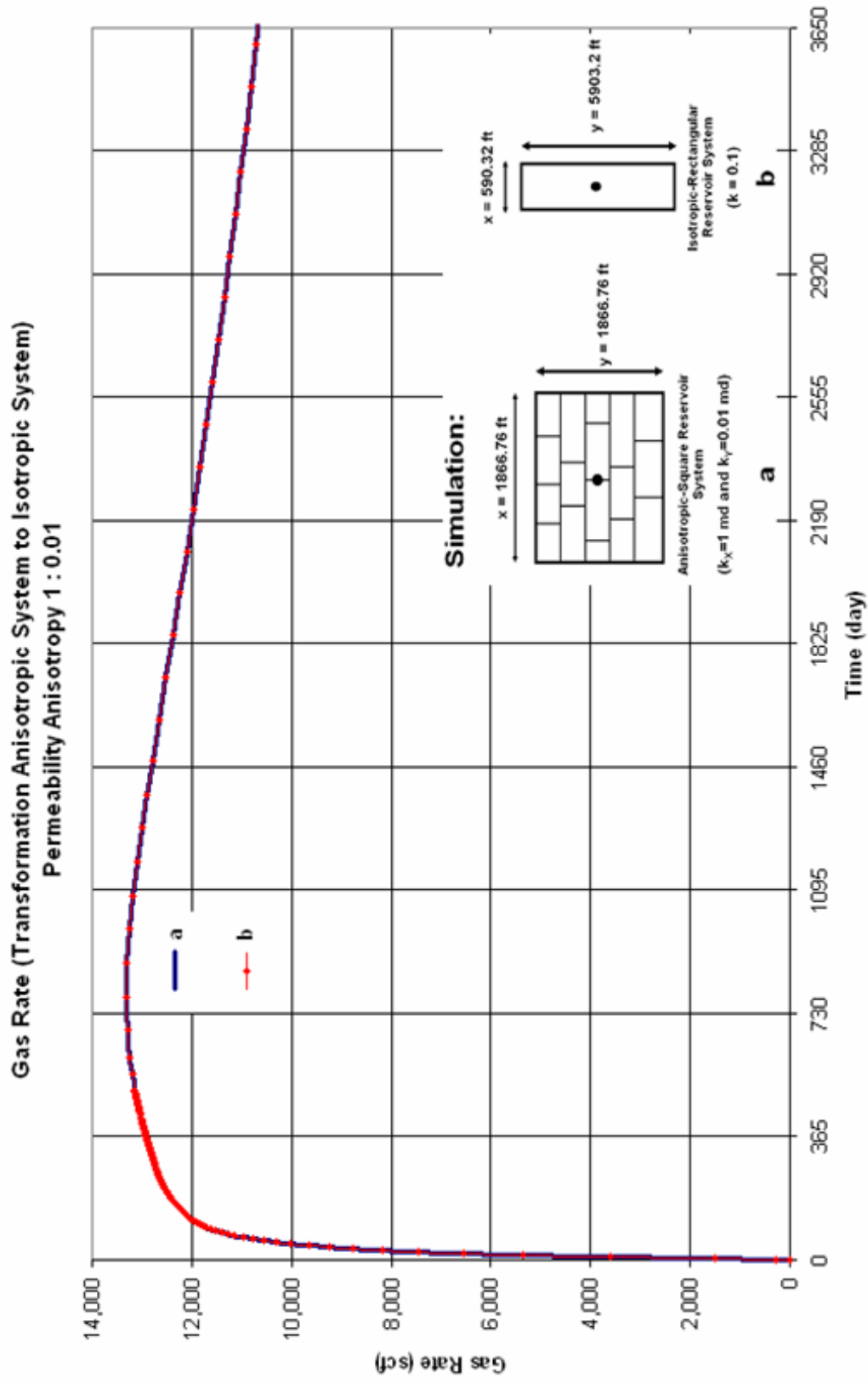


Fig. E.17—Gas rates for transformation of square-anisotropic 80 acre reservoir to rectangular-isotropic 80 acre reservoir with permeability anisotropy 1:0.01. Both of reservoir system show similar performance for gas production rate.

Cumulative Gas Production (Transformation Anisotropic System to Isotropic System)
Permeability Anisotropy 1 : 0.01

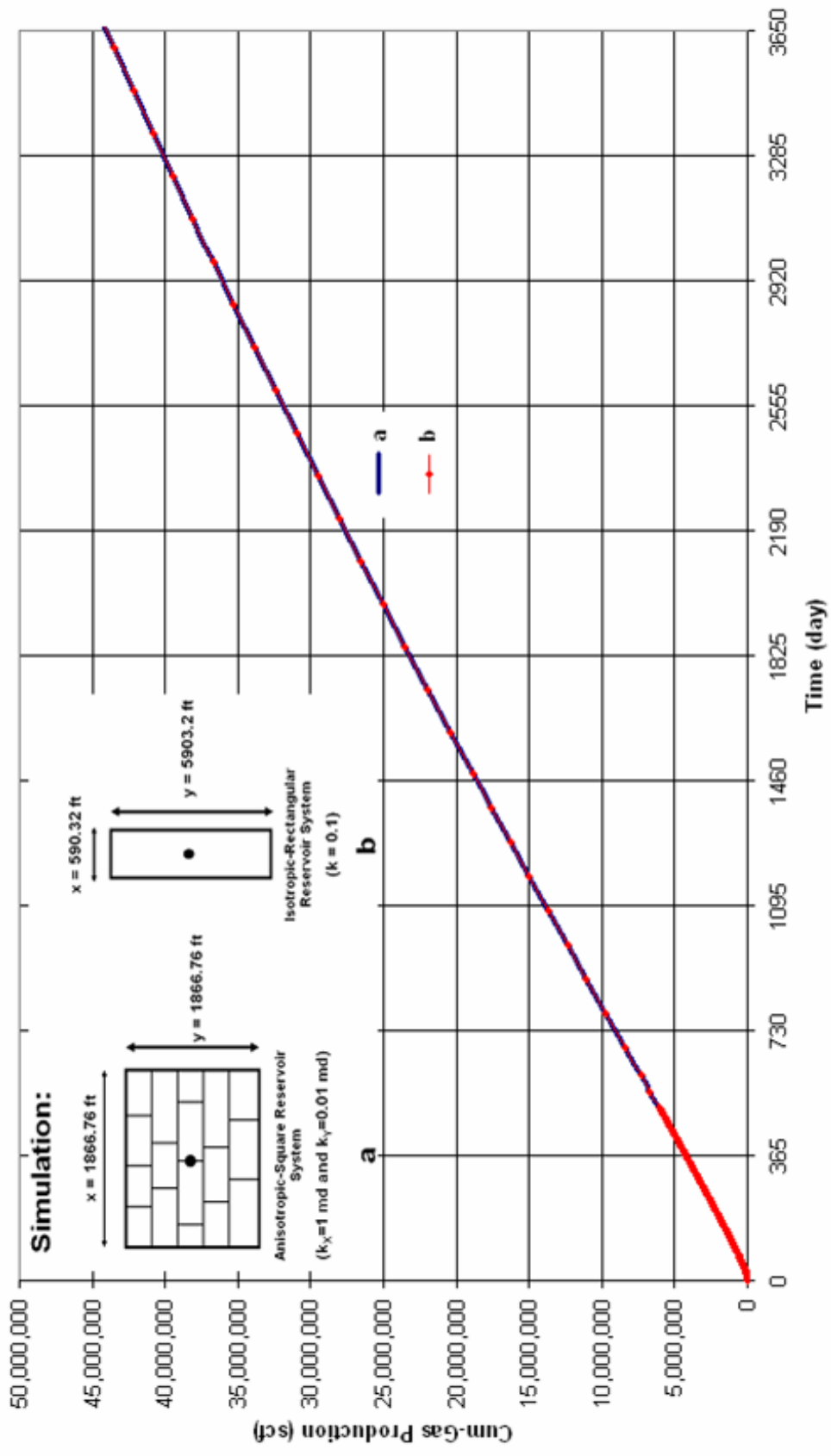


Fig. E.18—Cumulative gas production rates for transformation of square-anisotropic 80 acre reservoir to rectangular-isotropic 80 acre reservoir with permeability anisotropic 1:0.01. Both of reservoir system show similar performance for gas production rate.

VITA

NAME: Ismail Zulkarnain

PERMANENT ADDRESS: Komp. Taman Mutiara Blok CIV No. 10
Cimahi, West Java.
Indonesia-40265

EDUCATION: B.S., Petroleum Engineering (Cum Laude)
Institut Teknologi Bandung, West Java. Indonesia
October 2002

M.S., Petroleum Engineering (Sponsored by
Chevron Texaco)
Texas A&M University, College Station, Texas
December 2005